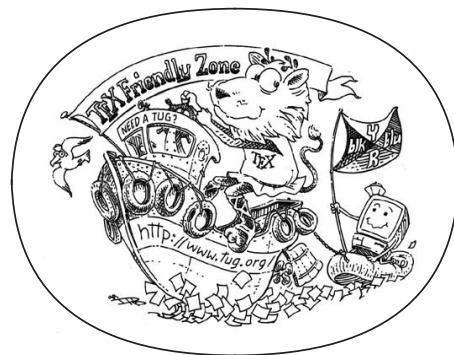


ON THE TRANSFER LEARNING PROPERTIES OF CONVOLUTIONAL NEURAL NETWORKS

MATTHIA SABATELLI



From Supervised to Deep Reinforcement Learning

September 2015 – version 4.2

ABSTRACT

Short summary of the contents... a great guide by Kent Beck how to write good abstracts can be found here:

<https://plg.uwaterloo.ca/~migod/research/beck00PSLA.html>

*You're never gonna grow if you don't grow now
You're never gonna know if you don't find out
You're never going back never turning around
You're never gonna go if you don't go now*

ACKNOWLEDGEMENTS

Put your acknowledgements here.

Many thanks to everybody who already sent me a postcard!

Regarding the typography and other help, many thanks go to Marco Kuhlmann, Philipp Lehman, Lothar Schlesier, Jim Young, Lorenzo Pantieri and Enrico Gregorio¹, Jörg Sommer, Joachim Köstler, Daniel Gottschlag, Denis Aydin, Paride Legovini, Steffen Prochnow, Nicolas Repp, Hinrich Harms, Roland Winkler, and the whole L^AT_EX-community for support, ideas and some great software.

Regarding LyX: The LyX port was initially done by Nicholas Mariette in March 2009 and continued by Ivo Pletikosić in 2011. Thank you very much for your work and the contributions to the original style.

¹ Members of GuIT (Gruppo Italiano Utilizzatori di T_EX e L^AT_EX)

CONTENTS

I PRELIMINARIES	3
1 SUPERVISED LEARNING AND DEEP NEURAL NETWORKS	5
1.1 Introduction	5
1.2 Statistical Learning Theory	5
1.3 Neural Networks	7
1.3.1 Multilayer Perceptrons	7
1.3.2 Stochastic Gradient Descent	9
1.3.3 Backpropagation	11
1.3.4 Loss Functions	12
1.3.5 Vanishing Gradients and Activation Functions .	13
1.4 Convolutional Neural Networks	15
1.4.1 Mathematical Operations	15
1.4.2 Popular Architectures	17
1.5 Conclusion	17
2 REINFORCEMENT LEARNING AND DEEP NEURAL NETWORKS	19
2.1 Introduction	19
2.2 Markov Decision Processes	20
2.3 Goals and Returns	22
2.4 Value Functions	24
2.5 Learning Value Functions	26
2.5.1 Monte Carlo Methods	26
2.5.2 Temporal Difference Learning	28
2.6 Function Approximators	31
2.6.1 Linear Functions	32
2.7 Deep Reinforcement Learning	33
2.8 Challenges and Desiderata	40
3 TRANSFER LEARNING	43
3.1 Introduction	43
3.2 Rationale of Transfer Learning	43
3.3 Mathematical Definitions	46
3.3.1 Supervised Learning	46
3.3.2 Reinforcement Learning	50
3.4 Deep Transfer Learning	51
3.4.1 General Framework	52
3.4.2 Literature Review	54
3.5 Relevance for this Dissertation	58
II TRANSFER LEARNING FOR DEEP SUPERVISED LEARNING	61
4 ON THE TRANSFERABILITY OF CONVOLUTIONAL NETWORKS	63

4.1	A First Empirical Study	63
4.2	Methodology	64
4.2.1	Transfer Learning	64
4.2.2	Datasets and Target Tasks \mathcal{T}_T	65
4.2.3	Convolutional Networks and Training Approaches	67
4.3	Results	68
4.3.1	From Natural to Non Natural Images	68
4.3.2	Discussion	72
4.3.3	From One Target Domain \mathcal{D}_T to Another	73
4.3.4	Selective Attention	74
4.4	Conclusion	75
5	NOVEL DATASETS FOR TRANSFER LEARNING	77
5.1	Challenges of Modern Computer Vision	77
5.2	The MINERVA Dataset	80
5.2.1	Data Collection	80
5.2.2	Annotation Process	81
5.2.3	Versions and Splits	81
5.3	Benchmarking	82
5.3.1	Classification	83
5.3.2	Object Detection	84
5.4	Results	85
5.4.1	Quantitative Analysis	85
5.4.2	Qualitative Analysis	88
5.5	Discussion and Critical Analysis	93
5.6	Future Work: towards more benchmarks	94
6	ON THE TRANSFERABILITY OF LOTTERY WINNERS	95
6.1	The Lottery Ticket Hypothesis	95
6.2	Datasets	98
6.3	Experimental Setup	99
6.4	Results	101
6.4.1	On the Importance of Finding Winning Initializations	102
6.4.2	On the Generalization Properties of Lottery Winners	103
6.5	Additional Studies	105
6.6	Related Work	108
6.7	Conclusion	110
III	TRANSFER LEARNING FOR DEEP REINFORCEMENT LEARNING	111
7	THE DEEP QUALITY-VALUE LEARNING FAMILY OF ALGORITHMS	113
7.1	Introduction	113
7.2	Preliminaries	114
7.3	Related Work	115

7.4 A Novel Family of Deep Reinforcement Learning Algorithms	117
7.4.1 DQV-Learning	118
7.4.2 DQV-Learning with Multilayer Perceptrons	119
7.4.3 DQV-Max Learning	119
7.5 Results	121
7.5.1 Global Evaluation	121
7.5.2 Convergence Time	124
7.5.3 Quality of the Learned Value Functions	124
7.6 Additional Studies	128
7.7 Discussion and Conclusion	130
8 ON THE TRANSFERABILITY OF DEEP-Q NETWORKS	133
9 CONCLUDING REMARKS	135
IV APPENDIX	137
BIBLIOGRAPHY	139

LIST OF FIGURES

Figure 1	A visualization of a perceptron.	8
Figure 2	The computational graph representing the mathematical operations performed by the perceptron represented in Fig. 1 and defined by Eq. 13.	8
Figure 3	The computational graph representing a simplified version of a multi-layer perceptron with one hidden layer. Note that no bias term is added after multiplying x and h_1 by W_1 and W_2 respectively.	11
Figure 4	The computational graph that results after having performed one forward pass through the network. We can see that the result of each mathematical operation is stored within a new node u that will be necessary for computing the partial derivatives required to perform stochastic gradient descent.	12
Figure 5	In the left plot a visualization of the vanishing gradient problem that can come from using a sigmoid non-linear activation function throughout a network. In the right plot a representation of typical non-linear activation functions within the $[-3, 3]$ range that are currently used by popular neural architectures.	14
Figure 6	A visual representation of how an agent interacts with an environment as modeled by a Markov decision process. Figure inspired from page 48 of the Sutton and Barto [188] textbook.	22
Figure 7	A visual representation of a simple MDP. For each state transition the corresponding reward is presented in red.	27
Figure 8	A visual representation of some of the Atari games that are part of the Arcade Learning Environment (ALE) [13]. From left to right Breakout, Seaquest, Qbert, Pong, MsPacman, KungFu-Master, Enduro and Space Invaders. Most of these games will be of interest in chapters 7 and 8. Image courtesy of	37

Figure 9	A visualization of the three possible desired outcomes that can come from adopting Transfer Learning strategies as initially defined by Langley [93] and later by Lazaric [95].	45
Figure 10	A visualization of two datasets that can be used for performing inductive transfer learning. On the left we represent instances of the popular MNIST dataset [227], while on the right instances of the Kuzushiji-MNIST dataset [32]. We see that both datasets share the same domain $\mathcal{D}_S = \mathcal{D}_T$ (black and white images), but are associated to different tasks $\mathcal{T}_S \neq \mathcal{T}_T$ (classification of digits vs classification of Japanese letters).	48
Figure 11	Two datasets that are representative of transductive transfer learning. On the left we show images coming from the Fashion-MNIST dataset [225], while on the right we report instances of the same dataset that are colored. In this case tasks among datasets are shared $\mathcal{T}_S = \mathcal{T}_T$ (classification of clothes), but the respective images come from different domains $\mathcal{D}_S \neq \mathcal{D}_T$ (black and white vs RGB images).	49

Figure 12	A simplified visual representation of the different deep transfer learning training paradigms that are considered throughout this thesis. The first plot represents a model that comes as pre-trained on a source task but which will not update most of its weights during the training stage (represented in gray): the only trainable parameters of this network are the ones that parametrize the final layer of the model and that are represented in green. In the second plot we visually represent a model that is parametrized with weights that have been learned on a certain source task, and that get “unfrozen” when the network gets trained on the target task, therefore defining the model as fully trainable. Lastly we visualize a model that does not come as pre-trained on any source task, and that is therefore initialized with random weights instead (represented by the various colours). As already mentioned throughout this chapter, the main goal of TL is to obtain a model that if trained with the first two approaches results into a final performance that is better than the one that would be obtained after adopting the last approach.	53
Figure 13	A visualization of the images that are used for our experiments. It is possible to see how the samples range from images representing plates made of porcelain to violins, and from Japanese artworks to a more simple picture of a key. . .	66
Figure 14	Comparison between the fine-tuning approach (θ_i) versus the off-the-shelf one (θ_i^-) when classifying the material of the heritage objects of the Rijksmuseum dataset. We can observe that for three out of four neural architectures the first approach leads to significant improvements when compared to the latter one. Furthermore, we can also observe that training a randomly initialized model from scratch (solid orange line) leads to worse results than fine-tuning a network that comes as pre-trained on the ImageNet dataset.	69

Figure 15	A similar analysis as the one which has been reported in Figure 14 but for the second and third classification tasks (left and right figures respectively). The results show again the significant benefits that fine-tuning (reported by the dashed line plots) has when compared to the off-the-shelf approach (reported by the dash-dotted lines) and how this latter strategy miserably under-performs when it comes to artist classification. Furthermore we again see the benefits that using a pre-trained model has over training the architecture from scratch (solid orange line).	71
Figure 16	A visualization of the saliency maps that are obtained when trying to classify an artist of the Rijksmuseum collection (first row of images) with either an ImageNet pre-trained model that is used as simple feature extractor(second row of images), or with the same kind of model which gets fine-tuned (third row of images). We can observe that after getting fine-tuned the network develops novel selective attention mechanisms that allow it to shift its attention from e.g., the buildings depicted in the paintings to the people represented at the bottom.	75
Figure 17	Some examples that show the limitations of object detectors that are trained on photorealistic images only. In the first image, we see how a model confidently detects a 'frisbee' for a 'lute', while in the second image, we can observe how next to being unable to detect the people in the painting, it also mistakenly detects the frame as a 'tv-monitor'. Similar limitations can be observed in the final image, where we can see that the persons within the painting are only correctly detected as long as they are either sitting or standing.	79
Figure 18	Samples from Minerva.	81
Figure 19	A visual representation of the distribution of the hypernym classes that are present within Minerva-0 and that define the Minerva-Hypernym benchmark.	83
Figure 20	True Positive (TP) vs False Positive (FP) analysis on the Minerva-Hypernym benchmark for $\text{IoU} \geq 10$ and $\text{IoU} \geq 50$	89

Figure 21	True Positive (TP) vs False Positive (FP) analysis on the Minerva-5 benchmark for $\text{IoU} \geq 10$ and $\text{IoU} \geq 50$	89
Figure 22	True Positive (TP) vs False Positive (FP) analysis on the Minerva-Hypernym benchmark for $\text{IoU} \geq 10$ and $\text{IoU} \geq 50$	90
Figure 23	Saliency maps obtained after fine-tuning an ImageNet pre-trained ResNet50 on the Minerva-Hypernym benchmark. The first image corresponds to the original image, while the second and fourth images, and the third and fifth images, respectively report the performance of the Grad-CAM and Grad-CAM ++ methods.	91
Figure 24	Some examples of successful detections that have been obtained on the IconArt dataset with a model fine-tuned on the Minerva-Hypernym benchmark.	92
Figure 25	Examples of false detections of 'stringed instruments' within some images representing 'nudity' that are part of the IconArt dataset.	93
Figure 26	Additional examples of false detections of 'stringed instruments' that are triggered by the presence of objects close to hands and fingers.	93
Figure 27	Examples of false detections that are due to the strong resemblance between long martial objects and (mostly) 'wind instruments'.	93
Figure 28	Examples of geometrical patterns that mistakenly yield the detection of instruments.	94

Figure 29 A visual representation of the LTH as introduced by Frankle and Carbin [50]. Let us consider a simplified version of a two hidden layer feedforward neural network as is depicted in the first image on the left. The LTH states that within this neural network, there exist multiple smaller networks (represented in green), which can perform just as well as their larger counterpart. Training these sparse models from scratch successfully is only possible as long as their weights are initialized with the same values that were also used when the larger (black) model was initialized. Furthermore, the structure of these sparse models appears to be crucial as well, as it is not possible to randomly extract any subset of weights from an unpruned model and successfully train the resulting sparse network (represented in red in the last figure) from scratch. We visually represent the performance of models that are the winners of the LTH in the two plots reported in Figure 30. . . 96

Figure 33	An overview of the results showing that sparse models that are the winners of the LTH (represented by the coloured lines) significantly outperform unpruned networks which get randomly initialized and trained from scratch (dashed black line). This happens to be the case on all tested datasets, no matter whether a winning initialization comes from a natural image source or not. It is however worth mentioning that, especially on the biomedical datasets, natural image tickets get outperformed by sparse networks that are the winners of the LTH on a biomedical dataset. On the other hand this is not the case when it comes to the classification of arts where natural image tickets outperform the ones which are found within artistic collections.	104
Figure 34	Our results showing the advantages of transferring lottery winners over pruned models that are fully fine-tuned on natural datasets (CIFAR-10/100). We can observe that their performance is overall inferior to the one of lottery tickets and that these models are significantly less robust to pruning. We believe that the reason behind their poor performance revolves around the fact that, once completely trained on a specific source task, and after having gone through the pruning stage, these models lose the necessary flexibility that is required for them to adapt to a new task.	106
Figure 35	Our results showing the benefits of transferring lottery winners that have been identified on a related source task. We can observe that on the Mouse-LBA dataset, winning tickets that were obtained on the Human-LBA dataset are the ones that are the most robust ones to pruning, while on the Artist 2 dataset we can observe that lottery winners that have been obtained on the Artist 1 dataset are both more robust to pruning, while they also yield overall better performance.	107

Figure 36	Our study showing that the robustness to large pruning rates of lottery winners does not depend from the size of the training dataset. We can observe that even when lottery tickets after are trained on only 25% of the dataset their performance remains stable with respect to the fraction of pruned weights. These results suggest that the less stable performance of Bone-Marrow lottery tickets observed in Fig. 33 does not depend from the small training set.	108
Figure 37	Our preliminary results that show the benefits in terms of convergence time that can come from jointly approximating the V function alongside the Q function. We can observe that the DQV-Learning algorithm yields faster convergence when compared to popular algorithms which only approximate the Q function: DQN and DDQN.	120
Figure 38	Learning curves obtained during training on three different Atari games by DQV and DQV-Max, and DQN and DDQN. We can observe that on these games both DQV and DQV-Max converge significantly faster than DQN and DDQN and that they obtain higher cumulative rewards on the Enduro environment.	125
Figure 39	Results investigating the extent to which the DQN algorithm suffers from the overestimation bias of the Q function. We can observe that on the Pong environment during the early stages of training, the $Q(s_{t+1}, a)$ estimates quickly grow, while on the Enduro game the values estimated by the Q network keep indefinitely growing, therefore making the algorithm significantly diverge from the real return that is obtained by a trained agent.	127
Figure 40	Results investigating the extent to which the DDQN algorithm suffers from the overestimation bias of the Q function. We can observe that compared to the analysis presented in Fig. 39, the DDQN algorithm prevents its Q-Network from diverging since on both Atari environments the $Q(s_{t+1}, a)$ estimates do not diverge from the observed real return of a trained agent. Results that replicate the findings reported by van2018deep.	127

- Figure 41 Results investigating the extent to which the DQV algorithm suffers from the overestimation bias of the Q function. We can observe that the performance of the algorithm is similar to the one observed in Fig. 40 for the DDQN algorithm. On both environments the estimated cumulative reward does not diverge from the real return that is obtained by the end of training, therefore suggesting that DQV-Learning does not suffer from the overestimation bias of the Q function. It is also worth noting the difference between the real return obtained by the DQN and the DDQN algorithms on the Enduro environment, and the one obtained by DQV. As can be seen by the black line, the real return obtained by a DQV agent is higher than DQN and DDQN's one, a result which shows that DQV converges to a better policy than DQN and DDQN. 128

Figure 42 Results investigating the extent to which the DQV-Max algorithm suffers from the overestimation bias of the Q function. We can observe that on the Pong environment the value estimates of the algorithm are comparable to the ones of DDQN and DQV, therefore showing the DQV-Max also diverges significantly less than DQN. On the Enduro environment we can observe that the algorithm does diverge, although, differently from what is reported in Fig. 39, the $Q(s_{t+1}, a)$ estimates seem to converge towards an upper bound (≈ 15). Similarly to what is reported in Fig. 41 we can again observe that the real return obtained by a trained agent is higher compared to the one obtain by DQN, DDQN and DQV, therefore confirming the results presented in Table 14 which see the DQV-Max algorithm as the best performing algorithm on the Enduro game. 129

Figure 43 Our results which aim to approximate the V and the Q function with a unique, shared parameterized network, an approach that is heavily inspired by multi-task learning studies that can be found in supervised learning [27, 125, 232]. We can see that this extension of DQV, named Hard-DQV, significantly underperforms the original DQV-Learning algorithm. 131

Figure 44 Our extensions of DQV that aim to reduce the amount of trainable parameters of the algorithm by following an approach similar to the one presented by Wang et al. [212] when "Dueling Networks" for DRL have been introduced. We can observe that among all the three Dueling-DQV extensions, only the Dueling-DQV-3rd one yielded good performance, but as highlighted by the results obtained on the Enduro environment, its performance is still inferior when compared to the one of the original DQV algorithm.

Figure 45 Learning curves obtained when reducing the capacity of the convolutional networks that approximate the V and the Q functions. We can observe that albeit each value function is approximated with its own parametrized network, the tiny-dqv extension still yields worse performance. These results highlight that it is not sufficient to simply have two separate neural networks for DQV to perform well, but that a crucial role in DQV's performance is played by the capacity of the networks that are used as well.¹³²

LIST OF TABLES

Table 1	An overview of the two datasets that are used in our experiments. For each heritage collection we report with N_t the amount of samples constituting the datasets and with Q_t the number of labels. Lastly, we also report if there are common labels between the two heritage collections.	66
Table 2	An overview of the results obtained by the different models on the testing set when classifying the heritage objects of the Rijksmuseum. The overall best performing architecture is reported in a green cell, while the second best performing one is reported in a yellow one. The additional columns “Params” and “ \mathcal{X} ” report the amount of parameters the networks have to learn and the size of the feature vector that is used as input for the softmax classifier.	72
Table 3	The results obtained on the classification experiments performed on the Antwerp dataset with models that have been initially pre-trained on ImageNet (θ^i) and the same architectures which have been fine tuned on the Rijksmuseum dataset (θ^r). Our results show that the latter pre-trained networks yield better results both if used as off the shelf feature extractors and if fine tuned.	73
Table 4	An overview reporting how many images N_t and instruments I_t are present within the splits of the Minerva-0, Minerva-5 and Minerva-10 versions of the MINERVA dataset.	82
Table 5	Results obtained when classifying the bounding boxes of the three different MINERVA benchmarks with models that do not come as pre-trained on any sort of source task \mathcal{T}_S . We can see that their performance is significantly worse than the one that is obtained when the same models come as pre-trained (see Table 6 and Table 7).	87

Table 6	Results obtained when classifying the bounding boxes of the three different MINERVA benchmarks after adapting transfer learning and considering the ImageNet dataset as the only source task \mathcal{T}_S . We observe that, compared to the results presented in Table 5, this approach yields significant benefits, therefore confirming the results presented in Chapter 4.	87
Table 7	Results obtained when classifying the bounding boxes of the three different MINERVA benchmarks after adapting transfer learning and considering the ImageNet and the Rijksmuseum collection as source domains \mathcal{D}_S . Similarly to what was observed in Table 6, we can again see that transfer learning yields significant benefits although this weight initialization strategy does mostly not outperform the more common ImageNet one.	87
Table 8	Average Precision (%) obtained when fine-tuning a pre-trained YOLO-V3 object detector on the Minerva-Hypernyms dataset. We can observe that satisfying results are obtained for both IoU thresholds when it comes to the detection of stringed instruments, whereas detecting the remaining four hypernyms of MINERVA appears to be much more challenging.	88
Table 9	Average Precision (%) obtained on the Minerva-5 benchmark. We can observe that the fine-tuned model successfully detects 'Harps', 'Lutes' and 'Violins', whereas the detection of 'Shawns' and 'Trumpets' can be improved.	89
Table 10	Average Precision (%) obtained on the Minerva-10 benchmark. Similarly to what was presented in Table 9, we can again observe that the model successfully detects the first three most occurring instruments within the dataset, whereas it appears to perform poorly on the remaining instrument classes.	89
Table 11	A brief overview of the seven different datasets which have been used in this work. As usual throughout this thesis N_t corresponds to the total amount of samples that are present in the dataset, while Q_t represents the number of classes.	99

Table 12	The results comparing the performance that is obtained on the testing-set by the best pruned model winner of the LTH, and an unpruned architecture trained from scratch. The overall best performing model is reported in a green cell, while the second best one in a yellow cell. We can observe that pruned models winners of the LTH perform significantly better than a larger over-parametrized architecture that gets trained from scratch. As can be seen by the results obtained on the Mouse-LBA and Artist 1 datasets the difference in terms of performance can be particularly large ($\approx 20\%$).
Table 13	Some additional information about the lottery winners which performance is reported in Table 12. For each winning ticket we report the fraction of weights that is pruned from an original ResNet-50 architecture and that therefore characterizes the level of sparsity of the overall best performing lottery ticket. The results in the Scratch-Training column are not reported since these are unpruned models that are trained from scratch.
Table 14	The results obtained by DQV and DQV-Max on a subset of 15 Atari games. We can see that our newly introduced algorithms have a comparable, and often even better performance than DQN and DDQN. As highlighted by the green cells the overall best performing algorithm in our set of experiments is DQV-Max while the second-best performing algorithm is DQV (as reported by the yellow cells). Specific attention should be given to the games BankHeist and Enduro where DQV and DQV-Max are the only algorithms which can master the game with a final super-human performance.

LISTINGS

SYMBOLS AND NOTATION

π policy

INTRODUCTION

This dissertation is based on several peer-reviewed publications. The main contributions underlying this work are:

- Sabatelli et al. [159] "*Deep transfer learning for art classification problems.*" Proceedings of the European Conference on Computer Vision (ECCV) Workshops, 2018.
- Sabatelli et al. [158] *Deep Quality Value (DQV) Learning.*" Advances in Neural Information Processing Systems (NeurIPS), Deep Reinforcement Learning Workshop, 2018.
- Sabatelli, Kestemont, and Geurts [157] "*On the transferability of winning tickets in non-natural image datasets.*" Proceedings of the 16th International Joint Conference on Computer Vision, Imaging and Computer Graphics Theory and Applications (VISAPP), 2021.
- Sabatelli et al. [162] "*The deep quality-value family of deep reinforcement learning algorithms*" Proceedings of the International Joint Conference on Neural Networks (IJCNN). IEEE, 2020.
- Sabatelli et al. [163] "*Advances in Digital Music Iconography: Benchmarking the detection of musical instruments in unrestricted, non-photorealistic images from the artistic domain.*" DHQ: Digital Humanities Quarterly 15.1 2021.
- "*On the Transferability of Deep-Q Networks.*" Under Review.

Throughout the Ph.D. several other peer-reviewed papers have been published, however these are not directly presented in this thesis. The following works are either the result of external collaborations, or have served for reporting preliminary results of ongoing research:

- Sabatelli et al. [161] "*Approximating two value functions instead of one: towards characterizing a new family of Deep Reinforcement Learning algorithms*" Advances in Neural Information Processing Systems (NeurIPS), Deep Reinforcement Learning Workshop, 2019
- Leroy et al. [101] "*QVMix and QVMix-Max: Extending the Deep Quality-Value Family of Algorithms to Cooperative Multi-Agent Reinforcement Learning.*" Proceedings of the AAAI-21 Workshop on Reinforcement Learning in Games, 2021.

- Hammond et al. [62] "*Forest Fire Control with Learning from Demonstration and Reinforcement Learning*". Proceedings of the International Joint Conference on Neural Networks (IJCNN). IEEE, 2020.
- Banar et al. [9] "*Transfer Learning with Style Transfer between the Photorealistic and Artistic Domain*." IST International Symposium on Electronic Imaging. Computer Vision and Image Analysis of Art, 2021.

Part I
PRELIMINARIES

SUPERVISED LEARNING AND DEEP NEURAL NETWORKS

OUTLINE

structure ...

1.1 INTRODUCTION

1.2 STATISTICAL LEARNING THEORY

We start by defining a Supervised Learning (SL) problem with a triplet containing the following elements:

- An input space \mathcal{X} ,
- An output space \mathcal{Y} ,
- A joint probability distribution $P(X, Y)$.

Let us define with \mathcal{F} the set of all functions f that can be produced by a certain learning algorithm. In SL the main goal is to find a function $f : \mathcal{X} \rightarrow \mathcal{Y} \in \mathcal{F}$ that minimizes the expectation over $P(X, Y)$ of a certain loss ℓ , based on the predictions made by f and the correct outputs defined in \mathcal{Y} .

This expectation is also known as the **expected risk**, or generalization error, and is defined as:

$$R(f) = \mathbb{E}_{(\mathbf{x}, y) \sim P(X, Y)} [\ell(y, f(\mathbf{x}))], \quad (1)$$

where f is built from a limited set of observations that define the SL problem we would like to solve. Such observations constitute the **learning set** \mathcal{L} which is defined by N pairs of input vectors and output values $(\mathbf{x}_1, y_1), \dots, (\mathbf{x}_N, y_N)$ where $\mathbf{x}_i \in \mathcal{X}$ and $y_i \in \mathcal{Y}$.

As $P(X, Y)$ is unknown and \mathcal{L} is finite, one cannot evaluate the quantity defined in Eq. 1, however, one can compute an estimate of it instead. To this end it is common to use part of the learning set \mathcal{L} for constructing a **training set** $\mathcal{L}_{\text{Train}}$, of size M , that can be used for computing the **empirical risk**, or training error, as follows:

$$\hat{R}(f, \mathcal{L}_{\text{Train}}) = \frac{1}{M} \sum_{(\mathbf{x}_i, y_i) \in \mathcal{L}_{\text{Train}}} \ell(y_i, f(\mathbf{x}_i)). \quad (2)$$

Computing Eq. 2 results in an unbiased estimate that can be used for finding a good approximation of the optimal function f^* that minimizes Eq. 1. Formally this corresponds to satisfying the equality

$$f_{\mathcal{L}_{\text{Train}}}^* = \arg \min_{f \in \mathcal{F}} \hat{R}(f, \mathcal{L}_{\text{Train}}), \quad (3)$$

which is known as the empirical risk minimization principle [209]. As mentioned by empirical risk minimizers converge in the limit to optimal models:

$$\lim_{N \rightarrow \infty} f_{\mathcal{L}_{\text{Train}}}^* = f^*. \quad (4)$$

With these concepts in place we can summarize the goal of SL as finding a function f that on average makes good predictions over $P(X, Y)$. To this end, when explaining the data generating process underlying $P(X, Y)$, f does not have to be too ‘simple’ nor too ‘complex’. In order to assess this let $\mathcal{Y}^{\mathcal{X}}$ be the set of all functions $f : \mathcal{X} \rightarrow \mathcal{Y}$. The minimal expected risk over all these functions is defined as

$$R_B = \min_{f \in \mathcal{Y}^{\mathcal{X}}} R(f), \quad (5)$$

and is called the **Bayes risk**. When minimized, the quantity defined in Eq. 5 results in the best possible function f_B , which is called the Bayes model. If the capacity of the hypothesis space \mathcal{F} chosen for finding f is too low, then it follows that $R(f) - R_B$ will be large for any $f \in \mathcal{F}$, including f^* and $f_{\mathcal{L}_{\text{Train}}}^*$. Similarly, if the capacity of \mathcal{F} is too high then albeit $R(f) - R_B$ will be small, $f_{\mathcal{L}_{\text{Train}}}^*$ can fit $\mathcal{L}_{\text{Train}}$ arbitrarily well such that:

$$R(f_{\mathcal{L}_{\text{Train}}}^*) \geq R_B \geq \hat{R}(f_{\mathcal{L}_{\text{Train}}}^*, \mathcal{L}_{\text{Train}}) \geq 0. \quad (6)$$

When f is too simple then it is said to **underfit** the data, whereas it is said to **overfit** it when it is too complex. As a result, one wants both the expected risk R and the empirical risk \hat{R} minimizers to be as low as possible. To achieve this we can again evaluate the performance of $f_{\mathcal{L}_{\text{Train}}}^*$ by computing the empirical risk defined in Eq. 2 on a separate independent dataset known as the **testing set** $\mathcal{L}_{\text{Test}}$. Note however that this quantity should be used for model evaluation purposes only, and not for model selection ones, which is usually done through a separate dataset called the **validation set**.

So far we have defined the concepts of expected risk and empirical risk with respect to a loss function ℓ , however, we have not yet seen how this loss function looks like in practice. In SL ℓ changes based on the characteristics of Y . This allows us to distinguish between two different SL problems: **classification** and **regression**. In the first case \mathcal{Y} comes in the form of a finite set of classes $\{c_1, c_2, \dots, c_i\}$, whereas in the latter case $\mathcal{Y} = \mathbb{R}$. For classification the arguably most straightforward loss function is the 0 – 1 loss defined as

$$\ell(f(\mathbf{x}, y)) = \mathbb{1}(f(\mathbf{x}) \neq y), \quad (7)$$

while for regression problems ℓ can either come in the form of the squared error loss:

$$\ell(f(\mathbf{x}, y) = (y - f(\mathbf{x})))^2 \quad (8)$$

or in the form of the absolute error loss

$$\ell(f(\mathbf{x}, y)) = |y - f(\mathbf{x})|, \quad (9)$$

depending on how much one wants to penalize the errors made by f .

While several SL algorithms adopting empirical risk minimization principles exist, throughout this dissertation we will only focus on artificial neural networks, a family of techniques that will be reviewed hereafter.

1.3 NEURAL NETWORKS

1.3.1 Multilayer Perceptrons

The first mathematical model developed with the intention of mimicking the biological processes underlying the human brain was proposed by Rosenblatt [150]. Inspired by the work of McCulloch and Pitts [113], Rosenblatt developed the [perceptron](#), the simplest form of artificial neural network able of tackling supervised learning binary classification problems. Given an input vector \mathbf{x} the perceptron produces the following output:

$$f(\mathbf{x}) = \begin{cases} 1 & \text{if } \sum_i w_i x_i + b \geq 0 \\ 0 & \text{otherwise} \end{cases} \quad (10)$$

which is given by summing up each input x with a certain weight w and a final additional bias term b . The result of this sum is then passed through the sign non-linear activation function which yields output h :

$$\text{sign}(x) = \begin{cases} 1 & \text{if } x \geq 0 \\ 0 & \text{otherwise} \end{cases} \quad (11)$$

The way the perceptron works is visually represented in Fig. 1 and can be summarized as follows:

$$f(\mathbf{x}) = \text{sign}\left(\sum_i w_i x_i + b\right). \quad (12)$$

Interestingly, Eq. 12 can also be rewritten in terms of tensor operations. This allows us to express the perceptron classification rule as

$$f(\mathbf{x}) = \text{sign}(\mathbf{w}^\top \mathbf{x} + b), \quad (13)$$

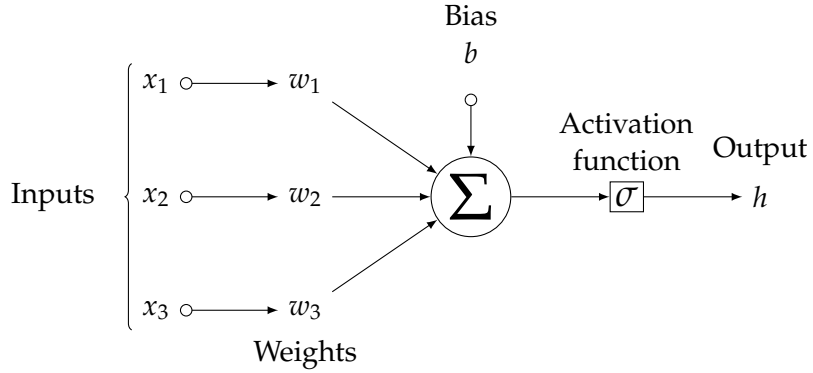


Figure 1: A visualization of a perceptron.

and to conveniently visualize its mathematical operations through a [computational graph](#), a directed graph where each node represents a certain mathematical operation. The computational graph of Eq. 13 is represented in Fig. 2 and can be considered as the main building block of artificial neural networks.

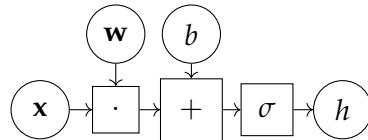


Figure 2: The computational graph representing the mathematical operations performed by the perceptron represented in Fig. 1 and defined by Eq. 13.

Eq. 13 summarizes the computations that are performed by one single input where $\mathbf{x} \in \mathbb{R}^p$, $\mathbf{w} \in \mathbb{R}^p$ and $b \in \mathbb{R}$. However, the computation capabilities of such a single unit are very limited and can rarely be adopted to solve complex tasks. To overcome this, one can stack several units in parallel such that they create a layer with q outputs defined as:

$$\mathbf{h} = \sigma(\mathbf{W}^\top \mathbf{x} + \mathbf{b}), \quad (14)$$

where $\mathbf{h} \in \mathbb{R}^q$, $\mathbf{x} \in \mathbb{R}^p$, $\mathbf{W} \in \mathbb{R}^{p \times q}$, $\mathbf{b} \in \mathbb{R}^q$. To increase the flexibility and capabilities of the model even further, one can then compose a sequence of L layers

$$\begin{aligned} \mathbf{h}_0 &= \mathbf{x} \\ \mathbf{h}_1 &= \sigma(\mathbf{W}_1^\top \mathbf{h}_0 + \mathbf{b}_1) \\ &\dots \\ \mathbf{h}_L &= \sigma(\mathbf{W}_L^\top \mathbf{h}_{L-1} + \mathbf{b}_L) \end{aligned} \quad (15)$$

and define a [multilayer perceptron](#) (MLP), also known as feedforward neural network. From now on we will refer to an MLP as $f(\mathbf{x}; \theta)$ where $\theta = \{\mathbf{W}_k, \mathbf{b}_k, \dots | k = 1, \dots, L\}$.

Now that we defined the mathematical computations that are performed by a feedforward neural network we move on to explaining how one can train these kind of models to perform empirical risk minimization.

1.3.2 Stochastic Gradient Descent

Training a neural network consists in finding parameters θ such that a loss function $\mathcal{L}(\theta)$, also denoted as the **objective function**, is minimized. Such loss functions are typically expressed as a sum of the losses ℓ_n incurred by each sample n in a training set of size N , and can be expressed in the following form:

$$\mathcal{L}(\theta) = \sum_{n=1}^N \ell_n(\theta). \quad (16)$$

When neural networks are used, \mathcal{L} has to be differentiable as this allows to minimize it through first order optimization algorithms. Among such methods, the arguably most straightforward one is gradient descent, which updates the parameters θ proportionally to the negative gradient of \mathcal{L} . This is done by applying the following update rule:

$$\begin{aligned} \theta_{t+1} &= \theta_t - \gamma_t (\nabla \ell(\theta_t))^T \\ &= \theta_t - \gamma_t \sum_{n=1}^N (\nabla \ell_n(\theta_t))^T, \end{aligned} \quad (17)$$

where t is a time counter variable, and $\gamma \geq 0$ is the learning rate, sometimes also denoted as the step-size parameter. We can easily observe that computing Eq. 19 can become computationally very expensive as it requires to evaluate gradients from all individual functions ℓ_n . This property is in fact what defines gradient descent as a batch optimization method, which makes it unfortunately unsuitable for dealing with large datasets. A possible solution to this computational burden consists in reducing the amount of computation required by the sum in Eq. 19 by simply considering a small, random batch of samples of the training set. In the extreme case, one can even just estimate the gradient on one single, randomly chosen, training sample, which is a method called Stochastic Gradient Descent (SGD). While it is true that this approach gives an unbiased estimate of the true gradient, its estimate can also be very noisy, which is the reason behind why it is preferable to evaluate the gradient for a mini-batch of samples instead than on one single, unique sample. A large body of work has investigated the effect that the batch-size has on neural network training [84, 85, 146]; however, so far no exact rule for determining an optimal batch-size exists. Yet, provided that enough computational resources are available, large mini-batches are usually preferred as they will re-

sult in more accurate estimates of the gradient, and therefore reduce the variance in the parameter update θ_{t+1} .

When the optimization surface is made of valley floors, gradient descent has the limitation of being very slow. To deal with such issue, several works have designed optimization strategies which make gradient based optimization faster and more efficient. The most straightforward improvement to the gradient descent algorithm is the one proposed by Rumelhart, Hinton, and Williams [153] who suggested to use of an additional term in the update rule presented in Eq.19, named **momentum**. This term, simply keeps track of what happened when the parameters were updated at $t - 1$ and determines the next parameters' update as a linear combination between the current and previous gradients. This results in the following update rule:

$$\theta_{t+1} = \theta_t - \gamma_t ((\nabla \ell(\theta_t)))^\top + \alpha \Delta \theta_t \quad (18)$$

where

$$\begin{aligned} \theta_t &= \theta_t - \theta_{t-1} \\ &= \alpha \Delta \theta_{t-1} - \gamma_{t-1} (\nabla \ell(\theta_{t-1}))^\top, \end{aligned} \quad (19)$$

and $\alpha \in [0, 1]$, which accelerates the optimization process and allows the algorithm average out noisy estimates of the gradient.

Next to adding a momentum term to improve the performance of gradient descent, another common method that can accelerate its convergence revolves around dynamically adapting the learning rate parameter γ . Popular neural network optimizers such as RMSProp [197], AdaGrad [42], and the very well-known Adam optimizer [86], all adapt this method. While discussing these algorithms into detail is out of the scope of this thesis, we refer the reader to the work of Ruder [152], which provides a nice overview of the most common gradient descent optimization algorithms, and to the work of Schmidt, Schneider, and Hennig [169] who empirically evaluate their performance across different networks and machine learning problems.

Before ending this section it is worth noting that next to SGD-like methods, there also exist several alternative algorithms that can be used for optimization problems. Among such methods, we mention second order optimization techniques such as Newton, Quasi-Newton and the Conjugate gradient methods discussed in [193]. While these algorithms are able to minimize the empirical risk faster and even better than SGD, they do not result in equally good generalization performance. Recall from Sec. 1.2, that in SL minimizing the expected risk is just as important as minimizing the empirical risk, which is a property that the aforementioned second order optimization algorithms do not have. This key result, first presented by Bottou and Bousquet [21], is what motivates the use of SGD-like optimizers in deep learning.

1.3.3 Backpropagation

From Eq. 19 we can note that a crucial role in the optimization process is played by the gradient $\nabla \ell(\theta)$. As we have seen in Sec. 1.3.1 neural networks can be considered as a composition of nested functions k for $k = 0, \dots, K - 1$, where each function comes with its own parameters θ_k . Therefore the gradient comes in the form of a vector which contains all the partial derivatives of the loss ℓ with respect to the weights θ that parametrize the neural network:

$$\nabla \ell(\theta) = \left[\frac{\partial \ell}{\partial \theta_0}(\theta), \dots, \frac{\partial \ell}{\partial \theta_{K-1}}(\theta) \right]. \quad (20)$$

As the number of functions increases, so does the complexity of the gradient, therefore an efficient way of calculating it is necessary. The backpropagation algorithm is a special case of a more general technique, called [automatic differentiation](#), that allows to evaluate the gradient of complicated functions numerically and automatically. This is done by exploiting the chain rule, which can be applied recursively on the computation graph that keeps track of all the arithmetic operations that are performed by the network.

To this end let us define a simplified version of a two hidden layer perceptron f that is parametrized with weight matrices \mathbf{W}_1 and \mathbf{W}_2 . When given input data \mathbf{x} the network produces a prediction \hat{y} which results from traversing the computational graph represented in Fig. 3. During the traversal, also known as the [forward pass](#), the result of

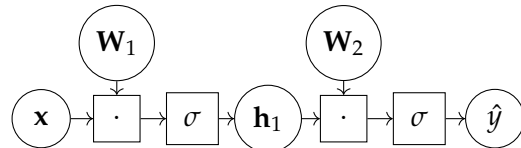


Figure 3: The computational graph representing a simplified version of a multi-layer perceptron with one hidden layer. Note that no bias term is added after multiplying \mathbf{x} and \mathbf{h}_1 by \mathbf{W}_1 and \mathbf{W}_2 respectively.

each mathematical operation is stored within its own output variable u (see Fig. 4) Having such an annotated graph it is now possible to compute all partial derivatives efficiently by traversing the graph backwards ([backward pass](#)), and by applying the chain rule which in its general form states that:

$$\frac{d\ell}{d\theta_i} = \sum_{k \in \text{parents}(\ell)} \frac{\partial \ell}{\partial u_k} \frac{\partial u_k}{\partial \theta_i}. \quad (21)$$

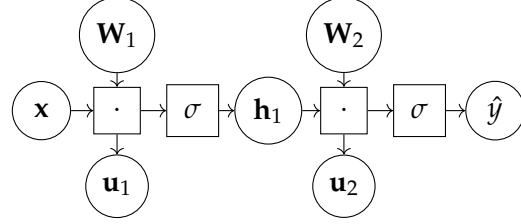


Figure 4: The computational graph that results after having performed one forward pass through the network. We can see that the result of each mathematical operation is stored within a new node \mathbf{u} that will be necessary for computing the partial derivatives required to perform stochastic gradient descent.

Therefore taking as example \mathbf{W}_1 , the derivative of the network's output \hat{y} with respect to this weight matrix is given by:

$$\begin{aligned} \frac{d\hat{y}}{d\mathbf{W}_1} &= \frac{\partial\hat{y}}{\partial u_2} \frac{\partial u_2}{\partial h_1} \frac{\partial h_1}{\partial u_1} \frac{\partial u_1}{\partial \mathbf{W}_1} \\ &= \frac{\partial\sigma(u_2)}{\partial u_2} \frac{\partial \mathbf{W}_2^\top h_1}{\partial h_1} \frac{\partial\sigma(u_1)}{\partial u_1} \frac{\partial \mathbf{W}_1^\top \mathbf{x}}{\partial \mathbf{W}_1}. \end{aligned} \quad (22)$$

1.3.4 Loss Functions

Defining an appropriate loss function is a task that has important practical implications when it comes to the design of the neural architecture. Just like for any other type of machine learning model, the choice of which loss function to minimize depends from the SL task we would like to solve. Fortunately, since neural networks are parametric models, their loss functions are not too different from the ones that are typically used by e.g., linear models such as . The most important concept underlying the loss functions used by neural networks is that of **maximum likelihood estimation**. As many other parametric models, neural networks implicitly define a distribution $p(Y|\mathbf{x}; \theta)$. This is convenient as it makes it possible to exploit the cross-entropy between the training data and the model's predictions. Therefore, no matter whether we are dealing with a classification problem or a regression one, the loss function that will be adopted by a neural network will always come in the following general form:

$$\mathcal{L}(\theta) = -\mathbb{E}_{(\mathbf{x}, y) \sim P(X, Y)} \log p_{\text{model}}(Y|\mathbf{x}). \quad (23)$$

Typical loss functions that derive from Eq. 23 (see Chapter 5 of [59] for the exact derivations) are the mean squared error (MSE) loss

$$\mathcal{L}(\theta) = \frac{1}{2} \mathbb{E}_{(\mathbf{x}, y) \sim P(X, Y)} \|y - f(\mathbf{x}; \theta)\|^2 \quad (24)$$

which is used for tackling regression problems, and the categorical cross-entropy loss

$$\mathcal{L}(\theta) = -\mathbb{E}_{(x,y \sim P(X,Y))} \sum_{i=1}^C y^i \log f(x; \theta) \quad (25)$$

which is used for multi-class classification problems, where C is the number of classes we would like to classify.

Based on whether Eq. 24 or Eq. 25 is minimized, the final layer of a neural network comes in different forms. As the goal of a regression problem is to predict a single numerical value, it follows that the final layer simply consists of one individual unit that is necessary for estimating $\mathcal{Y} \in \mathbb{R}$. One single output unit is also used for binary classification problems, where it is combined with the sigmoid activation function

$$\sigma(x) = \frac{1}{1 + \exp(-1)} \quad (26)$$

which allows to model a Bernoulli distribution over a binary variable. For classification problems, where $C > 2$, and the goal is to represent the distribution over a discrete variable that can have C possible values, the sigmoid function can be generalized to a softmax function by producing a vector for $i = 1, \dots, C$ such that:

$$\text{Softmax}(\mathbf{z})_i = \frac{\exp(z_i)}{\sum_{j=1}^C \exp(z_j)}. \quad (27)$$

We can observe that Eq. 27 makes the log probabilities, typically estimated by the second-last layer of a network, positive and sum up to one, therefore successfully modeling a multinoulli distribution. While the aforementioned output layers are arguably the most popular it is worth noting that several other types of output layers exist. Since throughout this dissertation none of these additional layers will be used in practice we will not describe them here and refer the reader to Chapter 6 of [59] for more information about this topic.

1.3.5 Vanishing Gradients and Activation Functions

A typical problem of neural networks that come with many hidden layers is given by vanishing gradients. Recall from Sec. 1.3.3 that in order to perform SGD we first need to collect all the partial derivatives of the network's output with respect to its parameters. As we do this by applying the chain rule this can have the drawback of making the gradient decrease exponentially with respect to the depth of the network. As a result deeper layers can become particularly hard to train, since no information necessary for updating the respective weights will be contained within the gradient. The most common

cause of this problem is given by the activation function that is used for introducing non-linearity across the network. For example, let us consider the sigmoid function presented in Eq. 26 and its derivative which comes in the following form:

$$\frac{d\sigma}{dx}(x) = \sigma(x)(1 - \sigma(x)). \quad (28)$$

As we can see from the first image of Fig. 5, the maximum value of Eq. 28 is 0.25. If we then use this value when adopting the chain rule as done in Eq. 22, and assume the network comes with a large number of hidden layers, it is easy to see that the gradient $\frac{d\hat{y}}{dW_1}$ will shrink to zero as the number of layers increases. The sigmoid function is not the only activation function which suffers from this phenomenon, which is also not restricted to feedforward neural networks. In fact as first presented by another non-linear activation function suffering from the vanishing gradient problem is the hyperbolic tangent

$$\tanh(x) = \frac{1 - \exp(-2x)}{1 + \exp(-2x)}. \quad (29)$$

As can be seen in the second plot of Fig. 5 the tanh is very similar in shape to the sigmoid. This activation function is largely used within Recurrent Neural Networks (RNNs), a particular type of neural network that can be unfolded into very deep MLPs. For many years its vanishing gradient issues have questioned whether RNNs could be trained and used in practice, a problem which has been successfully solved with the introduction of the Long Short Term Memory (LSTM) cells [75].

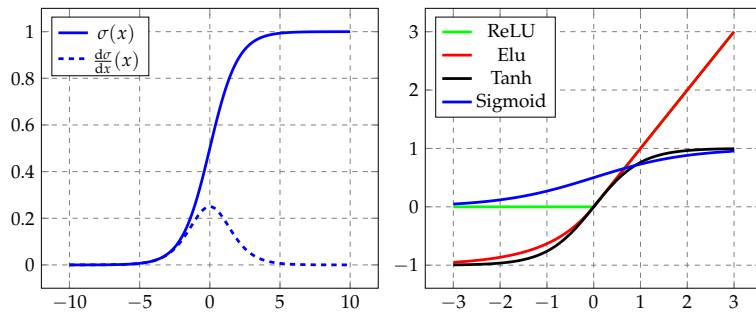


Figure 5: In the left plot a visualization of the vanishing gradient problem that can come from using a sigmoid non-linear activation function throughout a network. In the right plot a representation of typical non-linear activation functions within the $[-3, 3]$ range that are currently used by popular neural architectures.

Another solution to the vanishing gradient problem is to use the Rectified Linear Unit (ReLU) activation function (represented in green in Fig. 5), which is arguably the most popular choice when it comes to the design of deep neural networks. This activation function is simply defined as

$$\text{ReLU}(x) = \max(0, x). \quad (30)$$

Its derivative has the appealing property of staying constant to 1 whenever a unit is activated as defined by:

$$\frac{d}{dx} \text{ReLU}(x) = \begin{cases} 0 & \text{if } x \leq 0 \\ 1 & \text{otherwise} \end{cases} \quad (31)$$

A potential drawback of ReLU is that whenever its input is negative gradient based methods could not be used for learning, as the unit will have a value of 0. To overcome this several activation functions that generalize the ReLU to negative inputs have been proposed within the literature [33, 67, 110], among which we mention the Elu [33] that is visually represented in red in the last plot of Fig. 5.

1.4 CONVOLUTIONAL NEURAL NETWORKS

Convolutional Neural Networks (CNNs) are a family of artificial neural networks that are particularly well suited for problems involving high-dimensional inputs such as images or videos. This kind of data in fact prohibits the use of the multi-layer perceptrons presented in Sec. 1.3.1, as it requires to represent images as unstructured vectors, which is a process that for obvious computational reasons is not feasible. Furthermore MLPs present some additional limitations: first and foremost, due to their fully connected structure, they do not involve any sort of parameter sharing across the network. Second, as the output of each unit in a layer is given as input to all the units in the subsequent layer, the interaction among all such neurons is also extremely dense. CNNs address these limitations by exploiting **sparse weight sharing** strategies that result into neural networks that are significantly more memory and computationally efficient.

1.4.1 Mathematical Operations

As their name suggests, the key mathematical operation behind CNNs is that of **convolution**. A convolution operation is performed over two arguments: an input vector $\mathbf{x} \in \mathbb{R}^W$, and a kernel $\mathbf{u} \in \mathbb{R}^w$. Its output is a new vector of size $W - w + 1$ such that:

$$(\mathbf{x} * \mathbf{u}[i]) = \sum_{m=0}^{w-1} x_{m+i} u_m, \quad (32)$$

where $*$ technically denotes the cross-correlation operation, namely a convolution operation that does not flip the kernel. The process described in Eq. 32 can easily be generalized to multi-dimensional tensors such as images which can in fact be seen as three-dimensional tensors $\mathbf{x} \in \mathbb{R}^{C,W,H}$, of width and height W and H respectively, defined over the RGB color domain ($C = 3$). Similarly one can also define a three-dimensional kernel $\mathbf{u} \in \mathbb{R}^{C,w,h}$ whose purpose is to

slide over the input tensor \mathbf{x} and which yields a two-dimensional output tensor \mathbf{o} of size $(H - h + 1) \times (W - 1 + 1)$ that is computed as follows:

$$\begin{aligned}\mathbf{o}_{i,j} &= \mathbf{b}_{i,j} + \sum_{c=0}^{C-1} (\mathbf{x}_c \circledast \mathbf{u}_c)[j, i] \\ &= \mathbf{b}_{i,j} + \sum_{c=0}^{C-1} \sum_{n=0}^{h-1} \sum_{m=0}^{w-1} \mathbf{x}_{c,n+j,m+i} \mathbf{u}_{c,n,m},\end{aligned}\tag{33}$$

where \mathbf{b} and \mathbf{u} are learnable parameters. Within the deep learning literature, \mathbf{o} is also referred to as a [feature map](#) [59].

Note that by adopting a convolution approach, one input unit in the network only affects as many output units as defined by the size of the kernel, which improves the computational efficiency of the network greatly. Furthermore, each member of the kernel is used across the entire image, which means that the parameters that define a convolution operation are shared alongside the different locations that are visited by \mathbf{u} . The way the kernel interacts with its respective tensor is usually defined by two additional components that both play an important role in the design of convolutional networks. The first of these components is [padding](#) which is a technique that adds some extra values around the perimeter of the input tensor \mathbf{x} , with the aim of preserving the information that is depicted around its corners. Second, there is the concept of [strides](#) which defines by how many elements at a time we wish to slide \mathbf{u} over \mathbf{x} . As the goal of CNNs is that of downsampling the input tensor in a computationally efficient manner, it is usually good practice to have strides larger than one, albeit this comes at the cost of extracting features less thoroughly.

Convolutional networks typically perform several convolutions in parallel, as multiple kernels are used. The output of each convolution is then passed through a non linear activation function such as the ones that we represented in Fig. 5. To downsample the resulting feature maps even further, a [pooling](#) function is usually adopted. Its idea is to summarize the output of the convolving process at a certain location of the feature map through a summary statistic. This reduces its size while at the same time preserves the presence of the detected features. There are two common pooling operations one can choose from: max-pooling [234], which given a three dimensional tensor $\mathbf{x} \in \mathbb{R}^{C \times (rh) \times (sw)}$ produces a tensor $\mathbf{o} \in \mathbb{R}^{C \times r \times s}$ by simply keeping the maximum value of a feature map within a certain rectangular neighborhood such that

$$\mathbf{o}_{c,j,i} = \max_{n < h, m < w} \mathbf{x}_{c,rj+n,si+m},\tag{34}$$

and average pooling, which instead computes the mean of a feature map such that

$$\mathbf{o}_{c,j,i} = \frac{1}{hw} \sum_{n=0}^{h-1} \sum_{m=0}^{w-1} \mathbf{x}_{c,rj+n,si+m}.\tag{35}$$

Besides reducing the size of a feature map, pooling operations have also the important benefit of making the representations learned by the network invariant to small translations. In fact, one could translate the input by a small amount and still obtain the same output after pooling. Note however, that albeit desirable in most cases, there are situations where adopting pooling strategies should be avoided [19, 160].

1.4.2 *Popular Architectures*

Mention general structure here

1.5 CONCLUSION

2

REINFORCEMENT LEARNING AND DEEP NEURAL NETWORKS

OUTLINE

This chapter introduces the research field of Reinforcement Learning (RL) and presents how its algorithms can successfully be combined with neural networks. The successful marriage between RL and deep neural networks comes with the name of Deep Reinforcement Learning (DRL) and has gained tremendous attention from the machine learning community. Despite its recently gained popularity, however, we will also see that many of the concepts underlying today's most popular DRL breakthroughs date back to a time when training neural networks was not the common practice it is nowadays. We start by providing a general introduction to the field of RL in Sec. 2.1 where we describe the main objectives of this machine learning paradigm and see how it differs from the supervised learning setting that we have described in the previous chapter. We then present the mathematical framework that underpins the development of RL algorithms in Sec. 2.2, 2.3 and 2.4. In Sec. 2.5 and Sec. 2.6 we describe how one can create RL algorithms and why it is desirable to integrate the resulting algorithms with neural networks. In Sec. 2.7 we describe the field of DRL and introduce some of the most popular techniques that have been proposed over the years. This chapter ends with Sec. 2.8 where we discuss a few of the main challenges that currently characterize DRL and that have served as inspiration for the research that will be presented in Chapters 7, 8 and 9 of this dissertation.

2.1 INTRODUCTION

In the previous chapter, we have described Supervised Learning (SL), a machine learning framework that aims at constructing models which can answer statistical questions about data coming in the form of input-output pairs. When these models are built successfully, it is possible to use them to make predictions about the behavior of new unseen data. Training SL models is a process which from some perspective is very static. Datasets are divided into training, validation, and testing sets, and besides providing a model with a large set of samples drawn from these datasets, there is no real interaction between the learning algorithm and the data that drives the learning process. In Reinforcement Learning (RL), this drastically changes. The

goal is not anymore to learn a mapping between a set of fixed input samples and their respective targets, but to train an algorithm that learns how to interact with an environment. RL is, therefore, a much more dynamic learning paradigm, where the concept of time is omnipresent and is critical for the development of algorithms that not only need to solve a specific problem but additionally also have to be able to adapt themselves while training progresses. What makes RL so challenging is that these algorithms have to learn how to interact with the environment without any form of supervision and therefore can not rely on e.g., examples of successful interactions.

In RL, a learning algorithm is usually denoted as the [agent](#), and it can come in numerous forms: it can range from being a self-driving car that needs to learn how to drive to a recommendation system whose goal is to propose products to users navigating the web. More generally, we define an RL agent as any system that, given a specific situation, has to choose which action to perform. However, there is one more additional component that makes RL the challenging machine learning setting it is. It is not enough for an agent to just learn how to interact with the environment, it is even more desirable for it to learn an interaction which can be defined ‘intelligent’. Going back to the self-driving car example, an ‘intelligent’ agent would not only be a car that can drive autonomously but a car that is also able to do this while complying with the driving code. Because of this concept of learning how to make (intelligent) decisions while interacting, the problems tackled by RL algorithms are also referred to as optimal decision making problems, which are also the target of research fields other than machine learning as, control theory. Interestingly both worlds try to solve the same set of problems, one by tackling them through algorithms that are denoted as ‘intelligent’, while the other through the development of algorithms that are ‘optimal.’ Throughout this dissertation, we will not make a clear distinction between these two worlds and will assume that algorithms resulting in intelligent behaviors will correspond to behaviors that are also optimal. Nevertheless, we encourage the reader that has finished reading this chapter to assess whether acting optimally necessarily coincides with acting intelligently.

2.2 MARKOV DECISION PROCESSES

Before starting to develop RL algorithms for sequential decision making problems, we need to formulate the problem within a specific mathematical framework: in RL this framework is that of Markov Decision Processes (MDPs) [143, 144]. Throughout this dissertation, we will characterize MDPs, and the resulting RL concepts, by using the mathematical notation that was used by Sutton and Barto [188] in their seminal book about RL, although it is worth noting that within

in the literature, different formulations can be found for expressing the same kind of concepts [16–18, 25].

We start by introducing the following elements:

- A set of possible states \mathcal{S} , that can be visited by an agent while it is interacting with the MDP, where $s_t \in \mathcal{S}$ denotes the state being visited at time-step t .
- A set of possible actions \mathcal{A} that are available to the agent when it is in a certain state, where $a_t \in \mathcal{A}(s_t)$ denotes the action that is performed by the agent in state s at time-step t .
- A transition function $\mathcal{P} : \mathcal{S} \times \mathcal{A} \times \mathcal{S} \Rightarrow [0, 1]$ that defines the probability for an agent to visit state s_{t+1} , based on its current state and the action which will be performed thereafter.
- A reward function $\mathfrak{R} : \mathcal{S} \times \mathcal{A} \times \mathcal{S} \Rightarrow \mathbb{R}$ which returns a reward signal r_{t+1} when an agent performs action a_t in state s_t and transits to s_{t+1} .
- A discount factor denoted as $\gamma \in [0, 1]$.

Based on these concepts a MDP is defined by the following tuple $\langle \mathcal{S}, \mathcal{A}, \mathcal{P}, r, \gamma \rangle$ and is also commonly denoted in the RL literature as the **environment**. The way the agent interacts with this environment is given by its **policy** π , defined as a probability distribution over $a \in \mathcal{A}(s)$ for each $s \in \mathcal{S}$:

$$\pi(a|s) = \Pr \{a_t = a | s_t = s\}, \text{ for all } s \in \mathcal{S} \text{ and } a \in \mathcal{A}. \quad (36)$$

A policy can be deterministic if $\forall s : \pi(s, a) = 1$ for exactly one $a \in \mathcal{A}(s)$ and $\pi(s, b) = 0$ for all other $b \in \mathcal{A}(s)$, while it is stationary if it does not change over time. In both cases we can define it as follows:

Definition 1 *A policy is a mapping from states to actions $\pi : \mathcal{S} \Rightarrow \mathcal{A}$.*

The elements of the MDP allow us to properly model the dynamics of an agent interacting with its environment, an interaction which can be summarized as follows: at each time-step t the environment provides the agent with a certain state s_t , the agent then performs action a_t which results into the reward signal r_{t+1} . After performing such action the agent will enter into a new state s_{t+1} . This continuous interaction with the environment is also known as the Reinforcement Learning loop, and can technically be infinite. However, this is never the case in practice, since an agent will eventually visit a state that only transits to itself (denoted as terminal), which will therefore stop the agent-environment interaction. We visually represent the Reinforcement Learning loop in Fig. 6.

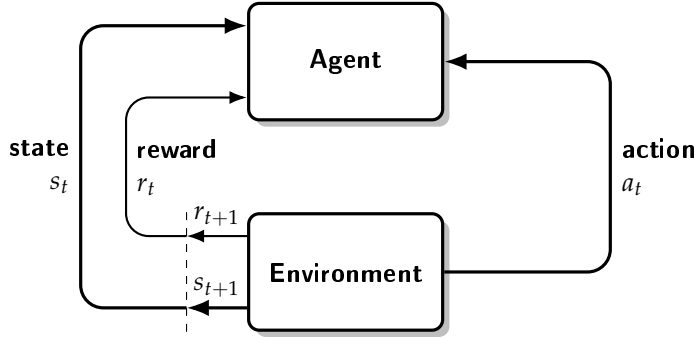


Figure 6: A visual representation of how an agent interacts with an environment as modeled by a Markov decision process. Figure inspired from page 48 of the Sutton and Barto [188] textbook.

Each interaction of the agent with the environment is defined as an **episode**, which consists of one, or several trajectories τ , that come in the form of the following sequence:

$$\langle (s_t, a_t, r_t, s_{t+1}) \rangle, t = 0, \dots, T - 1 \quad (37)$$

where T is a random variable representing the length of the episode.

A key property of the environment is that it fulfills the Markov property which is defined as follows:

Definition 2 *A discrete stochastic process is Markovian if the conditional distribution of the next state of the process only depends from the current state of the process.*

This implies that the only information that is necessary for predicting to which state an agent will step next are s_t and a_t , a concept which can be expressed formally as:

$$p(s_{t+1}|s_t, a_t, s_{t-1}, a_{t-1}, \dots) = p(s_{t+1}|s_t, a_t). \quad (38)$$

Interestingly, the same property also holds for the reward that the agent will get, meaning that the reward that an agent obtains is only determined by its previous action, and not by the history of all previously taken actions, as defined by:

$$(r_t|s_t, a_t, \dots, s_1, a_1) = p(r_t|s_t, a_t). \quad (39)$$

2.3 GOALS AND RETURNS

So far, we have defined all the elements that model an agent's interaction with an environment while introducing some of its fundamental properties. However, we do not yet know what the purpose of this interaction is. In RL, an agent's goal is defined with respect to the reward signal r_t that is returned by the reward function \mathfrak{R} and is very straightforward: maximizing the total amount of reward it receives

while interacting with the environment. In the simplest case, we can define this as:

$$G_t = r_t, r_{t+1}, r_{t+2}, \dots, r_T. \quad (40)$$

While simple and intuitive, this formulation has one major drawback: it treats each reward signal equally since it does not distinguish rewards that are obtained in the near future, r_t , from the ones that will be obtained in the more distant future, r_{T-1} . To deal with this issue, we need an additional concept known as [discounting](#), and that is governed by the discount rate parameter γ , also known as the discount factor. γ allows us to weight the different reward signals based on how close or distant in the future these rewards are received by the agent. By introducing γ in Eq. 40 we can now define the expected discounted return as:

$$G_t = r_t + \gamma r_{t+1} + \gamma^2 r_{t+2} + \dots \quad (41)$$

$$= \sum_{k=0}^{\infty} \gamma^k r_{t+k+1}. \quad (42)$$

The role of γ can be interpreted as follows: a reward obtained k time steps in the future is only worth γ^{k-1} times what it would be worth if received immediately. It is easy to see how different γ values can result in different agent's behaviors. If $\gamma = 0$ an agent will only take into account immediate rewards, therefore aiming to maximize r_{t+1} only and resulting into having a "myopic" behavior. If γ approaches 1 the agent will become more "far-sighted", it will take future rewards into account more strongly and will therefore increase its chances of accessing rewards that will result into a higher cumulative return. Please note that by defining $\gamma \leq 1$, we can make the infinite sum presented in Eq. 42 finite as long as the sequence of rewards r_k is bounded.

While the role of γ is often taken for granted within the RL literature, it is worth noting that as mentioned by Hessel et al. [73] and Schmidhuber [168], γ is an artificial concept that is not present in fields such as traditional control theory or engineering. This is because γ corresponds to a concept that does not exist in the real world and that in practice distorts the actual value of r_t in an exponentially shrinking fashion. Even if it is considered standard practice to include a discount factor in the development of RL algorithms, it is worth noting that making γ part of the RL framework corresponds to including a form of "inductive bias" within the resulting algorithms. It is common knowledge that low discount factors result in poor performance and that it is therefore as beneficial as possible to set γ as close to 1, yet choosing an appropriate γ parameter can be more challenging than expected, especially when RL algorithms are combined with function approximators. Wiering and Van Hasselt [220] show that different algorithms prefer different discount factors,

while François-Lavet, Fonteneau, and Ernst [48] show the benefits of initially starting with a low discount factor which gradually gets increased while training progresses. Finally, Van Seijen, Fatemi, and Tavakoli [207] introduce a method that allows the use of low discount factors for approximate RL algorithms while at the same time highlighting that the common perception of the role of γ might need revision from the RL community.

2.4 VALUE FUNCTIONS

We are now ready to introduce the arguably most important concept underlying many RL algorithms: the concept of **value**. We can define the value of a state s , as well as the value of a specific policy π or of a particular action a , anyhow, independently from what we are considering, the notion of value is always directly linked to the concept of expected discounted return defined in Eq. 42. Given an MDP and a policy π , we can determine the value of a state s as a function that measures the expected return that the agent will receive when starting in s and following π thereafter.

$$V^\pi(s) = \mathbb{E} \left[\sum_{k=0}^{\infty} \gamma^k r_{t+k} \middle| s_t = s, \pi \right]. \quad (43)$$

$V^\pi(s)$ is also known as the state-value function and intuitively tells us how good or how bad it is for an agent to be in a certain state. While this function is only conditioned on the state that is being visited by the agent, we can also condition it on the actions that the agent takes. By doing so we will quantify how good or bad it is for the agent to take a certain action a in a certain state. This function comes with the name of state-action value function and is defined as follows:

$$Q^\pi(s, a) = \mathbb{E} \left[\sum_{k=0}^{\infty} \gamma^k r_{t+k} \middle| s_t = s, a_t = a, \pi \right]. \quad (44)$$

Both value functions are very powerful since they allow us to characterize an agent's behavior by quantitatively assessing its interaction with the environment. They can be seen as the agent's knowledge and represent its desirability of being in a specific state. As we will see in the coming sections, accurately modeling these value functions is one of RL's major goals.

A key property of $V^\pi(s)$ and $Q^\pi(s, a)$ is that both value functions satisfy a consistency condition that allows us to define both functions

recursively. For example let us consider the state-value function $V^\pi(s)$ presented in Eq. 43, we can rewrite it as:

$$\begin{aligned}
 V^\pi(s) &= \mathbb{E} \left[\sum_{k=0}^{\infty} \gamma^k r_{t+k} \mid s_t = s, \pi \right] \\
 &= \mathbb{E} [r_{t+1} + \gamma r_{t+2} + \gamma^2 r_{t+3} + \dots \mid s_t = s, \pi] \\
 &= \mathbb{E} [r_{t+1} + \gamma(r_{t+2} + \gamma r_{t+3} + \dots) \mid s_t = s, \pi] \\
 &= \mathbb{E} [r_{t+1} + \gamma V^\pi(s_{t+1}) \mid s_t = s, \pi] \\
 &= \sum_a \pi(s, a) \sum_{s+1} p(s_{t+1} \mid s, a) [\mathfrak{R}(s_t, a, s_{t+1}) + \gamma V^\pi(s_{t+1})].
 \end{aligned} \tag{45}$$

Similar steps can be followed when considering $Q^\pi(s, a)$ which can then be recursively defined as:

$$Q^\pi(s, a) = \sum_{s_{t+1}} p(s_{t+1} \mid s, a) (\mathfrak{R}(s_t, a, s_{t+1}) + \gamma \sum_{a_{t+1}} \pi(s_{t+1}, a_{t+1}) Q^\pi(s_{t+1}, a_{t+1})). \tag{46}$$

When it comes to sequential decision making, we are interested in maximizing each state's value or each state-action pair, since by doing so, we will be finding a policy π that is optimal. The **optimal policy** π^* is a policy that realizes the optimal expected return defined as:

$$V^*(s) = \max_{\pi} V^\pi(s), \text{ for all } s \in \mathcal{S} \tag{47}$$

and the optimal Q value function:

$$Q^*(s, a) = \max_{\pi} Q^\pi(s, a) \text{ for all } s \in \mathcal{S} \text{ and } a \in \mathcal{A}. \tag{48}$$

When we recursively define both optimal value functions as we did for Eq. 43 we obtain:

$$V^*(s_t) = \max_a \sum_{s_{t+1}} p(s_{t+1} \mid s_t, a) \left[\mathfrak{R}(s_t, a, s_{t+1}) + \gamma V^*(s_{t+1}) \right] \tag{49}$$

for the optimal state-value function, and

$$Q^*(s_t, a_t) = \sum_{s_{t+1}} p(s_{t+1} \mid s_t, a_t) \left[\mathfrak{R}(s_t, a_t, s_{t+1}) + \gamma \max_a Q^*(s_{t+1}, a) \right], \tag{50}$$

for the optimal state-action value function. Both value functions are well known to correspond to the Bellman **optimality** equations [14].

If the optimal Q function is learned it becomes a straightforward task to derive an optimal policy since one only needs to select the action which has the highest value in each state as defined by:

$$\pi^*(s) = \arg \max_{a \in \mathcal{A}} Q^*(s, a) \text{ for all } s \in \mathcal{S}. \tag{51}$$

It is also worth noting that the Q function and the V function satisfy the following equality

$$V^*(s) = \max_{a \in \mathcal{A}} Q^*(s, a) \text{ for all } s \in \mathcal{S} \quad (52)$$

which comes from the fact $V^*(s) \leq \max_{a \in \mathcal{A}} Q^*(s, a)$ for all $s \in \mathcal{S}$. As we will later see throughout this thesis this equality is particularly important for the development of many RL algorithms.

2.5 LEARNING VALUE FUNCTIONS

The V function and the Q function play a crucial role in the development of optimal decision making algorithms, and over the years, several methods have been introduced to learn them. While all these algorithms' ultimate goal is to yield an optimal policy, there exist cases for which learning these value functions is easier than others. The complexity of learning a value function depends on how many MDP components are known to the agent. If the agent has access to all five of the components of the MDP that we introduced in Sec. 2.2, these algorithms are part of a collection of methods that comes with the name of [Dynamic Programming](#) (DP). DP algorithms such as *value-iteration*, *policy-iteration* and variants [15, 215] learn an optimal value function, or optimal policy, by exploiting the fact that the transition function \mathcal{P} , and the reward function \mathfrak{R} of the MDP are known. While DP methods can be considered as the progenitors of many RL algorithms, we will not discuss them here since throughout this thesis, we will be interested in scenarios for which \mathcal{P} and \mathfrak{R} are unknown. Specifically, we will introduce novel methods that aim to learn an optimal value function without requiring to learn an approximation of the transition and reward functions ($\hat{\mathcal{P}}$ and $\hat{\mathfrak{R}}$) neither, therefore placing all contributions of this dissertation within the [model-free](#) RL literature.

2.5.1 Monte Carlo Methods

The first family of methods that can learn optimal value functions when no complete knowledge of the environment is available comes with the name of Monte Carlo (MC) methods. MC algorithms only require RL trajectories to discover an optimal policy and achieve this by sampling and averaging the rewards obtained while the agent is interacting with the environment. While MC methods can be used both for learning $V^*(s)$ and for learning $Q^*(s, a)$, in this section, we only present how one can learn the state-value function. MC algorithms' key idea relies on computing the actual sum of discounted rewards that an agent obtains once an episode finishes. This corresponds to computing the quantity defined in Eq. 40. Once this value

is computed, it can be used for updating the current value of each state with the following update rule:

$$V(s_t) := V(s_t) + \alpha [G_t - V(s_t)] \quad (53)$$

where $\alpha \in [0, 1]$ is the learning rate controlling how much we want to change the value estimate of a state based on G_t . As a practical example let us consider the MDP represented in Fig. 7. Let us assume that the starting state of the environment is s_0 while the terminal state of the environment is s_2 , and that the agent follows a policy π that results into the following state visits: s_1, s_0, s_2 . The rewards associated to each visited state are therefore $-1, +2$ and $+3$ respectively. If we set the discount factor to 0.99 we know that the real discounted return that is obtained at the end of the agent-environment interaction when starting in state s_0 is $\sum_{k=0}^{\infty} \gamma^k r_{t+k+1} = -1 + \gamma 2 + \gamma^2 3 \approx 3.92$. If we now assume that the value of s_0 has never been updated before and that is therefore 0, and that we set $\alpha = 0.5$, the result of one MC update for s_0 will be ≈ 1.96 .

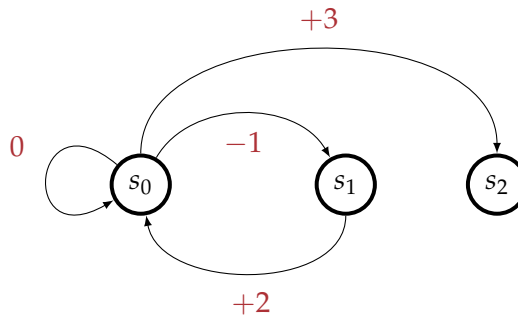


Figure 7: A visual representation of a simple MDP. For each state transition the corresponding reward is presented in red.

When dealing with MC learning, it can be possible that a certain state is visited more than once before a terminal state is reached. In the MDP represented in Fig. 7 this is the case for s_0 . If that happens, one must decide when to update $V(s)$ and which value to use as G_t , since different state visits result in different G_t values. There are two typical ways to deal with this: either update $V(s)$ only once, or one can update $V(s)$ each time the state is visited by simply using as G_t the average of all the different discounted returns. The first update strategy comes with the name of , while the latter is denoted as . While several successful applications of MC methods exist [79, 96, 107], a well known issue from this family of algorithms is that they suffer from highly biased updates. In fact, one needs to compute the sum presented in Eq. 40 over all visited states, resulting in returns with considerable variance. It is easy to see how this can become an issue, especially when the length of the episodes increases since the larger the episode's length, the more significant the variance of the

updates. Furthermore, an additional drawback of MC methods is that one must wait until the agent visits a terminal state before being able to perform an update that is based on Eq. 53, the latter drawback can result in slow learning and is addressed by the methods presented hereafter.

2.5.2 Temporal Difference Learning

Temporal Difference (TD) Learning [186, 190] is a learning paradigm that allows overcoming the issues mentioned above that characterize MC learning based methods. The key idea of TD-Learning is to update the value of each state with respect to a single MC update, therefore overcoming the hurdle of having to wait for the end of an episode before being able to update the value of a state. Just as MC methods TD-Learning algorithms also learn an optimal value function based on the experience that the agent collects. However, these algorithms base their updates only on the value of a single, consecutive state rather than on the real discounted return that is dependent on the entire sequence of visited states. Updating the value of a state with respect to the value of its successor state only is a technique that comes with the name of **bootstrapping**, and is a very effective design choice that reduces the variance in the updates. Bootstrapping can be used to learn the V function and the Q function and is at the core of the most popular model-free RL algorithms. The first and simplest form of TD-Learning was introduced by Sutton [186] for learning the state-value function with an algorithm that updates the value of a state based on the following learning rule:

$$V(s_t) := V(s_t) + \alpha [r_t + \gamma V(s_{t+1}) - V(s_t)]. \quad (54)$$

We can now clearly see that differently from what happens in the MC update presented in Eq. 53 the update of a state now only depends on the reward and the value of the next state. This quantity is denoted as the TD-error δ_t and is defined as:

$$\delta_t = r_t + \gamma V(s_{t+1}) - V(s_t). \quad (55)$$

where $r_t + \gamma V(s_{t+1})$ is also known as the TD-target. If we again consider the simple MDP represented in Fig. 7 and assume that the value of each state of the process is set to 0 while the discount factor γ is again set to 0.5, a TD update for $V(s_0)$ based on action a_3 will result into the new value estimate of 1.5. TD-Learning is a very effective strategy for building algorithms that can learn in an online, fully incremental fashion since one only needs to wait for a single time-step before updating the considered value function. Due to its striking simplicity, TD-Learning has been widely adopted by RL practitioners developing algorithms for learning the Q function. We will present some of the most important algorithms hereafter.

Q-LEARNING: introduced by Watkins and Dayan [214] is arguably the most popular model-free RL algorithm. It works by keeping track of an estimate of the state-action value function $Q : \mathcal{S} \times \mathcal{A} \rightarrow \mathbb{R}$ and updates each visited state-action pair with the following update rule:

$$Q(s_t, a_t) := Q(s_t, a_t) + \alpha [r_t + \gamma \max_{a \in \mathcal{A}} Q(s_{t+1}, a) - Q(s_t, a_t)]. \quad (56)$$

The key component of Q-Learning's update rule is the max operator, which characterizes its TD-error and that is necessary for constructing the TD-target. Since there are as many Q values as there are actions available to the agent, one must choose which Q value to use as a reference when updating the value of the state-action pair that the agent is currently visiting. The max operator simply chooses the state-action pair with the largest Q value, a simple design choice that has the appealing property of making Q-Learning converge to $Q^*(s, a)$ with probability 1 as long as all state-action pairs are visited infinitely often. Interestingly this guarantee holds even if the agent follows a random policy. The max operator also defines Q-Learning as an **off-policy** learning algorithm, since the Q values chosen for the construction of the TD-target might not correspond to the ones that are associated with the state that the agent will visit after having updated its Q function.

SARSA: also known as 'online Q-Learning' [154] can be seen as the most straightforward extension of the TD-Learning method presented in Eq. 54, and similarly to Q-Learning is an algorithm that aims at learning the state-action value function Q . The key idea of SARSA is to update a state-action value with respect to the Q value that is associated to the state that the agent will visit after a certain action is performed. Therefore, SARSA does not use the max operator within its TD-error and constructs TD-targets that represent the policy that the agent is following, a characteristic that defines SARSA as an **on-policy** RL algorithm. The way SARSA learns the Q function is given by the following update rule

$$Q(s_t, a_t) := Q(s_t, a_t) + \alpha [r_t + \gamma Q(s_{t+1}, a_{t+1}) - Q(s_t, a_t)], \quad (57)$$

where we can clearly see how the algorithm uses all the elements of the quintuple of events $(s_t, a_t, r_t, s_{t+1}, a_{t+1})$ a property that gives rise to the name *sarsa*. Not using the max operator in Eq. 57 results in an algorithm that, differently from Q-Learning, does not directly learn the optimal Q function anymore, but rather learns to estimate $Q^\pi(s, a)$. This has the drawback of not guaranteeing convergence to $Q^*(s, a)$ for any random policy anymore. To overcome this, SARSA needs an exploration policy that is greedy in the limit of infinite ex-

ploration [180]. This can be achieved with the popular ϵ – greedy selection policy which defines the action that the agent takes as:

$$a_t = \begin{cases} \arg \max_{a \in \mathcal{A}} Q(s_t, a) & \text{with probability } 1 - \epsilon \\ a \sim \mathcal{U}(\mathcal{A}) & \text{with probability } \epsilon \end{cases} \quad (58)$$

where ϵ is a hyperparameter that changes while training progresses. During early training iterations, its value is close to 1, while it approaches 0 by the end of training. This allows the agent to take actions that are representative of a large set of policies when the learned Q function does not yet correspond to $Q^*(s, a)$, while it will favor greedy actions at the end of training. This is a simple yet effective strategy to deal with the **exploration-exploitation** dilemma, and it is worth noting that its use is not limited to on-policy RL algorithms only. Furthermore, the method presented in Eq. 58 represents only one possible way of balancing exploration and exploitation, and although it is arguably the most popular of such methods, it is not the only existing one. We refer the reader to chapter 5 of [217] for a thorough analysis of different exploration algorithms.

DOUBLE Q-LEARNING: in some environments, Q-Learning is known to perform poorly. This poor performance stems from the fact that the algorithm largely overestimates some state-action values due to the max operator in its TD-error [196]. The max operator serves for constructing an approximation of the maximum expected action-value of a state, which, as discussed by Van Hasselt [204], is a technique that results in positively biased estimates [181, 183]. In some RL problems, this can significantly influence the learning procedure, which has led the RL community to develop a set of solutions that try to mitigate this bias [99, 100, 139, 235]. Among the different solutions, Double Q-Learning [204] is probably the most popular one. Its main idea is to keep track of two different state-action value functions, Q_1 and Q_2 , which get alternatively used for selecting which action to perform. When one of the two Q functions determines the action that maximizes the state-action value of the next state, the remaining value function is used for evaluating this estimate. This can be achieved with the following rule:

$$Q_1(s_t, a_t) := Q_1(s_t, a_t) + \alpha [r_t + \gamma Q_2(s_{t+1}, a^*) - Q_1(s_t, a_t)], \quad (59)$$

where $a^* = \arg \max_{a \in \mathcal{A}} (Q_1(s_{t+1}))$. Note that at each time step, only one of the two Q functions gets updated. While training progresses, the choice of which Q function to update is determined randomly. In the case it is Q_2 , the update rule is identical to the one presented in Eq. 59 with the only difference being that the role of the two Q functions is swapped. Double Q-Learning converges to the optimal state-action value function with probability 1 under the same conditions as

Q-Learning. Van Hasselt [204] shows that using two separate Q functions significantly mitigates the overestimation bias, yet this comes at the price of an algorithm that is twice more expensive in terms of memory requirements. It is also worth noting that although Double Q-Learning does not overestimate the state-action values, it might underestimate them, which in some environments can still yield poor performance.

QV(λ)-LEARNING: first introduced by Wiering [219] and further developed by Wiering and Van Hasselt [220] is an on-policy RL algorithm which differently from the previously introduced methods keeps track of an estimate of the state-value function $V : \mathcal{S} \rightarrow \mathbb{R}$ alongside the usual estimate of the state-action value function $Q : \mathcal{S} \times \mathcal{A} \rightarrow \mathbb{R}$. Since the goal is to jointly learn two value functions, QV(λ)-Learning requires two separate update rules. The V function is learned via the same form of TD-Learning that we introduced in Eq. 54, with the only difference being the addition of the eligibility traces $e_t(s)$ at the end of the update rule (an RL technique that we will not discuss in this dissertation). QV(λ)-Learning, therefore, learns the V function with the following update rule:

$$V(s) := V(s) + \alpha[r_t + \gamma V(s_{t+1}) - V(s_t)]e_t(s). \quad (60)$$

Since as discussed earlier only learning the V function is not sufficient for deriving an optimal policy one needs to learn the Q function as well. In QV(λ)-Learning this is done as follows:

$$Q(s_t, a_t) := Q(s_t, a_t) + \alpha[r_t + \gamma V(s_{t+1}) - Q(s_t, a_t)]. \quad (61)$$

An attractive property of the algorithm is that it uses the same TD-target ($r_t + \gamma V(s_{t+1})$) for defining the two different TD-errors that are required for learning the state-value and the state-action value functions. Among the main insights that motivate learning two value functions over one Wiering [219] mentions the possibility that the V function, since it does not depend on the agent's actions might converge faster than the Q function. As described earlier, the V function only depends on the state space of the MDP, which by definition is smaller than the state-action space. For a more in-depth and formal presentation of the conditions that show the benefits of jointly learning the V function alongside the Q function, we refer the reader to chapter 5 of [64].

2.6 FUNCTION APPROXIMATORS

If it is true that model-free RL algorithms are very powerful methods for learning an optimal policy when parts of the MDP are unknown, it is also true that all the algorithms mentioned above suffer from the **curse of dimensionality**. Model-free algorithms are typically

implemented in a tabular fashion, meaning that the state values, or state-action values, are stored within a table of sizes $|\mathcal{S}|$ and $|\mathcal{S} \times \mathcal{A}|$ respectively. Albeit straightforward and easy to implement, such an approach presents severe limitations. The first major drawback of the tabular representation approach is that it does not scale well with respect to the MDP complexity. If the environment's state and action spaces become very large, storing a table quickly becomes unfeasible in terms of storage space. Furthermore, tabular representations are also unable to deal with continuous states. A natural solution to this problem could consist of discretizing the state space; however, this approach still results in the aforementioned storage space issues when done thoroughly. Therefore, if one wants to use RL techniques, even when the state space of the MDP is large, a better solution is needed. This solution is based on [parametrized function approximation](#). In this context, the goal is not to learn the exact value function anymore but to rather replace its tabular representation with a parameterized function. This function's parameters can then be adjusted based on the RL algorithms that we introduced in Sec. [2.5.2](#).

2.6.1 Linear Functions

The most straightforward type of function approximator one can use is a linear function. Given a state-action tuple that gets represented as a feature vector $\mathbf{x} = [f_1(s, a), f_2(s, a), \dots, f_i(s, a)] \in \mathbb{R}^2$, and a function parametrized by a vector of parameters θ , as shown in [\[218\]](#) we can redefine the value of a state-action pair as:

$$Q(s, a) = \sum_i \theta_{i,a} \mathbf{x}_i(s). \quad (62)$$

Given a trajectory $\langle s_t, a_t, r_t, s_{t+1} \rangle$ the Q-Learning algorithm presented in Eq. [93](#) can now be used for updating the parameters θ for all i with the following update rule:

$$\theta_{i,a_t} := \theta_{i,a_t} + \alpha(r_t + \gamma \max_{a \in \mathcal{A}} Q(s_{t+1}, a) - Q(s_t, a_t)) \mathbf{x}_i(s_t). \quad (63)$$

We can observe that this update rule is equivalent to updating the parameter vector θ for minimizing the mean squared error loss between a given state-action tuple and Q-Learning's TD-target since

$$\mathcal{L}(\theta) = \frac{1}{2} (y_t - Q(s_t, a_t))^2 \quad (64)$$

$$\frac{\partial \mathcal{L}}{\partial \theta_{i,a_t}} = -(y_t - Q(s_t, a_t)) \mathbf{x}_i(s_t) \quad (65)$$

$$\theta_{i,a_t} := \theta_{i,a_t} + \alpha(r_t + \gamma \max_{a \in \mathcal{A}} Q(s_{t+1}, a) - Q(s_t, a_t)) \mathbf{x}_i(s_t). \quad (66)$$

Similar steps can be used for adapting all of the RL algorithms that we introduced in the previous section. As a representative example

for the on-policy learning case let us consider the SARSA algorithm. One can learn an approximation of the Q function by updating the parameters of a linear function as follows:

$$\theta_{i,a_t} := \theta_{i,a_t} + \alpha(r_t + \gamma Q(s_{t+1}, a_{t+1}) - Q(s_t, a_t))\mathbf{x}_i(s_t). \quad (67)$$

Among the different linear functions one can use there are CMACs [92], radial basis functions (RBFs) [134], linear neural networks [113] and linear support vector machines (SVMs). Although these techniques can successfully deal with the aforementioned curse of dimensionality problem, **non-linear** functions are usually preferred since their representational power is much larger than the one of linear methods. Throughout this dissertation, we are interested in non-linear functions that come in the form of deep neural networks. As we have seen in the previous chapter, neural networks such as e.g convolutional networks are able to learn very rich representations from their inputs. However, this also makes these kinds of models particularly challenging to train in an RL context. We will now describe how one can successfully deal with some of the challenges that characterize the use of deep neural networks in RL by presenting some of the most important algorithms that have been introduced over the years.

2.7 DEEP REINFORCEMENT LEARNING

Before looking into how RL algorithms should be integrated within deep neural networks, it is important to mention that RL techniques have been successfully used combined with (less powerful) neural networks for over three decades. In fact, the field known as **Connectionist Reinforcement Learning** (CRL) resulted in the very first algorithms that managed to outperform human experts on specific tasks. Among the multiple possible examples of this family of techniques, we mention the TD-Gammon program introduced by Tesauro [195]. TD-Gammon successfully learns an approximation of the popular Backgammon boardgame's evaluation function through the same TD-Learning methods that we presented in Sec. 2.5.2. Tesauro's program achieved a level of play that comparable to the one of the top human Backgammon players of its time and is even nowadays considered one of the most important RL breakthroughs. For a more detailed presentation about the successful applications of CRL algorithms, we refer the reader to [26].

While certainly successful for a certain set of problems (see for example chapter 1 of [156]), CRL techniques also present severe limitations. Since they only use multi-layer perceptrons as function approximators, these algorithms cannot be used for tackling problems where the state representation of the MDP is highly dimensional. To overcome this, more complicated and powerful networks are required.

Deep Reinforcement Learning (DRL) [7, 49, 102] is a research field that combines RL algorithms with deeper and more complex neural architectures. In value based model-free DRL we are interested in learning an approximation of an optimal value function with a deep neural network that comes with parameters θ

$$V(s; \theta) \approx V^*(s) \quad (68)$$

$$Q(s, a; \theta) \approx Q^*(s, a) \quad (69)$$

and that usually comes in the form of a convolutional neural network. We now describe some of the algorithms which have contributed to the development of DRL the most.

DEEP Q-LEARNING (DQN): just like Q-Learning is arguably the most important tabular model-free RL algorithm, so is DQN when it comes to DRL. First introduced by Mnih et al. [119] and then made popular by the work presented in [120] this algorithm can certainly be considered as the very first successful example of a neural network that is able to learn an approximation of the optimal state-action value function just from high sensory inputs (in this case images). As the name suggests, Deep Q-Learning (DQN)¹ is based upon the Q-Learning algorithm and aims at learning an approximation of the optimal state-action value function Q . This is done by reshaping Q-Learning's update rule, presented in Eq. 92, into a differentiable loss function that can be used for training a convolutional network with the following objective function:

$$\mathcal{L}(\theta) = \mathbb{E}_{(s_t, a_t, r_t, s_{t+1}) \sim U(D)} \left[(r_t + \gamma \max_{a \in \mathcal{A}} Q(s_{t+1}, a; \theta^-) - Q(s_t, a_t; \theta))^2 \right]. \quad (70)$$

We can start by observing that the general principles that characterize the algorithm are the same ones that made it possible to generalize Q-Learning to the use of linear function approximators, although it is worth noting that differently from when a linear function is used, the mapping between input and feature spaces is now not preserved anymore. Similarly to what we presented in Sec. 2.6.1, we can see from Eq. 93 that learning $Q(s, a, \theta)$ is again achieved by minimizing the squared error loss between the $Q(s_t, a_t; \theta)$ estimates and the off-policy TD-target

$$y_t^{DQN} = r_t + \gamma \max_{a \in \mathcal{A}} Q(s_{t+1}, a; \theta^-). \quad (71)$$

¹ In DQN the 'N' in the acronym stays for 'Network' and replaces the, arguably more intuitive, 'L' of Learning.

Despite this similarity, DQN requires some additional algorithmic design choices, without which it would result impossible to successfully train a neural network with Eq. 93. These additions, which significantly make DQN differ from the algorithm presented in Eq. 63 are the following:

- **Experience Replay:** a memory buffer, D , represented as a queue which stores RL trajectories of the form $\langle s_t, a_t, r_t, s_{t+1} \rangle$. Once this memory buffer is filled with a large set of these quadruples, DQN uniformly samples batches of trajectories for training its network. This makes it possible to exploit past trajectories multiple times by reusing them while training, which makes the overall algorithm more sample efficient. Furthermore, using a memory buffer also improves the stability of the training procedure. Recall that each trajectory is representative of a certain episode. By repeatedly randomly sampling a different τ from the memory buffer, a resulting mini-batch of trajectories will be representative of different episodes and of different policies. As a consequence, the correlation between trajectories within a mini-batch will be small. Although made popular by the DQN algorithm, using an experience replay buffer for tackling sequential decision making problems was already presented by Lin [105].
- **Target Network:** We can observe from Eq. 94 that the TD-target used by DQN for bootstrapping is not computed by the Q network that is being optimized (θ), but rather from a second separate network that is parameterized with θ^- . This second network has the same structure as the main Q network, but its weights do not change each time RL experiences are sampled from D . On the contrary, its weights are temporally frozen and only periodically get updated with the parameters of the main network θ as defined by an appropriate hyperparameter. Note that this is a design choice that is not motivated by the TD-Learning paradigm that we presented in Sec. 2.5.2, where we have seen that TD-Learning based methods learn in a fully online fashion by updating their value estimates based on their own future estimates. With a target-network, although the θ network still learns via the methods of temporal differences, it now requires an auxiliary, external model if it wants to successfully learn $\approx Q^*(s, a; \theta)$. Several works have studied the target network's role to understand why this design choice appears to be necessary for DRL, yet the DRL community does not fully understand the role of θ^- . For more about this topic, we refer the reader to .

With all these concepts in place we can show that given a training iteration i , differentiating this objective function with respect to θ gives the following gradient:

$$\nabla_{\theta_i} y_t^{DQN}(\theta_i) = \mathbb{E}_{(s_t, a_t, r_t, s_{t+1}) \sim U(D)} \left[(r_t + \gamma \max_{a \in \mathcal{A}} Q(s_{t+1}, a; \theta_{i-1}^-) - Q(s_t, a_t; \theta_i)) \nabla_{\theta_i} Q(s_t, a_t; \theta_i) \right]. \quad (72)$$

The DQN algorithm showcased its entire potential in [120] where Mnih and colleagues developed a convolutional neural network that trained with Eq. 93 learned how to successfully play most of the Atari games that are part of the popular Atari Arcade Learning Environment (ALE) [13], a well-known platform that even nowadays serves as a benchmark when for testing the performance of DRL algorithms. In the ALE, a DRL algorithm has to learn how to play 57 different emulations of Atari games which are specifically designed within a simulator (see Fig. 8 for a visualization of some of the games that are part of the ALE suite). Remarkably, DQN learned not only learned how to play most of the games of the platform but also achieved a final performance that, on most games, was superior to the one of human expert players. What is even more remarkable is that this was achieved by providing as inputs to the network the images representing the game only, therefore making the model learn just from its own experience in a pure model-free RL fashion. Since then, DQN has been successfully used for a large variety of applications ranging from healthcare [147, 200], robotics [83] and natural language processing [65, 126] to even particle physics [108, 164]. However, despite all these remarkable applications, the algorithm still comes with some drawbacks, some of which are addressed by the algorithms presented below.

DOUBLE DEEP Q-LEARNING (DDQN): Van Hasselt, Guez, and Silver [205] showed that the DQN algorithm suffers from the same issue that also characterizes the Q-Learning algorithm: the overestimation bias of the Q function. They show that DQN is prone to learn overestimated Q -values because the same values are used both for selecting an action ($\max_{a \in \mathcal{A}}$) and for evaluating it ($Q(s_{t+1}, a; \theta^-)$). This becomes clearer when re-writing DQN's TD-target presented in Eq. 94 as:

$$y_t^{DQN} = r_t + \gamma \max_{a \in \mathcal{A}} Q(s_{t+1}, a; \theta^-). \quad (73)$$

As a result, DQN tends to approximate the expected maximum value of a state, instead of its maximum expected value. As presented in Sec. 2.5.2, in the tabular case this can be solved by keeping track of two separate Q functions, and by randomly preferring one Q function over the other when it comes to selecting which action to execute.



Figure 8: A visual representation of some of the Atari games that are part of the Arcade Learning Environment (ALE) [13]. From left to right Breakout, Seaquest, Qbert, Pong, MsPacman, KungFu-Master, Enduro and Space Invaders. Most of these games will be of interest in chapters 7 and 8. Image courtesy of .

DDQN generalizes this idea and untangles the action selection process from its evaluation by taking advantage of the previously introduced target network θ^- . DDQN’s target stays the same as in DQN with the main difference being that the selection of an action, given by the online Q-network θ , and the evaluation of the resulting policy, given by θ^- , can now result into smaller overestimations simply by symmetrically updating the two sets of weights (θ and θ^-) which can easily be achieved by regularly switching their roles during training. While not always significantly impacting the performance of DQN (one can still act optimally even if some actions are associated to unrealistically high $Q(s, a)$ estimates), there are also cases for which the overestimation bias of the Q function significantly slows down the training process, and even prevents the DQN algorithm from improving its policy over time at all. We will come back to this issue in Chapter 7.

PRIORITIZED EXPERIENCE REPLAY (PER): we have seen that next to the target network θ^- an equally important role within the DQN algorithm is played by the experience replay memory buffer D . Schaul et al. [167] showed that the efficiency of how Deep Q-Networks use this buffer could be improved. Their claim stems from the fact that, as shown in Eq. 93, the RL trajectories that get sampled from the memory buffer when constructing a mini-batch of trajectories are sampled uniformly $\sim U(D)$. This approach’s main drawback is that it considers each τ stored in the buffer as equally important and representative for training. However, it is easy to imagine learning situations where some trajectories are more valuable than others. For example, at the beginning of training, most of the trajectories contained within D will

be representative of early agent-environment interactions. It is, therefore, safe to assume that the network will learn the $Q(s, a)$ estimates representative of these early dynamics much faster than it will learn the Q values, which are associated with trajectories occurring more rarely. The idea of PER is to use only highly informative trajectories when it comes to building the mini-batches that are used for training the network. The importance of different trajectories is given by their respective TD-error. PER ensures that the probability of sampling trajectories is proportional to their respective TD-errors: the higher the TD-error, the larger the probability for a specific τ to be sampled. In practice, given a trajectory τ , the probability of sampling it is given by the following equation:

$$P(\tau) = \frac{p_\tau^\alpha}{\sum_k p_k^\alpha} \quad (74)$$

where p_τ is $|\delta_\tau + \epsilon|$ with ϵ being a small positive number ensuring that the probability of sampling a trajectory remains positive even in the edge case where the TD-error is 0. Although simple and intuitive implementing a PER buffer is not that straightforward and still presents some algorithmic caveats that need to be taken into account. Yet, if done correctly it dramatically improves the sample efficiency of Deep Q-Networks [126].

DUELING NETWORKS: while the DDQN algorithm directly tackles a fundamental algorithmic bias that characterizes the way DQN learns the Q function, and PER addresses the inefficiency of its memory buffer, the contribution presented by Wang et al. [212] is of slightly different nature. Their work consists of a novel type of neural architecture called the Dueling Network. This is a contribution that resembles more the kind of progress that is made by the supervised learning community, which, as we discussed in the previous chapter, has put a lot of effort into developing novel neural architectures for tackling computer vision tasks. Nevertheless, Wang's work is a perfect example that showcases how in DRL, carefully designing the function approximator is just as important as properly defining its objective function. A Dueling network is a network that, after performing a series of convolutions, instead of directly outputting the state-action values for a specific state as DQN and DDQN do, adds some intermediate computations. The idea is to estimate the value of a state and the advantages for each action before outputting the final Q values. The state values are computed based on Eq. 43, while the advantage function A is simply the difference between the Q function and the V function:

$$A^\pi(s, a) = Q^\pi(s, a) - V^\pi(s). \quad (75)$$

To successfully estimate state values, advantages, and state-action values, the network requires a specific architecture consisting of three

separate streams. Each stream is responsible for estimating one of the three value functions and is initialized with its own parameters $\theta^{(\cdot)}$. The final Q function of the model is then obtained by combining what is learned by each stream as follows:

$$\begin{aligned} Q(s, a; \theta^{(1)}, \theta^{(2)}, \theta^{(3)}) = & V(s; \theta^{(1)}, \theta^{(3)}) + \\ & (A(s, a; \theta^{(1)}, \theta^{(2)}) - \max_{a_{t+1} \in \mathcal{A}} A(s, a_{t+1}; \theta^{(1)}, \theta^{(2)})). \end{aligned} \quad (76)$$

Building a network with different task-specific streams is a design choice that resembles the way models are built when tackling multi-task classification tasks. However, note that the output of each stream that either estimates the state values or the advantage function gets aggregated in a final layer that estimates the state-action values. Minimizing the objective function presented in Eq. 76 is done by following the same principles that DQN and DDQN also use. The idea of taking into account the V function when learning the Q function is a concept which will come back, in a different flavor, in chapters 7 and 8.

POLICY GRADIENT METHODS: so far we have only considered algorithms that are part of the action-value family of methods, which, as explained in Sec. 2.5 are techniques that derive an optimal policy from a learned Q function. Yet, there is a collection of algorithms that is able to learn a policy directly, and that therefore bypasses the requirement of having to consult state-action values when it comes to action selection. These methods, which have contributed to the development of DRL just as much as action-value methods, come with the name of Policy Gradients. They directly parametrize a policy at each time-step as $\pi(a|s; \theta) = \Pr_{t=1}^T a_t = a, s_t = s | \theta_t = \theta$ and seek to optimize the parameters θ such that the performance of the policy is maximized. Note that this is drastically different from all the methods which we have seen so far, where the aim, in fact, was to minimize the TD-error through gradient descent optimization. Since policy gradients aim to maximize their performance, they learn via gradient ascent and therefore update their parameters as follows

$$\theta \leftarrow \theta + \alpha \nabla \xi(\theta). \quad (77)$$

Here α is again the learning rate, and ξ is a measure that quantifies the performance of the policy. Similarly to action-value based methods, one can parametrize a policy either with a linear function or with a deep neural network. When the action space is discrete, it is common practice to parametrize π through the same exponential softmax distribution, which we have seen in the previous chapter when presenting neural networks trained for classification tasks. Therefore we have

$$\pi(a|s; \theta) = \frac{e^{h(s, a; \theta)}}{\sum_b e^{h(s, b; \theta)}} \quad (78)$$

where $h(s, a; \theta)$ is any function approximator. By doing so, policy gradient methods naturally deal with the exploration-exploitation trade-off since they simply assign different probabilities to the different actions. This also allows these methods to approach a deterministic policy (which cannot be achieved when using ϵ -greedy action selection) and makes these algorithms arguably easier to train since learning a policy could be easier than learning state-action returns. The fundamental result which allows optimizing any differentiable policy is the policy gradient theorem [189]. Sutton et al. [189] show that the gradient of π does not depend from the gradient of the state distribution and that it can therefore be expressed as follows:

$$\nabla \xi(\theta) = \sum_s \mu(s) \sum_a Q^\pi(s, a) \nabla \pi(a|s; \theta) \quad (79)$$

where $\mu(s)$ is the stationary on-policy distribution under π . By expressing the gradient as such, it is now possible to optimize π even when the state distribution of the environment is unknown (as discussed in Sec. 2.5). Policy gradient methods can be used for learning a policy through the same kind of techniques which in Sec. 2.5 were used for learning value functions. Within the Monte Carlo setting the arguably most important of such algorithms is REINFORCE [222], while Actor-Critic algorithms [53, 61, 103, 121, 170–172, 213] learn a policy with the additional help of a bootstrapped value function (typically V or A).

RAINBOW: from the examples above, it is clear that much fast progress has been achieved by the DRL community in creating algorithms capable of learning faster and better. Explaining all the individual value-based contributions that have made DRL the popular research field it is nowadays [69], is beyond the scope of this chapter, yet, if there is one algorithm that encapsulates most of the progress that the DRL community has achieved over the last years, that is Rainbow [72]. Rainbow is a single, almighty agent that integrates within the same algorithm most of the important breakthroughs that DRL researchers have introduced over the last decade, ranging from the previously mentioned DDQN algorithm and PER system to more recent techniques such as distributional DRL [12], multi-step learning, distributed training [121] and noisy networks [47] that allow for better exploration.

2.8 CHALLENGES AND DESIDERATA

Similar to what we did for the field of supervised-learning we now end this chapter by presenting some of the main limitations that currently characterize the field of DRL. We briefly describe three of the most significant challenges that have resulted in the research questions we have tried to address throughout this dissertation.

DIVERGENCE & ‘THE DEADLY TRIAD’ The combination of RL with function approximation can, unfortunately, result in unstable training and algorithms prone to diverge while learning. As a representative example of what it means for an RL algorithm to diverge, let us consider the following MDP firstly introduced by Tsitsiklis and Van Roy [201]. The MDP consists of three states s_0, s_1 and the terminal state s_3 . Each state is described by a single scalar feature ψ such that $\psi(s_0) = 1$ and $\psi(s_1) = 2$. The estimated state-value of each state is therefore given by $V(s) = \psi \times \omega$, where ω is the single weight we would like to update. The MDP is represented in Fig. Each state transition is associated with a reward of 0, which means that the optimal weight value for having perfect value predictions is $\omega^* = 0$. Let us now assume that we are updating the state-value function based on an on-policy learning scheme as discussed in Sec. 2.5.2. We then know that each time we are updating the state-value function for s_0 , the value of s_1 will, in expectation, also be updated multiple times. This however, changes if we are following an off-policy learning scheme since each time we update the state-value function for s_0 , we do not necessarily update the value of s_1 anymore. As shown by Van Hasselt et al. [206] if we would now update ω based on Eq. 54 we would have to modify ω as $\Delta\omega \propto r_t + \gamma(V(s_{t+1}) - V(s_t))$. Which results into $0 + \gamma 2\omega - \omega = \gamma 2\omega - \omega = (2\gamma - 1)\omega$. If we then set the discount factor $\gamma > 0.5$ as is common practice, we can see that we have $2\gamma > 1$, which will make any weight $\omega \neq 0$ be updated away from the desired value of 0.

Sutton and Barto [188] show that the cause of this type of divergence occurs when RL algorithms are combined with three concepts which we have already encountered in this chapter. These concepts are:

- Bootstrapping (Sec. 2.5.2)
- Off-Policy Learning (Sec. 2.5.2)
- Function Approximation (Sec. 2.6)

This combination is known as the ‘Deadly Triad’ of DRL, and it is well known that if all of these three elements are combined within the same algorithm, divergence cannot be avoided. However, if an agent can bypass the need to rely on either one of these elements, then instability can already be prevented. Several work has addressed the ‘Deadly Triad’ of DRL [46, 71, 206] to answer the natural question ‘*which element can be given up when developing DRL algorithms?*’ So far, the community seems to agree that giving up on function approximators is clearly not possible. As discussed in Sec. 2.6 even linear functions can already play a crucial role in developing algorithms that deal with large and complex MDPs. On the other hand, it is not yet known what to give up between off-policy learning and

bootstrapping; what is known however, is that also because of the ‘Deadly Triad’, successfully training DRL solutions can be computationally very expensive since long training times are required for training agents which constantly try not to diverge. We will introduce a solution to this issue in Chapter 7.

COMPUTATIONAL RESOURCES: while most of the DRL algorithms presented in this chapter naturally follow from the tabular RL literature and are therefore not particularly hard to implement, successfully training and benchmarking these algorithms is not an equivalently easy task. The aforementioned divergence issue reflects itself in DRL algorithms that work well only if combined with a large range of carefully chosen hyperparameters. If a few of these hyperparameters are not set correctly, the algorithms miserably fail to learn even the most simple tasks. Unfortunately, the intuition of even the most expert DRL practitioner is not enough for identifying which learning parameters work best. As an example, let us consider the previously described Rainbow agent [72]. The learning rate that yields successful training is set to 0.0000625, clearly this is a value that could only be identified after performing an exhaustive grid search over a large set of potential learning rates. If on top of this, we also consider that training an agent on the previously mentioned ALE is a process that can last from taking days to even weeks [82], it is clear that the computational resources that are required for successfully evaluating DRL algorithms might not be accessible to all of the DRL community. For an excellent position paper about this topic, we refer the reader to the work of Obando-Ceron and Castro [129]. It is, therefore, desirable to develop algorithms that do not require extraordinary computational costs or that, if they do, can limit this use by learning and converging faster. We address this issue in Chapter 7 and 8.

GENERALIZATION AND TRANSFERABILITY The limitation mentioned above can naturally be addressed by studying whether agents trained for solving specific tasks can generalize to new unseen problems. If this would be the case, this could have significant practical benefits. DRL algorithms would not have to be trained from scratch each time they face a new problem, limiting the aforementioned requirement of high computational costs significantly. Furthermore, as mentioned in the introduction of this dissertation, there is arguably nothing more intelligent than learning how to solve a problem than learning a solution to a problem that is general enough to a larger set of problems. We thoroughly study the degree of transferability of DRL algorithms in Chapter 8 and present how the RL community has already studied the transfer learning properties of RL algorithms in the coming chapter.

3

TRANSFER LEARNING

OUTLINE

We now present Transfer Learning (TL), a machine learning methodology that aims to create algorithms capable of retaining and reusing previously learned knowledge when getting trained on new, unseen problems. Most of the contributions presented within this dissertation are motivated by TL. Therefore, we now introduce the reader to this specific learning paradigm to provide him/her with all the preliminary knowledge that is necessary for fully understanding the research presented in the coming chapters. We start with a gentle introduction to TL in Sec. 3.1 where we describe the main concepts underlying TL and explain why it is desirable to have machine learning models that are transferable. We then show in Sec. 3.2 some practical, high-level examples that visually represent the benefits that can come from adopting TL strategies in machine learning. We will then provide more rigorous mathematical definitions of TL in Sec. 3.3 where we will characterize TL both for the supervised learning setting as for the reinforcement learning one. In Sec. 3.4 we thoroughly review how TL has been studied by the deep learning community in both settings. We end this chapter with Sec. 3.5, where we provide a summary of the most relevant TL concepts and show how they will play a role throughout the rest of this dissertation.

3.1 INTRODUCTION

- cogsci perspective on nature of intelligence
- practical benefits real world applications
- computational costs
- tl as a tool for understanding neural networks

3.2 RATIONALE OF TRANSFER LEARNING

Before mathematically defining TL, we start by building some intuition and visually represent how one can observe the benefits of TL in practice. We assume that we would like to solve a certain task and that we can choose between two different models: a model that has never dealt with any task before, and a second model, which is

identical to the first one with the major difference being that it has already seen a similar task in the past. Because of their different nature, we refer to the first model as a model trained from scratch and to the second model as a pre-trained model. Ideally, as mentioned in the previous section, we would like the latter model to perform better on the considered task than the first one. Yet, how can we assess if one model is better than the other one? As initially presented by Langley [93], and later generalized by Lazaric [95], we would like the performance of a pre-trained model to result in three possible improvements. If at least one of these improvements is observed while training, we can then consider the pre-trained model better than the scratch model. These improvements are the following:

- **Learning Speed Improvements:** in this scenario, the performance between a pre-trained model and a model trained from scratch is identical by the time training is finished; however, when this kind of improvement appears, we observe that the pre-trained model converges faster than the model trained from scratch. An example of this TL improvement is presented in the first plot of Fig. 9. The goal is to train a model such that by the end of training, its performance reaches a value of 200. We can clearly see that both models manage to converge to this desired performance value, but that the pre-trained model manages to converge already after ≈ 50 training iterations, whereas the model trained from scratch requires more than 200 training iterations to perform similarly. Also, note that the performance of both models at the beginning of training is identical, with both models starting with an initial performance of ≈ 20 .
- **Jumpstart Improvements:** similar to the previous case, also in this scenario, there are no significant differences between the performance of a pre-trained model and the performance of a scratch model by the end of training. However, this changes when we consider the very first training iteration. If jumpstart improvements appear, we can usually observe that when both models start their training process, the performance of the pre-trained model is much closer to the one that will be obtained by the end of training than the one of the scratch model. We visually report an example of this scenario in the third plot of Fig. 9. In this case, the goal is to train a model such that by the end of training its performance will be of ≈ -100 . We can clearly see that by the end of training both models are able to achieve this goal successfully, but that at the very first training iteration, the performance of the pre-trained model is significantly closer to the desired final performance (≈ -250) than the one of the scratch model (≈ -450).

- **Asymptotic Improvements:** when this TL improvement appears, the final performance of a pre-trained model is significantly higher than the one of a model trained from scratch. It is worth noting that similar to what happens when learning speed improvements are observed, also in this case, the performance of both models is identical when training begins, and that this TL improvement only presents itself after several training iterations. A visualization of this TL improvement can be observed in the last plot of Fig. 9 where we can observe that for the first ≈ 20 training iterations, there are no differences in terms of performance between a pre-trained model and a model trained from scratch. However, the more training iterations are performed, the more the pre-trained model starts outperforming the model trained from scratch, reaching a final performance that is almost twice as good by the 100th training iteration.

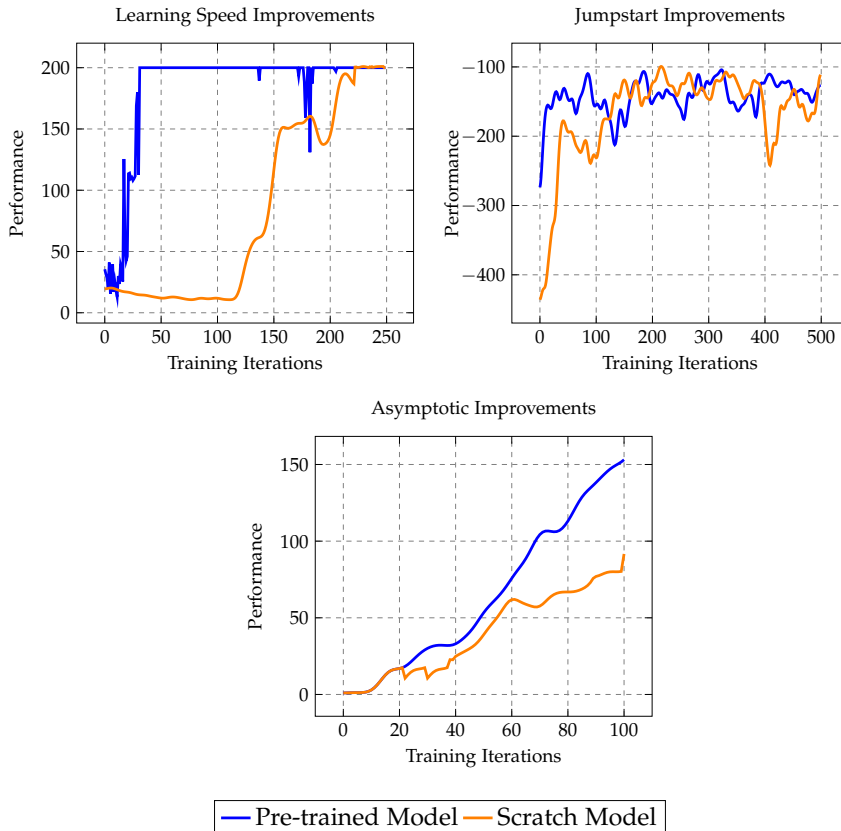


Figure 9: A visualization of the three possible desired outcomes that can come from adopting Transfer Learning strategies as initially defined by Langley [93] and later by Lazaric [95].

While the improvements presented in Fig. 9 are all highly desirable, it is worth noting that some of them can be preferable to others. In fact, the potential benefits of TL highly depend on the problem at

hand. For example, let us consider a training situation where the main goal is to minimize the overall training time of a model. In this particular case, jumpstart and learning speed improvements are more desirable than asymptotic improvements since the latter improvement might not result in a model that converges to a potentially desirable solution faster. On the other hand, if the main objective is that of training a model which performs as best as possible, then evidently, asymptotic improvements are preferred. It is also worth noting that the examples presented in Fig. 9 are not mutually exclusive and that, in practice, the benefits of TL can present themselves as a combination of improvements rather than in the form of a single, isolated improvement.

Now that we have introduced the key ideas behind TL and presented why adopting TL training strategies is beneficial, we move to formally characterizing this machine learning paradigm both from a supervised learning perspective as from a reinforcement learning one.

3.3 MATHEMATICAL DEFINITIONS

As is common throughout this thesis, we start by focusing on the supervised learning case.

3.3.1 Supervised Learning

The first two definitions that we provide are borrowed from Zhuang et al. [239] and are the ones of **domain** and **task**. The first one is defined as follows:

Definition 3 A domain \mathcal{D} is the combination between an input space \mathcal{X} and a marginal distribution $P(X)$, $\mathcal{D} = \{\mathcal{X}, P(X)\}$ where X denotes an instance set defined as $X = \{\mathbf{x} | \mathbf{x}_i \in \mathcal{X}, i = 1, \dots, n\}$.

Examples of domains can be natural images, time-series data, biomedical markers, etc. In supervised learning, we know that each domain is associated with its respective task, representing the problem we would like to solve. A task is defined as follows:

Definition 4 A task \mathcal{T} consists of a label space \mathcal{Y} and a decision function f , i.e., $\mathcal{T} = \{\mathcal{Y}, f\}$. The decision function f is implicit and can only be learned by sampling data from \mathcal{X} which comes in the form of $\{x_i, y_i\}$ pairs where x_i and $y_i \in \mathcal{Y}$.

Examples of possible decision functions f can be classifiers that categorize natural images in their respective classes or regressors that can predict future values in a time series. The key concept underlying TL is that, differently from the common supervised learning scenario where the only available information to a model is one domain and

one task, there is now access to at least two domains. The one that corresponds to the task we would like to solve called the **target-domain** \mathcal{D}_T , and an additional, possibly related, domain that comes with the name of the **source-domain** \mathcal{D}_S . With all these concepts in place, we can now define **Transfer Learning** as:

Definition 5 *Given one, or more, observations corresponding to $m^s \in \mathbb{N}^+$ source domain(s) and tasks(s) (i.e., $\{(\mathcal{D}_{Si}, \mathcal{T}_{Si} | i = 1, \dots, m^s)\}$) and some additional observation(s) about $m^T \in \mathbb{N}^+$ target domain(s) and task(s) (i.e. $\{(\mathcal{D}_{Tj}, \mathcal{T}_{Tj} | j = 1, \dots, m^T)\}$), transfer learning utilizes the knowledge implied in the source domains to improve the performance of the learned decision functions $f_j^T (j = 1, \dots, m^T)$ on the target domain(s).*

As pointed out by Pan and Yang [132] the condition that the source and the target domains might be different $\mathcal{D}_S \neq \mathcal{D}_T$ implies that either their respective input spaces are different as well $\mathcal{X}_S \neq \mathcal{X}_T$, or that their corresponding marginal distributions are different $P_S(X) \neq P_T(X)$. Similarly, if the tasks are different instead $\mathcal{T}_S \neq \mathcal{T}_T$, then either one between the output spaces, or the conditional distributions has to be different ($\mathcal{Y}_S \neq \mathcal{Y}_T$ or $P(Y_S | X_S) \neq P(Y_T | X_T)$).

Based on the consistency between the source and target input spaces \mathcal{X} , and the respective output spaces \mathcal{Y} , one can categorize TL into three following settings.

INDUCTIVE TRANSFER LEARNING This TL scenario is characterized by the fact that the target task \mathcal{T}_T is different from the source task \mathcal{T}_S , while the source domain \mathcal{D}_S and the target domain \mathcal{D}_T might, or might not be similar. As originally presented in [132] we define inductive transfer learning as:

Definition 6 *Given a source domain \mathcal{D}_S and a learning task \mathcal{T}_S , and a target domain \mathcal{D}_T and a learning task \mathcal{T}_T , inductive transfer learning aims to help to improve the target predictive function $f_T(\cdot)$ in \mathcal{D}_T by using the knowledge in \mathcal{D}_S and \mathcal{T}_S , where $\mathcal{T}_S \neq \mathcal{T}_T$.*

A key requirement of this type of TL is that some labeled data in the target domain is necessary for inducing the objective predictive function $f_T(\cdot)$. To build some more intuition about this kind of TL, let us assume that we would like to train a model on our target task \mathcal{T}_T , which corresponds to recognizing what kind of Japanese letter is depicted in an image. Instead of training a model only on a dataset of letters, we instead start from a model that has already been trained to recognize digits, which will therefore be our source task \mathcal{T}_S . Note that in this case, the source task and the target tasks are evidently different $\mathcal{T}_S \neq \mathcal{T}_T$ (classifying digits vs. classifying letters), but that the input space of the source and target domains is the same $\mathcal{X}_S = \mathcal{X}_T$, since it corresponds to black and white images as represented in Fig. 10. Please note that in this example, since we use a model



Figure 10: A visualization of two datasets that can be used for performing inductive transfer learning. On the left we represent instances of the popular MNIST dataset [227], while on the right instances of the Kuzushiji-MNIST dataset [32]. We see that both datasets share the same domain $\mathcal{D}_S = \mathcal{D}_T$ (black and white images), but are associated to different tasks $\mathcal{T}_S \neq \mathcal{T}_T$ (classification of digits vs classification of Japanese letters).

that is pre-trained on images representing digits, we assume that we have had access to some labeled data in the source domain in the past. However, the definition of inductive transfer learning does not require labeled data within the source domain to be strictly necessary.

TRANSDUCTIVE TRANSFER LEARNING Proposed initially by Arnold, Nallapati, and Cohen [6], this type of TL is characterized by the fact that the source and target tasks are the same $\mathcal{T}_S = \mathcal{T}_T$, but their respective domains are different $\mathcal{D}_S \neq \mathcal{D}_T$. It is also possible that the feature spaces between domains are the same but, if that is the case, then the marginal probability distributions are different $P(X_S) \neq P(X_T)$. In its original formulation, Arnold, Nallapati, and Cohen [6] assumed that all unlabeled data in the target domain is available at training time. However, we hereafter report the definition of Pan and Yang [132] who instead relax this condition and require only a subset of unlabeled target data to be seen at training time.

Definition 7 *Given a source domain \mathcal{D}_S and a learning task \mathcal{T}_S , and a target domain \mathcal{D}_T , and a learning task \mathcal{T}_T , transductive transfer learning aims to help to improve the target predictive function $f_T(\cdot)$ in \mathcal{D}_T by using the knowledge in \mathcal{D}_S and \mathcal{T}_S , where $\mathcal{D}_S \neq \mathcal{D}_T$ and $\mathcal{T}_S = \mathcal{T}_T$.*

As an example of transductive transfer learning let us assume that we would like to train a model to classify which type of clothing is depicted in an image. This time, differently from the inductive transfer learning case, the images in our target domain \mathcal{D}_T are not black and white anymore, but rather colored images; therefore, they are defined over the RGB domain (see the right image of Fig. 11). We now assume that we have access to a pre-trained model which has already been



Figure 11: Two datasets that are representative of transductive transfer learning. On the left we show images coming from the Fashion-MNIST dataset [225], while on the right we report instances of the same dataset that are colored. In this case tasks among datasets are shared $\mathcal{T}_S = \mathcal{T}_T$ (classification of clothes), but the respective images come from different domains $\mathcal{D}_S \neq \mathcal{D}_T$ (black and white vs RGB images).

trained to classify the same type of clothes, with the main difference being that the images constituting the source domain \mathcal{D}_S were black and white images (see the left image of Fig. 11). If we now train this pre-trained model on our colored dataset, we see that our setting fits the transductive transfer learning scenario: our considered domains are different $\mathcal{D}_S \neq \mathcal{D}_T$ (colored vs. black and white images), but their respective tasks are the same $\mathcal{T}_S = \mathcal{T}_T$, since a model is always trained to classify types of clothing.

Although this section, as this dissertation, primarily focuses on supervised learning, we hereafter still report for the sake of completeness a definition of unsupervised transfer learning, and see how this kind of TL connects to the types of TL that we have analyzed so far.

UNSUPERVISED TRANSFER LEARNING Arguably considered to be the most challenging and the least explored type of TL, unsupervised transfer learning is characterized by the total absence at training time of labeled data in both the source domain and the target domain. As mentioned by Pan and Yang [132], very little research work has so far explored this TL paradigm, with the only existing works exploring typical unsupervised learning topics such as clustering [34, 80, 145] and dimensionality reduction [211, 236, 237]. Unsupervised transfer learning is defined as follows:

Definition 8 *Given a source domain \mathcal{D}_S and a learning task \mathcal{T}_S , and a target domain \mathcal{D}_T , and a learning task \mathcal{T}_T , unsupervised transfer learning aims to help to improve the target predictive function $f_T(\cdot)$ in \mathcal{D}_T by using the knowledge in \mathcal{D}_S and \mathcal{T}_S , where $\mathcal{T}_S \neq \mathcal{T}_T$ and \mathcal{Y}_S and \mathcal{Y}_T are not observable.*

Based on this definition, we can note that unsupervised transfer learning is more similar to inductive transfer learning than to transductive transfer learning as we again assume that the source and the target tasks are different $\mathcal{T}_S \neq \mathcal{T}_T$.

3.3.2 Reinforcement Learning

When it comes to the Reinforcement Learning (RL) setup, the definition mentioned above of TL slightly changes and becomes arguably less general. Recall from Chapter 2 that in RL, the main goal is that of training an agent such that it becomes able to interact with its environment, a problem that is modeled with Markov Decision Processes (MDP). It follows that in the RL context, the previously introduced concept of domain \mathcal{D} (which could come in numerous flavors) now comes in the arguably more strictly defined form of an MDP \mathcal{M} . Just like domains, MDPs can either be representative of a source task, \mathcal{M}_S , or of a target task \mathcal{M}_T , with the latter case corresponding to the main RL problem we are interested in solving. Also, the previously introduced predictive function $f(\cdot)$ is now defined more precisely, as it corresponds to the task of learning an optimal policy π^* for \mathcal{M}_T . Based on these concepts, we give the following definition of TL for reinforcement learning that is adapted from the one proposed by Zhu, Lin, and Zhou [238].

Definition 9 *Given a source MDP \mathcal{M}_S and a target MDP \mathcal{M}_D , transfer learning in reinforcement learning aims to learn an optimal policy π^* for \mathcal{M}_D by exploiting some prior knowledge related to $\mathcal{M}_S, \mathcal{K}_S$, together with the knowledge that underlies $\mathcal{M}_T, \mathcal{K}_T$ such that:*

$$\pi^* = \arg \max_{\pi} \mathbb{E}_{s \sim \mu_0^t, a \sim \pi} [Q_{\mathcal{M}}^{\pi}(s, a)], \quad (80)$$

where $\pi = \zeta(\mathcal{K}_S \sim \mathcal{M}_S, \mathcal{K}_T \sim \mathcal{M}_T) : \mathcal{S}^t \rightarrow \mathcal{A}^t$ is a function mapping from the states to actions for \mathcal{M}_T learned thanks to both \mathcal{K}_S and \mathcal{K}_T .

Note that differently from the supervised learning case, we are now making explicit use of the concept of knowledge \mathcal{K} , which is what we would like to retain when moving from a source MDP \mathcal{M}_S to a target MDP \mathcal{M}_T . We do this because RL is a machine learning paradigm that is arguably, more complex than the supervised learning. A complexity that stems from the fact that in RL there are concepts such as e.g., rewards and policies, which are, by definition, not present in the supervised learning setup. As a result, \mathcal{K} can come in forms that it cannot take in SL, and correctly identifying which kind of knowledge to transfer between \mathcal{M}_S and \mathcal{M}_T is just as important as developing a method that successfully transfers this knowledge in the first place. As mentioned by Lazaric [95] \mathcal{K} can come in the following forms.

TRANSFER OF INSTANCES: in this scenario \mathcal{K} corresponds to RL trajectories coming in the form $\langle s_t, a_t, r_t, s_{t+1} \rangle$ and that have been collected on one, or possibly multiple, source MDPs \mathcal{M}_S . Such trajectories can then be used both in a model-based RL setting, as done by Taylor, Jong, and Stone [194], or for speeding up the process of learning a value function as described in [97] and [94]. Ideally, transferring RL trajectories should result in highly sample efficient algorithms, although it is worth noting that this property, albeit desirable, can constrain the source task \mathcal{M}_S and the target task \mathcal{M}_T to have similar transition models and reward functions. This instance of TL is usually used within the batch RL setup, where gathering experience samples for \mathcal{M}_T can be particularly expensive or time-consuming, which is a constraint that does not hold for \mathcal{M}_S . The typical challenge then consists of correctly identifying which of the samples coming from \mathcal{M}_S are the most informative ones for solving \mathcal{M}_T , as for example, studied by Tirinzoni et al. [199].

TRANSFER OF PARAMETERS: as we have seen in Chapter 2 it is often desirable to integrate RL algorithms with parametric function approximators. The main goal is then to train these parametric functions to learn an approximation of an optimal value function or policy. When parameter transfer is performed, the main idea is to start solving the problem modeled by the target task \mathcal{M}_T with a function that, instead of being initialized with random parameters, is initialized with parameters that have been learned on a certain source task \mathcal{M}_S . Examples of knowledge \mathcal{K} that fit this description are the parameters θ of a pre-trained Deep Q-Network, or the parameters that model an Actor-Critic agent.

While both representations are arguably the most popular ones, it is important to mention that as described by Tirinzoni, Sanchez, and Restelli [198] there are alternative possible ways of representing \mathcal{K} . Among such ways \mathcal{K} can come in the form of e.g., features [10, 114], rewards [89, 166] and options [179].

3.4 DEEP TRANSFER LEARNING

We now present the field of ‘Deep Transfer Learning’ (DTL), a machine learning paradigm that aims at performing TL when a source model comes in the form of a pre-trained convolutional neural network. We start by describing how one can exploit the availability of a pre-trained network when training a model on the desired target task and then present a thorough literature review that describes the most successful applications that the DTL community has so far achieved.

3.4.1 General Framework

Let us assume we would like to train a neural network on a regression task. Instead of initializing its weights randomly, we initialize it with weights that have already been optimized on a certain source task. We refer to the parameters of this pre-trained model as θ_S , where S stands again for ‘source’. When training the network on the target task, the main challenge revolves around deciding up to what extent the parameters θ_S should be modified by stochastic gradient descent. In practice, this corresponds to deciding how much of the knowledge contained in θ_S should be retained when training our pre-trained network on \mathcal{T}_T . Typically, one can choose between two different approaches:

- **Off the Shelf Extraction:** in this setting, the parameters θ_S of the pre-trained model are not changed when the network gets trained on the target task. Instead, the only weights that get optimized are the ones that are responsible for the final predictions of the model. In the regression example mentioned above, these weights would correspond to the ones parametrizing the network’s final output neuron. Similarly, if we would be dealing with a classification problem, we would only train the weights that constitute the final softmax layer of the model, as it is the part of the network responsible for outputting the predicted output classes. Since this approach does not involve any backpropagation operations, it is particularly desirable when computational resources are limited. In fact, one only needs to compute the forward pass in order to get the features from the pre-trained model. However, this approach also comes with the major limitation of not allowing the network to adapt to the target task as it assumes that all the knowledge that is required for solving \mathcal{T}_T is already contained within θ_S . In the context of convolutional neural networks, this corresponds to a model that has already learned all the features that are necessary for solving \mathcal{T}_T when getting trained on \mathcal{T}_S .
- **Fine-Tuning:** when this approach is adopted all the parameters θ_S that have been learned on the source task get optimized when training the network on the target task. Evidently, this training strategy is computationally more expensive than the previous one, as it involves all of the steps that characterize the successful training of neural networks that we discussed in Chapter 1. Despite being computationally more demanding, fine-tuning a network has the significant benefit of allowing a model to become target task-specific. In fact, whilst training, part of the knowledge contained within θ_S can be ‘forgotten’, which will result in a new set of parameters, θ_T , that can perform better on

\mathcal{T}_T than θ_S . From a practical perspective, however, it is important to train the model in such a way that the knowledge contained within θ_S does not get ‘forgotten’ too quickly while at the same time ensuring that the network stays flexible enough for successfully learning the target task. One possible way of achieving this is by using small learning rate values for training.

While both approaches come with pros and cons, the latter option is usually preferred if enough computational resources are available. In fact, as we will see in the coming section, the community seems to agree that it often results into better final performance. When DTL strategies are adopted it is usually good practice to compare the performance of a pre-trained model with the performance that is obtained by a model that is initialized randomly, and that gets therefore trained from scratch. Throughout this thesis we will constantly characterize the benefits of adapting TL strategies from this perspective, therefore, to add even more clarity to the concepts presented in this section, we also visually represent them in Fig. 12.

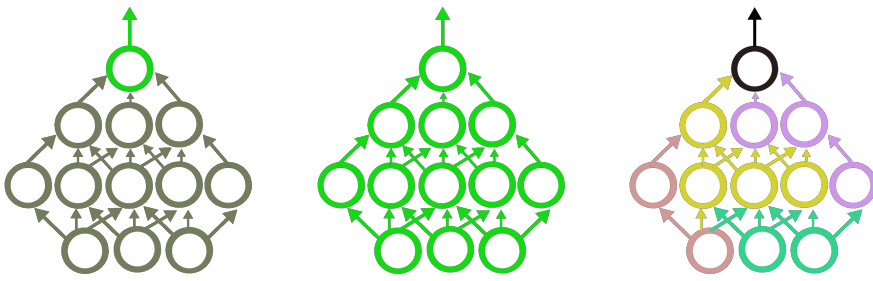


Figure 12: A simplified visual representation of the different deep transfer learning training paradigms that are considered throughout this thesis. The first plot represents a model that comes as pre-trained on a source task but which will not update most of its weights during the training stage (represented in gray): the only trainable parameters of this network are the ones that parametrize the final layer of the model and that are represented in green. In the second plot we visually represent a model that is parametrized with weights that have been learned on a certain source task, and that get “unfrozen” when the network gets trained on the target task, therefore defining the model as fully trainable. Lastly we visualize a model that does not come as pre-trained on any source task, and that is therefore initialized with random weights instead (represented by the various colours). As already mentioned throughout this chapter, the main goal of TL is to obtain a model that if trained with the first two approaches results into a final performance that is better than the one that would be obtained after adopting the last approach.

3.4.2 Literature Review

CONVOLUTIONAL NETWORKS AS FEATURE EXTRACTORS As soon as convolutional neural networks started to perform well on popular computer vision benchmarks, research investigating whether these networks could be transferred and reused for novel tasks started to bloom. Among the different works exploring this research direction, one of the very first ones is that of Donahue et al. [40] who evaluated whether features extracted from a convolutional neural network trained for image classification could also be used for tackling CV tasks such as scene recognition and domain adaptation. Donahue et al. [40] showed that this was indeed the case and publicly released the pre-trained model under the name of DeCAF intending to stimulate the CV community to investigate further the extent to which the features learned by this network were transferable to novel tasks. Almost concurrently, similar conclusions about the transferability of pre-trained convolutional networks were drawn by Oquab et al. [130], who showed the benefits of using a pre-trained convolutional model as feature extractor when dealing with object and action localization problems, and by Zeiler and Fergus [230] who first showed that on many problems it was more beneficial to simply train the final classification layer of a pre-trained network, than to train a randomly initialized model from scratch. While definitely promising, all these works restricted their experimental analysis to a relatively small set of CV problems, and it was only with the seminal work of Sharif Razavian et al. [175] that the deep learning community realized how powerful pre-trained networks could be. Sharif Razavian et al. [175] used the off the shelf (OTS) features of the pre-trained OverFeat network [174] for tackling numerous challenging CV problems and consistently reported a final performance that was superior to the one of the state of the art algorithms of the time. Next to providing a wealth of empirical evidence supporting the use of off-the-shelf features, their work also established the first training protocol for combining high dimensional OTS features with linear classifiers, such as SVMs, and dimensionality reduction techniques such as principal component analysis.

It did not take long before the scientific community started to investigate whether off-the-shelf features could also be used for problems outside the typical CV benchmarks, and therefore fully realized the potential of this TL approach. Among the very first practical applications, we mention the work of Van Ginneken et al. [203] who used the previously mentioned DeCAF model for (successfully) tackling the challenging medical task of pulmonary nodule detection. Along the same line of research, equally good results were obtained within the medical domain by Hernandez-Diaz, Alonso-Fernandez, and Bigun [70] who tackled the problem of periocular recognition,

and by Nguyen et al. [128] who considered the similar task of iris recognition.

Further successful applications of OTS classification, which go beyond the medical domain, are the ones reported by Sharma [176], who considered the handwriting recognition task of word spotting, and the one of Wolfshaar, Karaaba, and Wiering [223], who studied the task of gender classification. While all these research solely relied on an OTS feature extraction approach when addressing a CV problem, it is also worth noting that OTS features can be used in combination with more traditional CV feature engineering techniques such as SIFT [109] and HOG [35]. This research direction has been successfully explored by, e.g., Wang, Qiao, and Tang [210] who examined the task of human action understanding, and by Zhong, Sullivan, and Li [233] who addressed the problem of face localization.

ON THE BENEFITS OF FINE-TUNING Modern deep learning frameworks such as TensorFlow [1] and PyTorch [136], provide high level and easy to use APIs that make it possible to create and train deep learning models even without a necessarily strong machine learning background. Among the main reasons that have made deep learning so accessible there is the fact that the aforementioned deep learning libraries provide easy access to models that have already been trained on a large variety of CV tasks [44, 106, 155]. As a result, using pre-trained neural networks has become increasingly easy, which is among the reasons that allowed the deep learning community to explore whether fine-tuning pre-trained models could result in better performance than simply using them as OTS feature extractors. It is easy to see how this research question is of high practical interest and why it has therefore been heavily explored by practitioners working at the intersection of machine learning and fields such as, e.g., medicine [74, 192]. Among the first works exploring whether it is beneficial to fine-tune pre-trained models instead of using them as simple feature extractors, there is the one of Tajbakhsh et al. [192]. The authors consistently show that fine-tuning a pre-trained network outperforms the OTS feature extraction approach when it comes to four distinct medical imaging tasks and that, similarly to what was predicted by Zeiler and Fergus [230], pre-trained networks outperform models that are trained from scratch. A similar conclusion has also been reached by Mormont, Geurts, and Marée [124], who analyzed the same research question under the lens of image classification problems coming from the digital pathology field. They also show that fine-tuning yields better performance than OTS feature extraction, but they do not answer whether this TL strategy works better than training a network from scratch. The question of whether to fine-tune or not to fine-tune a neural network has also been explored outside of the CV domain. Among the different works, we mention

the one of Peters, Ruder, and Smith [140], who address this question from a Natural Language Processing (NLP) perspective. In line with what has been observed by the CV community, they also highlight the significant benefits that can come from fine-tuning popular NLP models such as ELMo [141] and BERT [37] as long as the source task is carefully chosen. By now, studies investigating the benefits coming from fine-tuning pre-trained models are countless and range over a large variety of domains that do not necessarily strictly involve CV problems [3, 22, 36, 39, 56, 76, 77, 88, 229].

ON THE ROLE OF IMAGENET AS \mathcal{T}_S Throughout this chapter, we have constantly referred to the concept of source domain \mathcal{D}_S and source task \mathcal{T}_S , two key elements without which the entire field of TL would not even exist. Albeit in the previous paragraphs we have mentioned the task of image classification as source task \mathcal{T}_S that can be used for pre-training convolutional networks, we have not explicitly described what this task consists of in practice. When adopting TL strategies for CV problems, the most common and, by far successful, approach is that of relying on models that have been trained for the ImageNet Large Scale Visual Recognition Challenge (ILSVRC) [155]. The ILSRVC dataset, more commonly referred to as the ImageNet dataset, is a collection of over one million natural images that are categorized among one thousand different classes. Until 2017 it was primarily considered to be the most complex and challenging problem of all CV and is among the main reasons which have yielded the deep learning community to develop most of the neural architectures that we described in Chapter 1. Due to the large number of samples constituting the dataset and the complexity of the tackled task, networks trained for the ILSVRC challenge are regularly used as pre-trained networks even when the target task \mathcal{T}_T does not involve the classification of natural images. Intuitively, the reasons behind this choice are very straightforward: on the one hand, it is safe to assume that some of the features that are learned by a network that receives as input more than one million images will, at least in part, correspond to the features that the same network would have to learn when getting trained from scratch on the desired target task.

On the other hand, it is also unlikely that the target task \mathcal{T}_T will be more complex than the source task \mathcal{T}_S since it is not common to deal with classification problems that involve more than 1000 classes. In this sense, as pointed out by Mensink et al. [117], it is reasonable to assume that if a network performs well on \mathcal{T}_S , it should also perform well on \mathcal{T}_T , as the latter task is essentially easier than the former. Despite these intuitive explanations, a large body of work has studied why it is beneficial to transfer ImageNet pre-trained models and the factors of influence of this dataset for TL. This question was first tackled by Huh, Agrawal, and Efros [78] who studied, among other

questions, how many examples and classes of the ImageNet dataset should be used for successfully pre-training a model. Perhaps surprisingly, they found that already half of the ImageNet data yielded a well-performing pre-trained network and that among the different 1000 classes, it was already enough to pre-train a network on a subset of 127 of them. Kornblith, Shlens, and Le [91] empirically studied the benefits of using ImageNet pre-trained models for 12 different classification problems and found that the better a model performs on ImageNet, the better it transfers to new unseen tasks. A similar study, which, however, yielded slightly different results, is the one of He, Girshick, and Dollár [66] who showed that there might not be significant differences in terms of final performance between using an ImageNet pre-trained network and a randomly initialized one, but that the first ones consistently converge faster than the latter. Finally, the recent work of Mensink et al. [117] shows that ImageNet pre-trained models always outperform models that are trained from scratch, but that this dataset might not necessarily always be the best possible source task for pre-training. It is worth noting that all the examples as mentioned earlier revolve around the field of supervised learning within CV, it naturally follows that different pre-training strategies, and therefore different source domains, need to be considered for other fields (see e.g. NLP). Since discussing these techniques would go beyond the main scope of this dissertation, we do not present them here. However, we refer the reader to [24, 37, 118, 151] for a discussion of pre-training strategies outside the CV and supervised learning domain.

THE DEEP REINFORCEMENT LEARNING SETTING While within the supervised learning setting, the body of work studying the transfer learning properties of neural networks is substantial, the same cannot be said when it comes to reinforcement learning. Although, as presented in Sec. 3.3.2 there exist many different approaches for performing TL in RL, the integration of such techniques with convolutional neural networks is much rarer. Perhaps the work that studies the TL properties of Deep Q-Networks in a flavor that is the closest to the TL approaches used in supervised learning that we presented in Fig. 12 is that of Farebrother, Machado, and Bowling [45]. The authors study whether convolutional neural networks that are trained with the DQN algorithm [120] are capable of learning features that are robust enough to allow the algorithm to generalize across different tasks. The results, obtained on four different Atari 2600 games do not provide a clear answer to this question: when Deep Q-Networks come as pre-trained on a particular game and simply get fine-tuned on a new different game, the authors fail in observing the benefits that this TL approach typically yields in the supervised learning context. However, if networks get pre-trained in combination with typ-

ical supervised learning regularization techniques such as dropout [182] and l_2 regularization, then the authors observe that fine-tuning these models results in a final performance that is better than the one of models trained from scratch. While indeed encouraging, these results were only obtained on a minimal set of RL environments, and it is unclear whether these conclusions would hold if a more extensive set of benchmarks, and algorithms, would be tested. A similar study, which arguably presents the same limitations, is the one performed by Tyo and Lipton [202]. On the same line with Farebrother, Machado, and Bowling [45] the authors study the effect of fine-tuning different pre-trained Rainbow agents [72] that use different weight initialization strategies. Results reported for three different Atari games show that fine-tuning is beneficial only for one single game but do not explain the TL properties of pre-trained Deep Q-Networks any further. A more thorough and successful study is the one presented by Parisotto, Ba, and Salakhutdinov [133], where the authors also investigate the effect of fine-tuning pre-trained DRL agents and show that this TL strategy can result in significant benefits. Their study, however, presents some significant differences when compared to the previous works. First, the DRL algorithm under scrutiny is a policy gradient algorithm which, as discussed in Chapter 2, is part of a family of techniques that is significantly different from the family DQN and Rainbow are part of. Second, their proposed Actor-Mimic algorithm does not come as pre-trained on a single Atari game anymore but is pre-trained in a multi-task learning setting instead. The algorithm, therefore, deals with different source-tasks \mathcal{T}_S during the pre-training stage, which is a strategy that results in algorithms that are more robust and suitable for TL [87].

3.5 RELEVANCE FOR THIS DISSERTATION

With all the concepts above and the ones presented in Chapters 1 and 2, we are now ready to end this first part of this dissertation by describing how all the aforementioned content will play a role throughout the rest of this thesis.

First, we start by noting that all the quantitative results that will be presented from now on will be defined with respect to the three TL benefits that we described in Sec. 3.2. No matter which kind of task we will be training neural networks for, we will always seek to identify at least one of the three possible benefits of adapting TL. The only chapter where we will not do this is Chapter 7, which instead will serve for introducing some novel DRL algorithms that will be studied from a TL perspective only in Chapter 8.

When it comes to all the research performed within the supervised learning setting, it is important to note that we will only consider the inductive transfer learning scenario. More specifically, we will

always study the extent to which neural networks pre-trained on natural images can generalize to non-natural datasets. The content of these datasets, and therefore the considered target tasks \mathcal{T}_T , will change from chapter to chapter, and so will the source task \mathcal{T}_S that will be used for pre-training. For the research involving reinforcement learning, we will instead only consider the TL setting that studies the transferability of parameters presented in Sec. 3.3.2. As a result, no matter whether we will tackle supervised learning problems or reinforcement learning ones, the experimental protocol that we will adopt will always consider the TL training strategies that we have described in Sec. 3.4.1 and presented in Fig. 12. Thus, the coming results will all contribute to the development of the field that studies the transferability of neural networks that we have reviewed in Sec. 3.4.

We will now move to present the results of our studies investigating the TL properties of convolutional neural networks trained for supervised learning problems.

Part II

TRANSFER LEARNING FOR DEEP SUPERVISED LEARNING

4

ON THE TRANSFERABILITY OF CONVOLUTIONAL NETWORKS

CONTRIBUTIONS AND OUTLINE

We now present a first study that characterizes the Transfer Learning (TL) properties of convolutional neural networks that come as pre-trained on the ImageNet dataset. We thoroughly investigate whether popular neural networks that have obtained state of the art results on this benchmark of natural images can perform equally well once used on non-natural datasets. Specifically, we explore whether it is possible to tackle three different target tasks \mathcal{T}_T that come in the form of art classification problems. We study the effects of different TL training approaches (off-the-shelf classification vs. fine-tuning), and explore whether it is possible to improve the TL performance of the considered pre-trained networks by allowing these models to have access to source domains \mathcal{D}_S other than the ImageNet dataset exclusively. The chapter is structured as follows: we start by providing the reader with some background information in Sec. 4.1. In Sec. 4.2 we present a brief theoretical reminder of the field of TL, a description of the datasets that we have used, and the methodological details about the experiments that we have performed. In Sec. 4.3 we present and discuss our results. A summary of the main contributions of this chapter is finally presented in Sec. 4.4.

This chapter is based on the publication Sabatelli et al. [159].

4.1 A FIRST EMPIRICAL STUDY

In the first part of this thesis, we have seen how convolutional neural networks became a crucial component in today's machine learning toolbox. Thanks to their ability to automatically learn relevant features, these neural networks have become the first algorithmic choice for problems involving high dimensional inputs. As seen in Chapters 1 and 2, convolutional networks can successfully be used for tackling both supervised learning problems, as reinforcement learning ones, provided that it is possible to represent the machine learning task we would like to solve through images¹. Furthermore, thanks to the development of the field of deep transfer learning (Chapter 3), it is now possible to find a broad range of successful applications that see the

¹ For the sake of simplicity we do not consider one-dimensional convolutions.

usage of convolutional networks outside the domain these networks were originally developed for (natural images) [90]. Yet, there still are some domains for which their applicability, and therefore potential transfer learning properties, have not been explored. A promising research field in this sense is that of [Digital Heritage](#) [135]. Due to a growing and rapid process of digitization, museums have started to digitize large parts of their cultural heritage collections, leading to the creation of several digital open datasets [4, 116]. The images constituting these datasets are mostly matched with descriptive metadata, which, as presented by Mensink and Van Gemert [116], can be used for defining a set of challenging machine learning tasks. However, the image samples in these datasets are very different in terms of quantity, size, and resolution from the images that typically constitute popular computer vision benchmarks; therefore, the computer vision potential of convolutional networks in this domain is largely unknown. In this chapter, we address this research question and present a first, thorough, empirical study that explores the potential that convolutional neural networks have to offer when transferred to the artistic domain. The next section moves towards providing the reader with a brief formal reminder of TL. We then introduce the three classification problems that are considered in our study, together with a brief description of the datasets. Finally, we present the neural architectures that we have used for the experiments.

4.2 METHODOLOGY

4.2.1 Transfer Learning

As seen in Chapter 1, a supervised learning (SL) problem can be identified by three elements: an input space \mathcal{X}_T , an output space \mathcal{Y}_T , and a probability distribution $p_T(x, y)$ defined over $\mathcal{X}_T \times \mathcal{Y}_T$ (where T stands for ‘target’, as this is the main problem we would like to solve). The goal of SL is then to build a function $f : \mathcal{X}_T \rightarrow \mathcal{Y}_T$ that minimizes the expectation over $p_T(x, y)$ of a given loss function ℓ assessing the predictions made by f :

$$E_{(x,y) \sim p_T(x,y)} \{\ell(y, f(x))\}, \quad (81)$$

where the only information available to build this function is a learning sample of input-output pairs $LS_T = \{(x_i, y_i) | i = 1, \dots, N_T\}$ drawn independently from $p_T(x, y)$. As introduced in Chapter 3, in the general transfer learning setting, one assumes that an additional dataset LS_S , called the source data, is available that corresponds to a different, but related, SL problem. More formally, the source SL problem is assumed to be defined through a triplet $(\mathcal{X}_S, \mathcal{Y}_S, p_S(x, y))$, where at least either $\mathcal{X}_S \neq \mathcal{X}_T$, $\mathcal{Y}_S \neq \mathcal{Y}_T$, or $p_S \neq p_T$. The goal of TL is then to exploit the source data LS_S together with the target data LS_T to po-

tentially find a better model f in terms of the expected loss (81) than when only LS_T is used for training this model. We have seen that depending on the availability of labels in the target and source data and on how the source and target problems differ, one can distinguish different TL settings (see Sec. ?? of Chapter 3). In what follows, we assume that labels are available in both the source and target data and that the input spaces \mathcal{X}_T and \mathcal{X}_S , that both correspond to color images, match. However, output spaces and joint distributions will differ between the source and target problems, as they will correspond to different classification problems (ImageNet object recognition versus art classification tasks). We, therefore, consider the inductive transfer learning setup and assume that information between the source and target problems is exchanged in the form of a neural network that comes as pre-trained on the source data.

4.2.2 Datasets and Target Tasks \mathcal{T}_T

For our experiments, we use two datasets that come from two different heritage collections. The first one contains the largest number of samples and comes from the Rijksmuseum in Amsterdam². On the other hand, our second ‘Antwerp’ dataset is much smaller. This dataset presents a random sample that is available as open data from a larger heritage repository: DAMS (Digital Asset Management System)³. This repository can be searched manually via the web interface or queried via a Linked Open Data API. It aggregates the digital collections of the foremost GLAM institutions (Galleries, Libraries, Archives, Museums) in the city of Antwerp in Belgium. Thus, this dataset presents a varied and representative sample of the sort of heritage data nowadays being collected at the level of individual cities across the globe. While it is much smaller, its coverage of cultural production is similar to that of the Rijksmuseum dataset and presents an ideal testing ground for the transfer learning task under scrutiny here. Both image datasets come with metadata encoded in the Dublin Core metadata standard [216]. We selected three well-understood classification problems:

- **Material classification:** which consists in identifying the material the different heritage objects are made of (e.g., paper, gold, porcelain, ...);
- **Type classification:** in which the neural networks have to classify in which artistic category the samples fall into (e.g., print, sculpture, drawing, ...);
- **Artist classification:** where the main goal is to match each sample of the dataset with its creator.

² <https://staff.fnwi.uva.nl/t.e.j.mensink/uval2/rijks/>

³ <https://dams.antwerpen.be/>



Figure 13: A visualization of the images that are used for our experiments.

It is possible to see how the samples range from images representing plates made of porcelain to violins, and from Japanese artworks to a more simple picture of a key.

As the goal is to tackle these classification problems through TL, we will refer to them as \mathcal{T}_T ①, \mathcal{T}_T ② and \mathcal{T}_T ③ respectively. As reported in Table 1 we can see that the Rijksmuseum collection is the dataset with the largest amount of samples per target task (N_t) and the highest amount of labels to classify (Q_t). Furthermore, it is also worth noting that there was no metadata available when it comes to the first classification task for the Antwerp dataset (as marked by the – symbol), and that there are some common labels between the two heritage collections when it comes to the classification of types (\mathcal{T}_T ②). A visualization reporting some of the images that are present in both datasets is shown in Figure 13.

Table 1: An overview of the two datasets that are used in our experiments.

For each heritage collection we report with N_t the amount of samples constituting the datasets and with Q_t the number of labels. Lastly, we also report if there are common labels between the two heritage collections.

\mathcal{T}_T	Dataset	N_t	Q_t	% of overlap
Material ①	Rijksmuseum	110,668	206	\emptyset
	Antwerp	–	–	
Type ②	Rijksmuseum	112,012	1,054	$\approx 15\%$
	Antwerp	23,797	920	
Artist ③	Rijksmuseum	82,018	1,196	\emptyset
	Antwerp	18,656	903	

We use 80% of the datasets for training while the remaining $2 \times 10\%$ is used for validation and testing respectively. Furthermore, we ensure that only classes which occur at least once in all the splits are used for our experiments. Naturally, in order to keep all comparisons

fair between neural architectures and different TL approaches, all experiments have been performed on the exact same data splits.

4.2.3 Convolutional Networks and Training Approaches

For our experiments, we use four pre-trained convolutional networks that were reviewed in Chapter 1 and that have all obtained state-of-the-art results on the ImageNet classification challenge. These neural architectures are VGG19 [178], Inception-V3 [191], Xception [30] and ResNet50 [226]. We use the implementations of the networks that are provided by the Keras Deep Learning library [31] together with their appropriate Tensorflow weights [1] that come from the Keras official repository as well. Since all architectures have been built in order to deal with the ImageNet dataset, we replace the final classification layer of each network with a new one. This final layer simply consists of a new softmax output, with as many neurons as there are classes to classify, which follows a 2D global average pooling operation. We rely on this dimensionality reduction step because we do not add any fully connected layers between the last convolution layer and the softmax output. Hence, in this way, we are able to obtain a feature vector, \mathcal{X} , out of the rectified activation feature maps of the network that can be properly classified. Since all experiments are treated as a multi-class classification problem, all networks minimize the categorical crossentropy function loss function. We investigate the potential of the TL approaches that were reviewed in Chapter 3, which, as a reminder, are: the off-the-shelf classification approach, which only trains the final softmax classifier on \mathcal{X} , which is retrieved from the different models after performing one forward pass of the image through the network and the fine-tuning approach, which differs from the previous one by the fact that together with the final softmax output the entire network is trained as well. From now on, we refer to the networks trained with the off-the-shelf classification approach as θ_i^- , while to the fine-tuned networks simply as θ_i , where i stands for the source task \mathcal{T}_S these models have been trained on, namely the ImageNet (i) dataset. In order to maximize the performance of all models, we follow some of the recommendations presented by Masters and Luschi [112] and train the networks with a relatively small batch size of 32 samples. We do not perform any data augmentation operations besides a standard pixel normalization to the $[0, 1]$ range and a re-scaling operation that resizes the images to the input size that the different models require. Regarding the stochastic optimization procedures of the different classifiers, we use two different optimizers, that after preliminary experiments, turned out to be the best-performing ones. For the off-the-shelf approach we use the RMSprop optimizer [197] which has been initialized with its default hyperparameters (learning rate = 0.001, a momentum value $\rho = 0.9$ and

$\epsilon = 1e - 08$). On the other hand, when we fine-tune the models, we use the standard Stochastic Gradient Descent (SGD) algorithm with the same learning rate, 0.001, and a Nesterov Momentum value [127] set to 0.9. Training has been controlled by the early stopping method [28] which interrupted training as soon as the validation loss did not decrease for 7 epochs in a row. The model which is then used on the testing set is the one that obtained the smallest validation loss while training.

4.3 RESULTS

Our experimental results are divided into two sections, depending on which kind of dataset has been used. We first report the results that we have obtained when using architectures that were pre-trained on the ImageNet dataset only and aimed to tackle the three classification tasks of the Rijksmuseum dataset that were presented in Section 4.2.2. We report these results in Section 4.3.1 where we explore the benefits of using the ImageNet dataset as source domain \mathcal{D}_S only, and how well such pre-trained models generalize when it comes to the artistic target domain. We then present the results from classifying the Antwerp dataset, using models that are both pre-trained on the ImageNet dataset and on the Rijksmuseum collection in Section 4.3.3. We investigate whether these neural architectures, which have already been trained to tackle art classification problems before, perform better than those trained on the ImageNet dataset only. All results show comparisons between the off-the-shelf classification approach and the fine-tuning scenario. In addition to that, in order to establish the potential benefits that TL from ImageNet has over training a model from scratch, we also report the results that have been obtained when training a network with weights that have been initially sampled from a He-Uniform distribution [67]. Since we take advantage of the work presented by Bidoia et al. [19] we use the Inception-V3 architecture. We refer to it in all figures as Scratch-V3 and always visualize it with a solid orange line. Figures 14 and 15 report the performance in terms of accuracy (%) that the models have obtained on the validation sets. While the performance that the neural architectures have obtained on the final testing set are reported in Tables 2 and 3.

4.3.1 From Natural to Non Natural Images

The first results that we report have been obtained on \mathcal{T}_T ①, namely the material classification task. We believe that this can be considered as the easiest classification task within the ones that we have introduced in Section 4.2.2 for two main reasons: first, the number of possible classes the networks have to deal with is more than five times smaller when compared to the other two challenges; second, we also

believe that this classification task is, within limits, the most similar one when compared to the original ImageNet challenge. Hence, the features that might be useful to classify the different natural images on the latter classification testbed might not be too dissimilar from the ones needed to properly recognize the material that the different samples of the Rijksmuseum collection are made of. If this were the case, we would expect a very similar performance between the off-the-shelf classification approach and the fine-tuning one. Comparing the learning curves of the two classification strategies in Figure 14, we observe that the fine-tuning approach leads to significant improvements when compared to the off-the-shelf one for three architectures out of the four tested ones. Note, however, that, in support of our hypothesis, the off-the-shelf approach can still reach high accuracy values on this problem and is also competitive with the model trained from scratch, with the crucial difference being that these models result in faster training as **jumpstart improvements** can be observed. This suggests that features extracted from networks pretrained on ImageNet are relevant for the target task \mathcal{T}_T of material classification.

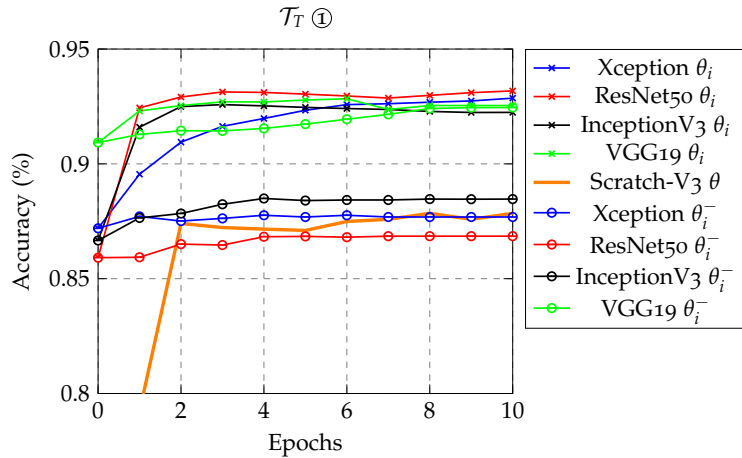


Figure 14: Comparison between the fine-tuning approach (θ_i) versus the off-the-shelf one (θ_i^-) when classifying the material of the heritage objects of the Rijksmuseum dataset. We can observe that for three out of four neural architectures the first approach leads to significant improvements when compared to the latter one. Furthermore, we can also observe that training a randomly initialized model from scratch (solid orange line) leads to worse results than fine-tuning a network that comes as pre-trained on the ImageNet dataset.

We can also observe that the ResNet50 architecture is the architecture that, when fine-tuned, performs overall best compared to the other three models. This happens despite it being the network that initially performed worse as a simple feature extractor in the off-the-shelf experiments. As reported in Table 2 we can see that this kind of behavior reflects itself on the separated testing set as well, where it ob-

tained the highest testing set accuracy when fine-tuned (92.95%), and the lowest one when the off-the-shelf approach was used (86.81%). It is worth noting that the performance between the different neural architectures do not strongly differ between each other once they are fine-tuned, with all models performing around $\approx 92\%$ on the final testing set. Furthermore, special attention needs to be given to the VGG19 architecture, which does not seem to benefit from the fine-tuning approach as much as the other architectures do. In fact, its off-the-shelf performance on the testing set (92.12%) is very similar to its fine-tuned one (92.23%). This suggests that this neural architecture is the only one that, in this task, and when pre-trained on ImageNet, can successfully be used as a simple feature extractor without relying on complete retraining.

When analyzing the performance of the different neural architectures on \mathcal{T}_T ② (type classification) and \mathcal{T}_T ③ (artist classification), respectively the left and right plots reported in Figure 15, we observe that on these problems the fine-tuning strategy leads to even more significant improvements when compared to what we observed in the previous experiment. The results obtained on the second task show again that the ResNet50 architecture is the architecture that leads to the worse results if the off-the-shelf approach is used (its testing set accuracy is as low as 71.23%), and similarly to what has been observed before, it then becomes the best performing model when fine-tuned, with a final accuracy of 91.30%. Differently from what has been observed in the previous experiment, the VGG19 architecture, despite being the network performing best when used as off-the-shelf feature extractor, this time performs significantly worse than when it is fine-tuned, which highlights the benefits of this latter training approach. Similar to what has been observed before, our results are again not significantly favoring any fine-tuned neural architecture, with all final accuracies being around $\approx 91\%$.

If the so far considered target tasks have highlighted the significant benefits of the fine-tuning approach over the off-the-shelf one, it is also important to note that the latter approach is still able to yield satisfying results. In fact, a final accuracy of 92.12% has been obtained when using the VGG19 architecture for tackling \mathcal{T}_T ①, and the same architecture reached a classification rate of 77.33% on \mathcal{T}_T ②. Despite the latter accuracy being very far in terms of performance from the one obtained when fine-tuning the network (90.27%), these results still show that models pre-trained on ImageNet do learn particular features that can also be used for classifying the material and the type of heritage objects, as **jumpstart improvements** can be observed in Fig. 14 and in the first plot of Fig. 15. However, when analyzing the \mathcal{T}_T ② results, we can see that this is partially not the case anymore.

When considering the third target task, we can observe that the Xception, ResNet50, and Inception-V3 architectures perform extremely

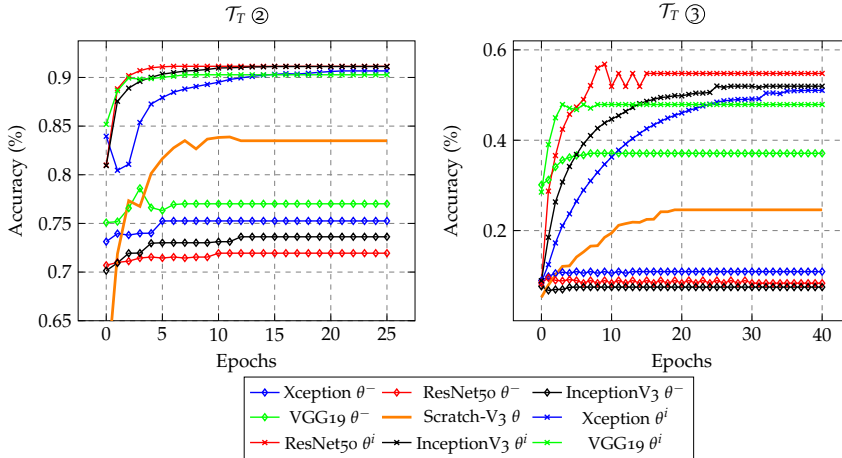


Figure 15: A similar analysis as the one which has been reported in Figure 14 but for the second and third classification tasks (left and right figures respectively). The results show again the significant benefits that fine-tuning (reported by the dashed line plots) has when compared to the off-the-shelf approach (reported by the dash-dotted lines) and how this latter strategy miserably underperforms when it comes to artist classification. Furthermore we again see the benefits that using a pre-trained model has over training the architecture from scratch (solid orange line).

poorly if not fine-tuned, with the latter two models not reaching a 10% classification rate. Better results are obtained when using the VGG19 architecture, which reaches a final accuracy of 38.11%. Most importantly, the performance of each model is again significantly improved when the networks are fine-tuned. As already observed in the previous experiments, ResNet50 outperforms the other architectures on the validation set. However, on the test set (see Table 2), the overall best performing network is Inception-V3 (with a final accuracy of 51.73%), which suggests that ResNet50 suffered from overfitting. It is important to state two major important points about this set of experiments. The first one relates to the final classification accuracy that is obtained by all models, and that at first sight might seem disappointing. While it is true that these classification rates are significantly lower when compared to the ones obtained in the previous two experiments, it is important to highlight how a large set of artists present in the dataset are associated to a minimal amount of samples. This reflects a lack of appropriate training data, which does not allow the models to learn all the necessary features for successfully dealing with this particular classification challenge. In order to do so, we believe that more training data is required. Moreover, it is worth pointing out that despite performing very poorly when used as off-the-shelf feature extractors, ImageNet pre-trained models do still perform better once they are fine-tuned than a model that is trained from scratch, as **asymptotic improvements** were observed in all our

experiments. This suggests that these networks do learn potentially representative features when it comes to the classification of artists, but in order to correctly classify them, fine-tuning is required.

Table 2: An overview of the results obtained by the different models on the testing set when classifying the heritage objects of the Rijksmuseum. The overall best performing architecture is reported in a green cell, while the second best performing one is reported in a yellow one. The additional columns “Params” and “ \mathcal{X} ” report the amount of parameters the networks have to learn and the size of the feature vector that is used as input for the softmax classifier.

\mathcal{T}_T	model	off the shelf	fine tuning	Params	\mathcal{X}
①	Xception	87.69%	92.13%	21K	2048
①	InceptionV3	88.24%	92.10%	22K	2048
①	ResNet50	86.81%	92.95%	24K	2048
①	VGG19	92.12%	92.23%	20K	512
②	Xception	74.80%	90.67%	23K	2048
②	InceptionV3	72.96%	91.03%	24K	2048
②	ResNet50	71.23%	91.30%	25K	2048
②	VGG19	77.33%	90.27%	20K	512
③	Xception	10.92%	51.43%	23K	2048
③	InceptionV3	.07%	51.73%	24K	2048
③	ResNet50	.08%	46.13%	26K	2048
③	VGG19	38.11%	44.98%	20K	512

4.3.2 Discussion

In the previous section, we have investigated whether four different architectures pre-trained on the ImageNet dataset can be successfully used to address three art classification problems. We have observed that this is particularly the case when it comes to classifying the material and the type, where in fact, an off-the-shelf classification approach already yielded satisfactory results. However, most importantly, we have also shown that the performance of all models can be significantly improved when the networks are fine-tuned and that an ImageNet initialization is beneficial when compared to training a randomly initialized network from scratch. Furthermore, we have also shown that ImageNet pre-trained models can still perform extremely poorly when they are used as simple feature extractors (as demonstrated by the experiments reported on \mathcal{T}_T ③). In the next section, we explore the performance of fine-tuned models trained to tackle two of the already seen target tasks on a different heritage collection. For

this problem, we will again compare the off-the-shelf approach with the fine-tuning one.

4.3.3 From One Target Domain \mathcal{D}_T to Another

Table 3 compares the results that we obtained on the Antwerp dataset when using ImageNet pre-trained models (θ^i) versus the same architectures that were fine-tuned on the Rijksmuseum dataset (θ^r). While looking at the performance of the different neural architectures, two interesting results can be highlighted. First, models which have been fine-tuned on the Rijksmuseum dataset outperform the ones pre-trained on ImageNet on both target tasks \mathcal{T}_T . This happens to be the case both when the networks are used as simple feature extractors and when they are fine-tuned. On \mathcal{T}_T ②, this result is not surprising since, as discussed in Section 4.2.2, the types corresponding to the heritage objects of the two collections partially overlap. This is, however, more surprising when it comes to the artist classification tasks \mathcal{T}_T ③ as there is no overlap at all between the artists of the Rijksmuseum and the ones from the Antwerp dataset. A second interesting result, which is consistent with the results presented in the previous section, revolves around the observation that it is always beneficial to fine-tune the networks over just using them as off-the-shelf feature extractors. Once the models get fine-tuned on the Antwerp dataset, these networks, which have also been fine-tuned on the additional source domain of the Rijksmuseum dataset, outperform the architectures that were pre-trained on ImageNet only. This happened to be the case for both target tasks \mathcal{T}_T , and for all considered architectures, as reported in Table 3. This demonstrates how beneficial it is for the models to have been trained on a similar source task and how this can lead to significant improvements both when the networks are used as feature extractors as when they are fine-tuned.

Table 3: The results obtained on the classification experiments performed on the Antwerp dataset with models that have been initially pre-trained on ImageNet (θ^i) and the same architectures which have been fine tuned on the Rijksmuseum dataset (θ^r). Our results show that the latter pre-trained networks yield better results both if used as off the shelf feature extractors and if fine tuned.

\mathcal{T}_T	model	θ^i + off the shelf	θ^r + off the shelf	θ^i + fine tuning	θ^r + fine tuning
②	Xception	42.01%	62.92%	69.74%	72.03%
②	InceptionV3	43.90%	57.65%	70.58%	71.88%
②	ResNet50	41.59%	64.95%	76.50%	78.15%
②	VGG19	38.36%	60.10%	70.37%	71.21%
③	Xception	48.52%	54.81%	58.15%	58.47%
③	InceptionV3	21.29%	53.41%	56.68%	57.84%
③	ResNet50	22.39%	31.38%	62.57%	69.01%
③	VGG19	49.90%	53.52%	54.90%	60.01%

4.3.4 Selective Attention

The benefits of the fine-tuning approach over the off-the-shelf one are clear from our previous experiments. Nevertheless, we do not have any insights yet about what exactly allows fine-tuned models to outperform the Imagenet only pre-trained architectures. In order to provide an answer to that, we investigate which pixels of each input image contribute the most to the final classification predictions of the networks. We do this by using the “VisualBackProp” algorithm presented by [20], which is able to identify which feature maps of the networks are the most informative ones with respect to their final prediction. Once these feature maps are identified, they get backpropagated to the original input image and visualized as a saliency map according to their weights. The higher the activation of the filters, the brighter the set of pixels covered by these filters are represented.

The results that we have obtained provide interesting insights into how fine-tuned models develop novel selective attention mechanisms over the images, which are very different from those that characterize the ImageNet only pre-trained networks. We report the existence of these mechanisms in Figure 16 where we visualize the different saliency maps between a model pre-trained on ImageNet and the same neural architecture, which has been fine-tuned on the Rijksmuseum collection. In Figure 16 we visualize which sets of pixels allow the fine-tuned model to successfully classify an artist of the Rijksmuseum collection that the same architecture was not able to recognize initially. It is possible to notice that the saliency maps of the latter architecture either correspond to what is more similar to a natural image, as represented by the central image of the first row of plots, or even to what appear to be non-informative pixels at all, as shown by the second image in the second row. However, when considering the fine-tuned model, we clearly observe that these saliency maps change. In this case, the network attends towards the set of pixels representing people at the bottom, suggesting that this allows the model to recognize the artist of the considered artwork appropriately.

These observations can be related to parallel insights in authorship attribution research [43], an established task from Natural Language Processing that is highly similar in nature to artist recognition. In this field, preference is typically given to high-frequency function words (articles, prepositions, particles etc.) over content words (nouns, adjectives, verbs, etc.), because the former are generally considered to be less strongly related to the specific content or topic of a work. As such, function words or stop words lend themselves more easily to attribution across different topics and genres. In art history, strikingly similar views have been expressed by the well-known scholar Giovanni Morelli (1816-1891), who published seminal studies in the field of artist recognition [224]. In Morelli’s view too, the attribution

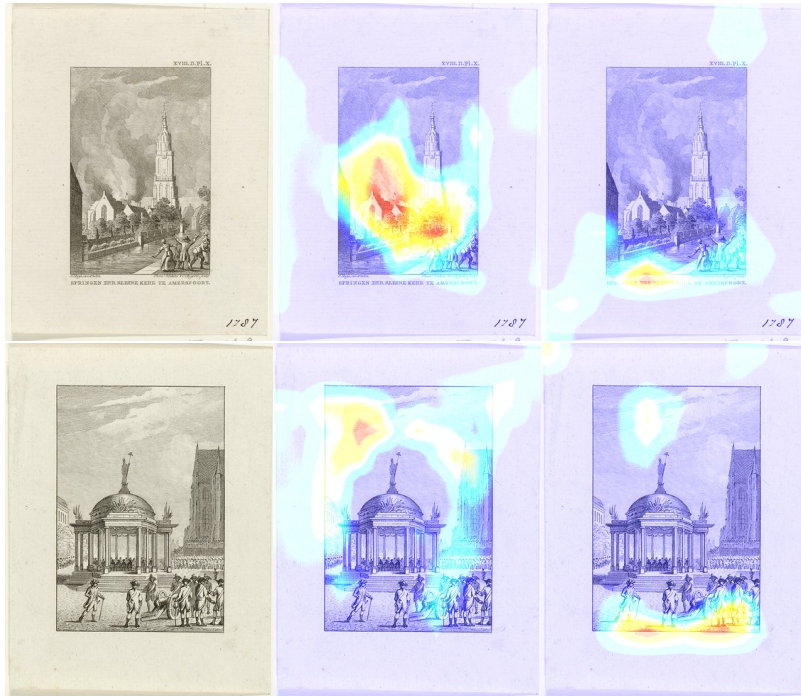


Figure 16: A visualization of the saliency maps that are obtained when trying to classify an artist of the Rijksmuseum collection (first row of images) with either an ImageNet pre-trained model that is used as simple feature extractor (second row of images), or with the same kind of model which gets fine-tuned (third row of images). We can observe that after getting fine-tuned the network develops novel selective attention mechanisms that allow it to shift its attention from e.g., the buildings depicted in the paintings to the people represented at the bottom.

of a painting could not happen on the basis of the specific content or composition of a painting, because these items were too strongly influenced by the topic of a painting or the wishes of a patron. Instead, Morelli proposed to base attributions to so-called *Grundformen* or small, seemingly insignificant details that occur frequently in all paintings and typically show clear traces of an artist's individual style, such as ears, hands or feet, a painting's function words, so to speak. The saliency maps above reveal a similar shift in attention when the ImageNet weights are adapted on the Rijksmuseum data: instead of focusing on higher-level content features, the network shifts its attention to lower layers in the network, seemingly focusing on insignificant details, that nevertheless appear crucial to perform artist attribution.

4.4 CONCLUSION

This chapter provides the first insights into the potential that TL can offer for art classification. We have investigated the behavior of con-

volutional networks which have been pre-trained initially on a very different classification task and shown how their performances can be improved when these networks are fine-tuned. Moreover, we have observed that such neural architectures perform better than if they are trained from scratch and that during the fine-tuning stage, they develop new saliency maps that can provide insights about what makes these models outperform the ones that are pre-trained on the ImageNet dataset only. Such saliency maps reflect themselves in the development of new features, which can then be successfully used by the models when classifying heritage objects from different heritage collections. It turns out that the fine-tuned models are a better alternative to the same kind of architectures that are pre-trained on ImageNet only and can serve the CV community, which will deal with similar machine learning problems.

TODO: wrap up the chapter

OUTLINE

In this chapter, we continue studying the transfer learning properties of convolutional neural networks trained on non-natural image distributions. To facilitate this process, we present MINERVA, a novel dataset that can be used both for object classification as for object detection. We report thorough experiments that highlight the challenges that can arise from using MINERVA as a computer vision testbed, while at the same time, we further characterize the benefits that can come from adopting transfer learning training strategies. The structure of this chapter is the following: in Sec. 5.1 we describe some of the limitations that currently define the field of computer vision and that have served as inspiration for the development of our newly introduced dataset. In Sec. 5.2 we present MINERVA, we thoroughly explain how its images have been collected and annotated, and how the resulting splits have served for the experiments that are presented in Sec. 5.3. We then report and discuss the results of our experiments in Sec. 5.4 and Sec. 5.5 respectively, before ending the chapter by identifying possible avenues for future work in Sec. 5.6.

This chapter is based on the publication Sabatelli et al. [163].

5.1 CHALLENGES OF MODERN COMPUTER VISION

If it is true that the results presented in the previous chapter show that it is possible to transfer pre-trained convolutional neural networks to non-natural image datasets successfully, it is equally true that some limitations might still need to be addressed. Above all, the need to fine-tune the networks instead of simply using them as feature extractors. As demonstrated by the experiments performed on the third classification problem of the Rijksmuseum dataset, it is clear that pre-trained models might only learn features that are relevant for their respective source task \mathcal{T}_S (ImageNet), which therefore might result in unsatisfying performance when an off-the-shelf training strategy is used. While this is a result that does not come as a surprise, as it would be unreasonable to expect pre-trained networks to act as universal feature extractors, this limitation can still have some important practical implications since it can prevent the deployment of computer vision systems outside the domain of natural images. As a

practical example, let us consider the first image presented in Fig. 17 and the computer vision task of object detection. We tackle this task with an object detector that is pre-trained on natural images only and that, therefore, has never seen any images coming from a domain other than the source domain \mathcal{D}_S . From the model's performance, it is clear that only one out of the two predictions made by the network is appropriate, as it fails in detecting the musical instrument depicted in the image by wrongly classifying it as a 'frisbee'. While certainly reasonable and fully justifiable, this kind of performance is the result of some limitations that currently characterize modern Computer Vision (CV), which we summarize as follows:

- **Photorealism and Data Scarcity:** it is well known that modern CV strongly gravitates towards photorealistic material since most of the datasets that are used in the field are representative of digitized, or born-digital, versions of photographs. Nevertheless, datasets like MNIST, CIFAR-10/100 and the already mentioned ImageNet play a crucial role in today's rapid development of the field, as they are constantly used as benchmarks by the community. While certainly suitable for defining different challenging CV tasks, it is worth noting that these datasets are also only partially representative of the physical world, as they do not actively attempt to distort the reality they depict. Unfortunately, datasets going beyond the photorealistic domain are either much rarer, or are not as popular as their photorealistic counterparts, a limitation that results into pre-trained models that fail in performing well when used outside from the natural world (see again first image of Fig. 17).
- **Modern Training Classes:** the performance depicted in the first image of Fig. 17 can largely be attributed to the fact that the model used for detecting the objects in the image has never been explicitly trained on images of musical instruments. As a result its predictions can only tend to be representative of the classes that have governed the training process. While this behavior has only to be expected, it can still serve as a surrogate for highlighting an important limitation of modern object detection datasets: datasets are not as diversified and heterogeneous as one might expect. As an example let us consider the popular Pascal-Voc [44] and MS-COCO [106] datasets. The first one tackles the detection of 20 classes, out of which more than a third constitute different kinds of transportation systems, such as 'trains', 'boats', 'motorcycles' and 'cars'. The latter, albeit more complex, mostly represents objects that are representative of the highly technological world we currently live in, with classes such as 'microwave', 'laptop' and 'remote control'. In practice, this results in models that gravitate towards

detecting objects in an image that are modern, a behavior that hurts not-technological classes such as the ‘person’ one, which should, but unfortunately is not, detected in the second image of Fig. 17.

- **Model Robustness:** the aforementioned limitation also results into models that learn features that are hardly general enough for successfully tackling different representations of the same class. As an example, let us consider the last image of Fig. 17: we can see that a model pre-trained on MS-COCO successfully detects the persons represented in the paintings only as long as their pose corresponds to a pose that can easily be found in the images depicting persons in photorealistic datasets. As soon as a person is depicted in a pose different from the one that usually characterizes a person in a photorealistic dataset (sitting or standing), then a pre-trained network mistakenly detects it like an animal.



Figure 17: Some examples that show the limitations of object detectors that are trained on photorealistic images only. In the first image, we see how a model confidently detects a ‘frisbee’ for a ‘lute’, while in the second image, we can observe how next to being unable to detect the people in the painting, it also mistakenly detects the frame as a ‘tv-monitor’. Similar limitations can be observed in the final image, where we can see that the persons within the painting are only correctly detected as long as they are either sitting or standing.

This chapter takes inspiration from these limitations and uses them as a surrogate for introducing novel datasets that can be used as a benchmark for CV researchers. The purpose of such datasets is twofold: on the one hand, they represent, at least in part, a solution to the aforementioned issues that currently characterize CV, while on the other hand, they allow us to continue studying the transfer learning properties of convolutional neural networks which we started exploring in the previous chapter.

5.2 THE MINERVA DATASET

We now introduce MINERVA, a novel annotated dataset that can be used for object detection. More specifically, the main task that we present is that of the detection of musical instruments in non-photorealistic, unrestricted image collections from the artistic domain. We start by describing how its images have been first collected and then annotated, while we then move on towards quantitatively characterizing the dataset from a machine learning perspective.

5.2.1 Data Collection

The images constituting MINERVA come from three different data sources, which allow the dataset to be highly varied and unrestricted. Its images cover a large range of periods, genres, and materials and are both of photorealistic and not-photorealistic nature as visually represented in Fig. 18. The three data sources are the following:

- RIDIM: which stays for *Repertoire International d'Iconographie Musicale* is an international digital inventory for musical iconography that functions as a reference image database. Developed and curated by Green and Ferguson [60] it has been designed to facilitate the discovery of music-related artworks. Among the three different considered data sources, the images coming from the RIDIM collection are the ones of the highest quality in terms of resolution.
- RMFAB/RMAH: which stays for *Royal Museums of Fine Arts of Belgium* and *Royal Museums of Art and History*. These images come from a larger pool of digitized images that have been manually selected based on whether they included depictions of musical instruments or not. Among the different data sources, the amount of images coming from RMFAB/RMAH within MINERVA is the lowest compared to the other two data sources. These images are of midrange resolution.
- Flickr: is a well-known image hosting service from which we downloaded a large dataset of images depicting musical instruments in the visual arts pre-dating 1800. Most of the images present within MINERVA come from Flickr, although their resolution is not always on par with the previous two data sources.

Once all these images have been collected we have started the labeling process.



Figure 18: Samples from Minerva.

5.2.2 Annotation Process

We manually annotated almost 10000 instruments by using the conventional method of rectangular bounding boxes. To this end, we have used the open-source Cytomine software [111], a rich web environment that allows highly collaborative analysis of multi-gigapixel imaging data. Initially developed for facilitating the task of image annotation in biomedical informatics, Cytomine has already been widely used for the annotation and creation of several datasets [124]. However, it is worth noting that its use within the present study is among the very first ones which use the software outside the context of large-scale bioimaging data. All the individual instruments within MINERVA have been unambiguously identified and labeled by using their MIMO codes. The MIMO (Musical Instrument Museums Online) initiative is an international consortium, well known for its online database of musical instruments, aggregating data and metadata from multiple heritage institutions [38]. An important contribution of Dolan [38] is the development of a uniform metadata documentation standard for the field, including a multilingual vocabulary that can be used for identifying musical instruments in an interoperable manner. We have followed this metadata standard and manually labeled the previously collected images within Cytomine as visually represented in Fig. ??.

5.2.3 Versions and Splits

MINERVA comes in four different, increasingly complex versions: Minerva-0 which is arguably the easiest version of the dataset where

the target task \mathcal{T}_T simply consists in detecting whether a musical instrument is present within an image or not. We, therefore, do not yet consider the task of predicting the class of the detected instrument. The second version of the dataset is Minerva-Hypernym where the goal is that of detecting all the images present within Minerva-0 and classify them according to their hypernym categories. All instruments present within MINERVA correspond to 5 different hypernyms which define them as: ‘stringed instruments”, ‘wind instruments”, ‘percussion instruments”, ‘keyboard instruments” and ‘electronic instruments’. The last two versions of MINERVA are Minerva-5 and Minerva-10 where the goal is to detect and classify the instruments depicted in the images according to the top 5 or top 10 most occurring classes. These classes are: ‘Lute”, ‘Harp”, ‘Violin”, ‘Trumpet”, ‘Shawn”, ‘Bagpipe”, ‘Organ”, ‘Horn”, ‘Rebec” and ‘Lyre”. Naturally, in Minerva-5 we only consider the first 5 of such classes, whereas in Minerva-10 we consider all 10 of them. Each version of the dataset comes with its training, validation, and testing splits, where we offer the guarantee that at least one of the instrument classes in the task is represented in each of the splits. Additionally, the splits are stratified so that the class distribution is approximately the same in each split. The number of images per split in each version is summarized in Table 4 where N_t corresponds to the number of images present within the split, whereas I_t denotes the number of total instruments. The hypernym version of the dataset is not reported as it shares the same images and splits as Minerva-0 (they both contain all instruments). However, a distribution of the hypernym classes within Minerva-Hypernym is reported in Fig. 19. All splits have been created with the scikit-learn software [137] by using 50% of the images for training and the remaining 50% for validation and testing (25% respectively).

Table 4: An overview reporting how many images N_t and instruments I_t are present within the splits of the Minerva-0, Minerva-5 and Minerva-10 versions of the MINERVA dataset.

\mathcal{T}_T	training-set		validation-set		testing-set	
	N_t	I_t	N_t	I_t	N_t	I_t
Minerva-0	1857	4243	1137	2288	1182	2102
Minerva-5	952	1589	540	852	721	1173
Minerva-10	1227	2147	680	1127	897	1506

5.3 BENCHMARKING

While MINERVA has been created with the primary intention of serving as a novel dataset for object detection, it can nevertheless still be

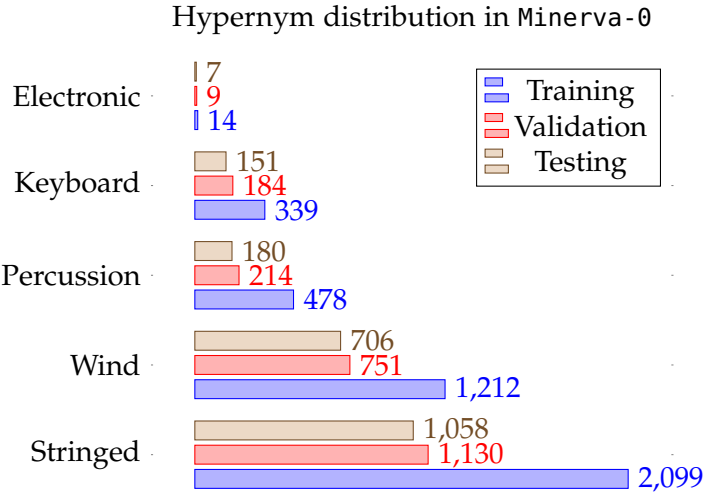


Figure 19: A visual representation of the distribution of the hypernym classes that are present within Minerva-0 and that define the Minerva-Hypernym benchmark.

used to test the classification performance of convolutional neural networks. Although this task is certainly easier than object detection, it is still of high interest as it provides a novel benchmark for further characterizing the transfer learning properties of neural networks that we started studying in the previous chapter. Therefore, we hereafter report results both for **classification** experiments as for **object detection** experiments. In the first section, we consider the target task \mathcal{T}_T of classifying the bounding boxes that have been annotated in MINERVA as standalone images, while in the second section, we aim at both detecting and classifying the content of the potentially detected bounding boxes. We hereafter describe the experimental protocol used for both sets of experiments in detail.

5.3.1 Classification

The experimental setup used for the classification experiments largely builds on top of the study that we presented in Chapter 4. We continue to explore whether popular neural architectures, which have obtained state-of-the-art results on the ImageNet benchmark, can perform equally well when trained on datasets of non-natural images. To this end, we again consider the well known VGG19 [178], InceptionV3 [191] and ResNet50 [226] neural architectures. As done in the previous chapter, we keep investigating the effect that different weight initialization strategies have on the final performance of the networks to characterize further the potential benefits that can come from adopting transfer learning. Specifically, we train the three considered neural architectures by following three different initialization strategies: 'random' which simply initializes the model's parameters after following

a He et al. [67] weight initialization strategy, ‘ImageNet’ which instead uses the weights that are obtained after training the networks on the ImageNet source task \mathcal{T}_S , and ‘RijksNet’ which are models that are trained both on the ImageNet dataset and on the Rijksmuseum collection, and that were also used for the final experiments reported in the previous chapter. As the benefits of fully fine-tuning the models over using them as off-the-shelf feature extractors were clear from the results obtained in Chapter 4, we now limit our analysis to this transfer-learning approach solely. We train all networks with the Adam optimizer [86] and by using an initial learning rate of 0.001. As already done for the previous study, we again controlled the training process by using early stopping and by interrupting the training regime as soon as the validation loss did not decrease for five epochs in a row. Naturally, all networks minimize the categorical crossentropy loss function.

5.3.2 Object Detection

For this set of experiments we explore the performance of a YOLO object detector [148], a popular neural architecture that has obtained state-of-the-art results on the MS-COCO object detection benchmark. YOLO treats the task of object detection as a standard regression problem by dividing an image into a $S \times S$ grid and by predicting for each grid cell B bounding boxes and C class probabilities. The main assumption behind YOLO is that any of the $S \times S$ cells contains at most the center of one single object, therefore for every image, cell index $i = 1, \dots, S \times S$, predicted box $j = 1, \dots, B$ and class index $c = 1, \dots, C$ we have the following components:

- $\mathbb{1}_i^{\text{obj}}$ which is 1 if there is an object in cell i , and 0 otherwise;
- $\mathbb{1}_{i,j}^{\text{obj}}$ which is 1 if there is an object in cell i and predicted box j that is the most fitting one, whereas is 0 otherwise;
- $p_{i,c}$ which is 1 if there is an object of class c in cell i , and 0 otherwise;
- x_i, y_i, w_i, h_i which are the coordinates of an annotated bounding box that are defined only if $\mathbb{1}_i^{\text{obj}} = 1$;
- $c_{i,j}$ which is the IoU between the predicted box and the ground truth target.

At training, YOLO computes the value of the $\mathbb{1}_{i,j}^{\text{obj}}$ for each image together with the respective $c_{i,j}$, and then minimizes the following multi-part loss function:

$$\begin{aligned}
& \lambda_{\text{coord}} \sum_{i=1}^{S \times S} \sum_{j=1}^B \mathbb{1}_{i,j}^{\text{obj}} \left((x_i - \hat{x}_{i,j})^2 + (y_i - \hat{y}_{i,j})^2 + (\sqrt{w_i} - \sqrt{\hat{w}_{i,j}})^2 + (\sqrt{h_i} - \sqrt{\hat{h}_{i,j}})^2 \right) \\
& + \lambda_{\text{obj}} \sum_{i=1}^{S \times S} \sum_{j=1}^B \mathbb{1}_{i,j}^{\text{obj}} (c_{i,j} - \hat{c}_{i,j})^2 + \lambda_{\text{noobj}} \sum_{i=1}^{S \times S} \sum_{j=1}^B (1 - \mathbb{1}_{i,j}^{\text{obj}}) \hat{c}_{i,j}^2 \\
& + \lambda_{\text{classes}} \sum_{i=1}^{S \times S} \mathbb{1}_i^{\text{obj}} \sum_{c=1}^C (p_{i,c} - \hat{p}_{i,c})^2
\end{aligned}$$

where $\hat{p}_{i,c}$, $\hat{x}_{i,j}$, $\hat{y}_{i,j}$, $\hat{w}_{i,j}$, $\hat{h}_{i,j}$ and $\hat{c}_{i,j}$ are the predictions of the network.

In our experiments, we use the YOLO-V3 version of the network introduced by Redmon and Farhadi [149] and initialize it with the weights that are obtained after training the network on the MS-COCO dataset. Regarding the stochastic optimization procedure, we use two different optimizers: we train the network with the Adam optimizer for the first 10 epochs, while we then use the RMSprop optimizer for the remaining training epochs, which are again controlled through early stopping. To assess the final performance of the model, we follow an evaluation protocol that is typical for object detection problems in CV [106]. Each detected bounding box is compared to the bounding box, which has been annotated on the Cytomine platform. We only consider bounding boxes for which the confidence level is ≥ 0.05 , following the protocol established by Everingham et al. [44]. We then compute the "Intersection over Union" (IoU) for measuring how much the detected bounding-boxes differ from the ground-truth ones. To assess whether a prediction can be considered as a true positive or a false positive, we define two increasingly restrictive metrics: first, $\text{IoU} \geq 10$ and, secondly, $\text{IoU} \geq 50$. This approach is inspired by the work of Gonthier et al. [58], where the authors report results for both IoU thresholds when assessing the performance of their weakly supervised learning system on the IconArt dataset.

5.4 RESULTS

5.4.1 Quantitative Analysis

CLASSIFICATION We start by discussing the results obtained with our classification experiments. The performance of all models is reported in Tables 5, 6 and 7, where we present the accuracy that the networks have obtained on the different MINERVA testing sets, together with their respective F-1 scores. To this end for a given class

c , a ground truth label y and a model's prediction \hat{y} , let us introduce the notions of precision and recall. The first is computed as:

$$P(c) = p(y = c | \hat{y} = c) = \frac{TP}{TP + FP}, \quad (82)$$

while the latter as

$$R(c) = p(y = c | \hat{y} = c) = \frac{TP}{TP + FN}. \quad (83)$$

Both quantities can be used for computing the F-1 score as follows:

$$F_1(c) = 2 \cdot \frac{P(c) \cdot R(c)}{P + R}. \quad (84)$$

Similarly to the results reported in Chapter 4 we again report the best performing architecture in a green cell, while the second-best performing model in a yellow one.

We can start by observing that among all the results presented in the three different tables, the best performing models are either the ones reported in Table 6 or the ones presented in Table 7. This confirms the results that were presented in the previous chapter: fine-tuning pre-trained models yields significantly better results than training models from scratch, even when the source and the target tasks can be particularly different (as is the case for musical instruments classification). While the results of this study confirm the conclusions that were drawn at the end of Chapter 4, they also provide some additional insights that were not observed before. First, it appears that the best performing architecture is not ResNet50 anymore, but rather the arguably older InceptionV3, a result which seems to suggest that there is no overall best-performing architecture for all target tasks \mathcal{T}_T , and that the best architecture is highly problem dependent. Second, and perhaps arguably more surprising, we can also see that differently from what was observed in the last experiment in Chapter 4, it appears to be more beneficial to transfer models pre-trained on ImageNet only, instead of models that are additionally trained on the Rijksmuseum collection. Indeed, as can be observed by the results presented in Tables 6 and 7, the latter pre-training strategy outperforms the first one only when the ResNet50 and the InceptionV3 architectures are trained on the Minerva-5 benchmark. These results can be explained as follows: in Chapter 4 the target task \mathcal{T}_T tackled with a model pre-trained on the Rijksmuseum collection corresponded to the original source task \mathcal{T}_S (classification of 'types' and 'artists'). In these experiments, however, albeit coming from similar domains, the considered source task \mathcal{T}_S and target task \mathcal{T}_T are unrelated, which could work in favor of an arguably more general ImageNet weight initialization.

Table 5: Results obtained when classifying the bounding boxes of the three different MINERVA benchmarks with models that do not come as pre-trained on any sort of source task \mathcal{T}_S . We can see that their performance is significantly worse than the one that is obtained when the same models come as pre-trained (see Table 6 and Table 7).

\mathcal{T}_T	ResNet50		InceptionV3		VGG19	
	Accuracy (%)	F1	Accuracy (%)	F1	Accuracy (%)	F1
Minerva-Hypernym	50.33	13.39	51.80	14.02	50.12	13.12
Minerva-5	40.83	21.88	40.49	21.65	41.26	22.01
Minerva-10	32.85	0.09	32.18	0.09	19.72	0.03

Table 6: Results obtained when classifying the bounding boxes of the three different MINERVA benchmarks after adapting transfer learning and considering the ImageNet dataset as the only source task \mathcal{T}_S . We observe that, compared to the results presented in Table 5, this approach yields significant benefits, therefore confirming the results presented in Chapter 4.

\mathcal{T}_T	ResNet50		InceptionV3		VGG19	
	Accuracy (%)	F1	Accuracy (%)	F1	Accuracy (%)	F1
Minerva-Hypernym	76.64	58.56	79.40	60.07	76.54	57.39
Minerva-5	60.41	49.10	72.06	68.89	70.43	68.42
Minerva-10	55.37	41.65	60.1	45.12	44.22	40.12

Table 7: Results obtained when classifying the bounding boxes of the three different MINERVA benchmarks after adapting transfer learning and considering the ImageNet and the Rijksmuseum collection as source domains \mathcal{D}_S . Similarly to what was observed in Table 6, we can again see that transfer learning yields significant benefits although this weight initialization strategy does mostly not outperform the more common ImageNet one.

\mathcal{T}_T	ResNet50		InceptionV3		VGG19	
	Accuracy (%)	F1	Accuracy (%)	F1	Accuracy (%)	F1
Minerva-Hypernym	72.26	52.66	75.80	57.03	66.41	40.35
Minerva-5	68.71	64.10	73.66	70.29	48.33	33.92
Minerva-10	52.85	41.55	55.51	45.77	37.52	15.22

OBJECT DETECTION The results for this set of experiments are reported in terms of average precision as for each class; we report the area under the precision-recall curve that is obtained by setting IoU ≥ 10 and ≥ 50 as explained in Sec. 5.3.2. We start by discussing the performance that is obtained after fine-tuning a pre-trained YOLO-V3 model on the Minerva-0 benchmark, where, as a reminder, the goal is that of simply detecting a musical instrument within an image without classifying it. For an IoU ≥ 10 we report an average precision of 35.33%, while for an IoU ≥ 50 , a final score of 22.31%. Both scores demonstrate that the model is successfully able to detect the musical

instruments within MINERVA and that, on this task, its performance is on par with the one that is reported on more common object detection benchmarks [106]. More specifically, the model detects an instrument 1386 times, out of which when an $\text{IoU} \geq 10$ is considered, 878 detections correspond to true positives, whereas 508 detections are false positives. Naturally, the model’s performance decreases when an $\text{IoU} \geq 50$ is considered, as the amount of true positive detections decreases to 648 and the number of false positives increases to 738.

We report a similar quantitative analysis for the Minerva-Hypernym, Minerva-5 and Minerva-10 benchmarks. We do this in Tables 8, 9 and 10 where we present the different average precision scores, and in Figures 20, 21 and 22, where we visualize the true vs false positives detections. We can see that out of these three benchmarks, the Minerva-Hypernym one appears to be the most challenging one as it results in the worst-performing models independently from which IoU threshold is considered. We can observe from Fig. 20 that the model can detect ‘stringed instruments’ successfully, whereas its performance in detecting the remaining four hypernyms of the dataset is drastically worse. When it comes to the Minerva-5 benchmark, we can observe from Table 9 that the model can successfully detect three instruments out of the five instruments which constitute this benchmark, namely ‘Harps’, ‘Lutes”, and ‘Violins”. These results are only second to the ones obtained on Minerva-0, although the considered target task T_T is now significantly harder. Similar detections have been obtained after fine-tuning the model on the Minerva-10 benchmark. Here we can again observe (see Table 10 and Fig. 22) that the network can only successfully detect the first three most occurring instruments of the dataset, whereas for the ‘Horn”, ‘Bagpipe” ‘Rebec” and ‘Lyre” classes even no detections at all are made.

Table 8: Average Precision (%) obtained when fine-tuning a pre-trained YOLO-V3 object detector on the Minerva-Hypernyms dataset. We can observe that satisfying results are obtained for both IoU thresholds when it comes to the detection of stringed instruments, whereas detecting the remaining four hypernyms of MINERVA appears to be much more challenging.

	Stringed	Wind	Percussion	Keyboard	Electronic	Mean
AP $\text{IoU} \geq 10$	28.22	4.58	2.55	7.36	0	6.03
AP $\text{IoU} \geq 50$	20.95	2.91	1.84	4.47	0	8.54

5.4.2 Qualitative Analysis

We now characterize the performance of the aforementioned fine-tuned models from a qualitative perspective.

Table 9: Average Precision (%) obtained on the Minerva-5 benchmark. We can observe that the fine-tuned model successfully detects ‘Harps’, ‘Lutes’ and ‘Violins’, whereas the detection of ‘Shawns’ and ‘Trumpets’ can be improved.

	Harp	Lute	Violin	Shawn	Trumpet	Mean
AP IoU ≥ 10	55.60	36.51	12.21	1.75	1.3	21.47
AP IoU ≥ 50	46.80	26.93	7.64	1.01	1.07	16.69

Table 10: Average Precision (%) obtained on the Minerva-10 benchmark. Similarly to what was presented in Table 9, we can again observe that the model successfully detects the first three most occurring instruments within the dataset, whereas it appears to perform poorly on the remaining instrument classes.

	Harp	Lute	Violin	Shawn	Trumpet	Organ	Rebec	Lyre	Horn	Bagpipe	Mean
AP IoU ≥ 10	46.88	33.74	6.73	0.59	1.83	6.1	0	0	0	0	9.58
AP IoU ≥ 50	39.81	25.40	4.82	0.59	0.14	6.1	0	0	0	0	7.68

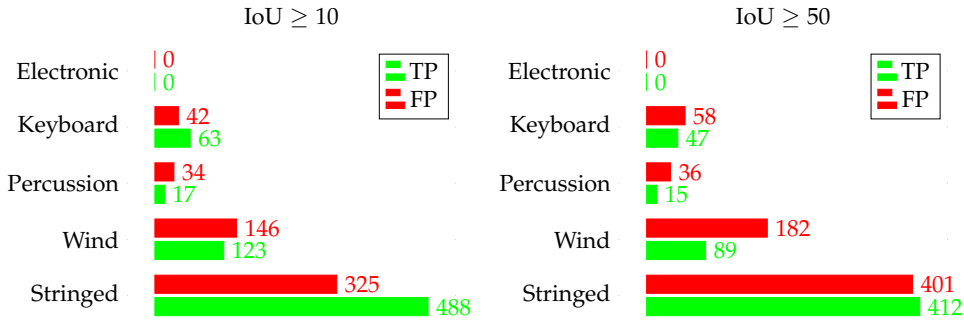


Figure 20: True Positive (TP) vs False Positive (FP) analysis on the Minerva-Hypernym benchmark for $\text{IoU} \geq 10$ and $\text{IoU} \geq 50$.

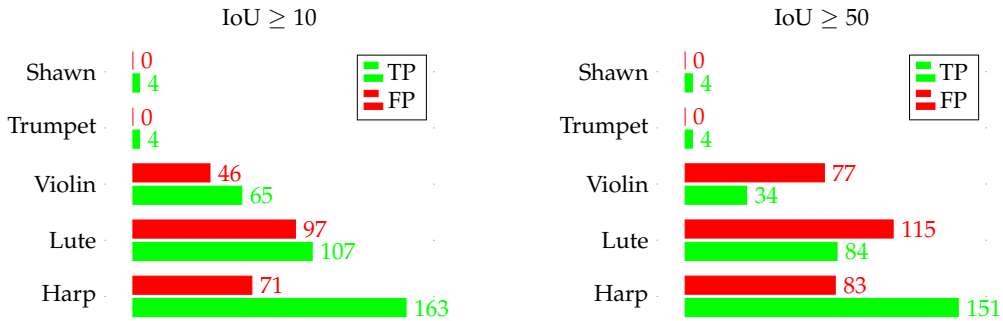


Figure 21: True Positive (TP) vs False Positive (FP) analysis on the Minerva-5 benchmark for $\text{IoU} \geq 10$ and $\text{IoU} \geq 50$.

OBJECT CLASSIFICATION For the classification experiments, we keep building on top of the study presented in the previous chapter and perform a qualitative evaluation of the models that is based on the visualization of saliency maps, as this allows us to investigate which visual properties in the image are exploited by the networks

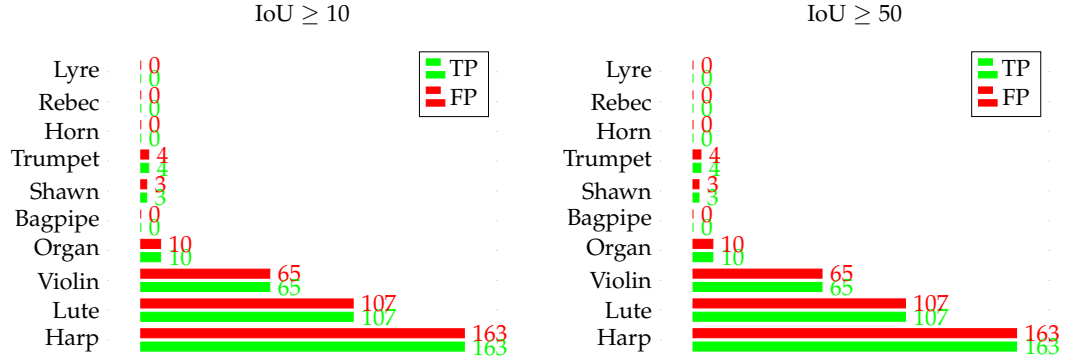


Figure 22: True Positive (TP) vs False Positive (FP) analysis on the Minerva-Hypernym benchmark for $\text{IoU} \geq 10$ and $\text{IoU} \geq 50$.

for correctly classifying the instruments in MINERVA. We hereafter report saliency maps that are obtained after fine-tuning an ImageNet pre-trained ResNet50 model on the Minerva-Hypernym benchmark, and that are computed with two different, gradient-based techniques: Grad-CAM [173] and Grad-CAM ++ [29]. Examples of computed saliencies are reported in Fig. 23. We can observe that the model focuses on two broad types of regions within the image: properties of the instruments themselves (which can be expected), but also the immediate context of the instruments, and more specifically, the way they are operated, handled, or presented. Let us, for example, consider the ‘stringed instruments’ category: as can be seen from the images in the first and third row of Fig. 23, the network happens to focus more on the strings of the instruments rather than on the, arguably more representative, resonance body of the instrument (which is however of interest in the second row of images). When it comes to the ‘percussion instrument’ represented in the fourth row and the ‘wind instrument’ represented in the last row, we can again observe that the model considers the fingers handling the instruments at least as important as the instruments themselves.

While saliency maps can produce appealing visual explanations of the performance of neural networks, it is also worth noting that the output of these methods should also be critically assessed. As reported by Alqaraawi et al. [5] saliency maps do not always necessarily explain the model’s predictions, and there is a large body of work questioning their reliability [8, 165, 177]. Nevertheless, we also believe that they can still be interesting to visually inspect, as long as the resulting saliencies are taken with a grain of sand.

OBJECT DETECTION Regarding the models trained for object detection, we visually investigate the quality of the predictions on the IconArt dataset [58], a database of ≈ 6000 paintings that have been collected with the aim of detecting classes that are specific to the analysis of artworks. Among such classes, IconArt tackles the detec-

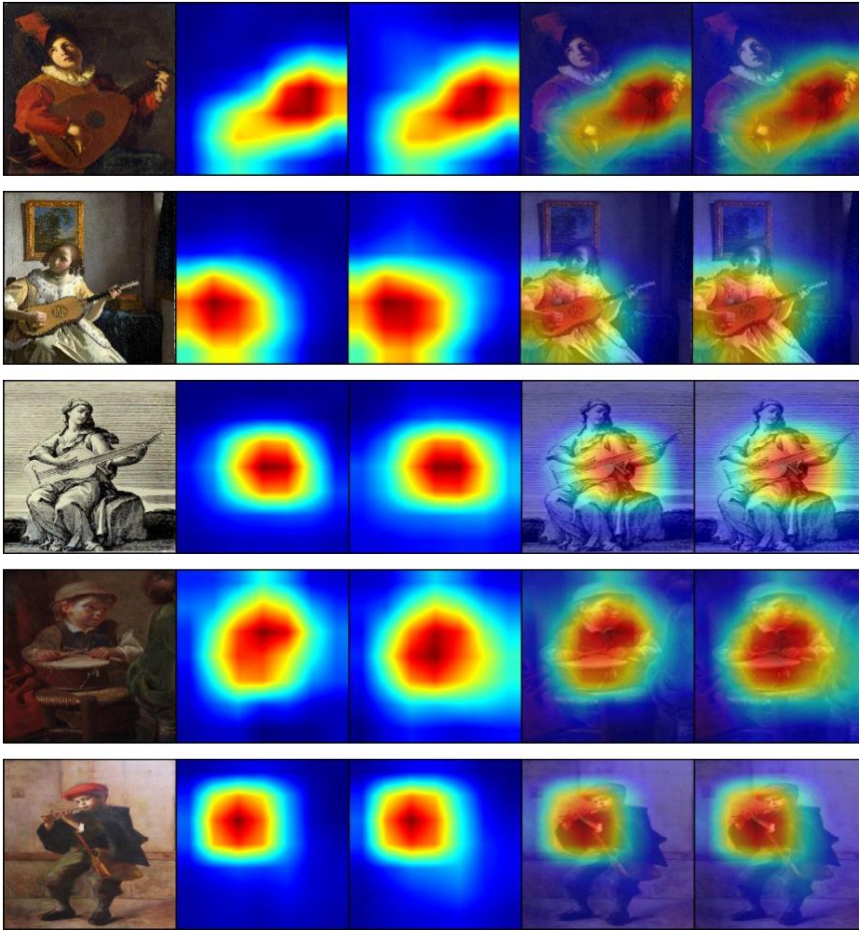


Figure 23: Saliency maps obtained after fine-tuning an ImageNet pre-trained ResNet50 on the Minerva-Hypernym benchmark. The first image corresponds to the original image, while the second and fourth images, and the third and fifth images, respectively report the performance of the Grad-CAM and Grad-CAM ++ methods.

tion of ‘angels’, ‘Jesus’ and ‘Mary’, or more simply ‘ruins’. IconArt however, does not come with any ground truth labels that are suitable for the task of instruments detection, as the dataset has been built for different purposes. Yet, musical instruments might still be depicted within its images, and trying to detect them corresponds to a nice proof of concept that can show the benefits of deploying MINERVA pre-trained models to different artistic collections. In Fig. 24 we show some successful examples of detections that were obtained after testing the performance of a YOLO-V3 model that was fine-tuned on the Minerva-Hypernym benchmark. We see that the model can successfully detect musical instruments within this new artistic collection, a result that can be exploited by art historians interested in the study of musical instruments.

While these results are undoubtedly nice and encouraging, it is arguably of even more considerable interest analyzing the model’s

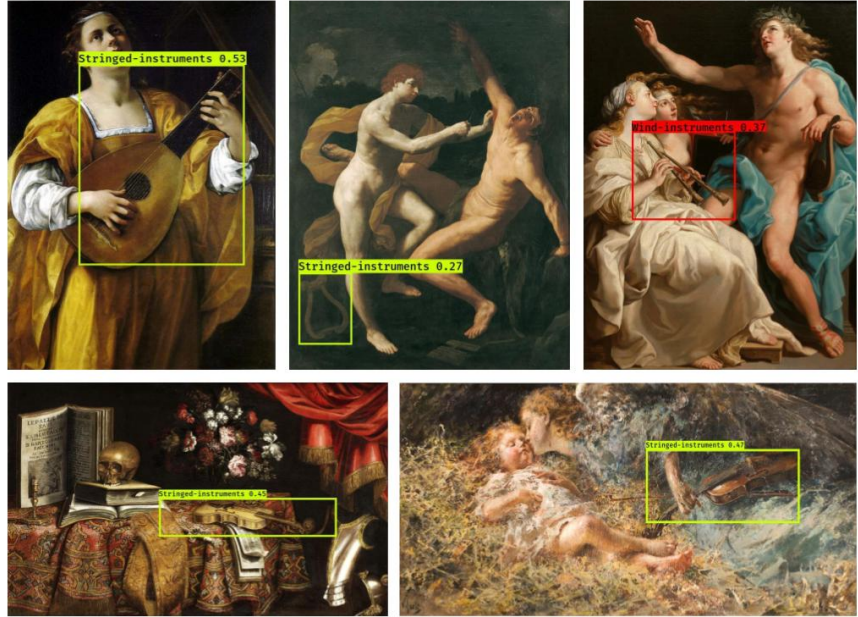


Figure 24: Some examples of successful detections that have been obtained on the IconArt dataset with a model fine-tuned on the Minerva-Hypernym benchmark.

erroneous detections. To this end, we have manually identified the incorrect model’s predictions and grouped them into different categories. This process resulted in novel insights that, at least in part, explain the performance of the models that we have quantitatively assessed in Sec. 5.4.1. First and foremost, we have noticed that the model strongly gravitates towards the detection of ‘stringed instruments’ (a result which was already observed in Fig. 20). We believe that two main reasons drive such detections: the significant presence of dual, conic contour curves of naked women’s bodies, which are reminiscent of the resonance box of guitar-like instruments (see Fig. 25), and the presence of book-like objects that, just as instruments, are mostly depicted next to hands and fingers (see Fig. 26). We have then also observed that long, often martial objects such as swords, arrows, and spears are mistakenly detected as ‘wind instruments’. We believe that the reason for this is that the shape between such objects and one of the instruments like ‘shawns’, is very similar, and sometimes even hard to distinguish for the human eye (see Fig. 27). Lastly, we have noticed that musical instruments are often mistakenly detected when regular patterns or parallel grids of straight lines (e.g. folds in clothing or wheel spokes) are present within the images. We hypothesize that the model associates these patterns to the presence of strings (see Fig. 28) within stringed instruments.



Figure 25: Examples of false detections of ‘stringed instruments’ within some images representing ‘nudity’ that are part of the IconArt dataset.



Figure 26: Additional examples of false detections of ‘stringed instruments’ that are triggered by the presence of objects close to hands and fingers.



Figure 27: Examples of false detections that are due to the strong resemblance between long martial objects and (mostly) ‘wind instruments’.

5.5 DISCUSSION AND CRITICAL ANALYSIS

In this chapter, we have introduced MINERVA, the first sizable benchmark dataset for identifying and detecting musical instruments in unrestricted, digitized images from the realm of the visual arts. We hope that this dataset can serve as a novel test-bed for the computer vision community as it provides, at least in part, a solution to some of the challenges that currently define the field (see Sec. 5.1). Our benchmark experiments have highlighted the feasibility of our newly proposed classification and object detection tasks and served us for



Figure 28: Examples of geometrical patterns that mistakenly yield the detection of instruments.

further characterizing the degree of transferability of pre-trained convolutional neural networks. While, when it comes to the classification experiments presented in the first part of Sec. 5.4.1, the obtained results are lower in terms of accuracy when compared to the classification tasks that we tackled in the previous chapter, they nevertheless provide strong evidence in favor of adapting transfer learning. At the same time, these experiments also show how challenging the simple task of image classification can be, as we believe there is definitively room for improving the results presented in Tables 6 and 7. Similarly, the results presented in the second part of Sec. 5.4.1 show that it is equally possible to transfer models that have been initially built for the detection of objects in natural images and to use them on non-natural image distributions. We again believe that albeit satisfying results on MINERVA have been obtained by starting with an MS-COCO weight initialization, better performance than the one reported in Tables 8, 9 and 10 can be obtained. To this end, we recommend taking into account the qualitative analysis that we presented in Sec. 5.4.2. Overall, our study is a first step towards creating novel, arguably more challenging computer vision test-beds that we hope can be used to further characterize the potential, and limitations, of modern state-of-the-art neural networks. To this end, the methodological protocol that was used for the creation of MINERVA has already inspired the development of new datasets and experimental studies that will be briefly reviewed in the next section.

5.6 FUTURE WORK: TOWARDS MORE BENCHMARKS

Something about Yann's MSc. thesis

6

ON THE TRANSFERABILITY OF LOTTERY WINNERS

CONTRIBUTIONS AND OUTLINE

In Chapters 4 and 5, we have always performed Transfer Learning (TL) with large and deep convolutional neural networks, as this is the type of models which have obtained state-of-the-art results in the naturalistic domain. While all the studies presented so far aimed at characterizing the TL properties of popular convolutional architectures, we explore a different approach in this chapter. We use TL as a tool for not only exploiting the performance of pre-trained neural networks but also for characterizing a relatively new deep learning phenomenon that comes with the name of the “Lottery Ticket Hypothesis” (LTH). Specifically, we investigate whether lottery winners found on datasets of natural images contain inductive biases that are generic enough to generalize to non-natural image distributions. To do so, we present the first results that study the transferability of winning initializations in this particular training setting. Furthermore, we also show that the LTH offers a novel way for doing TL when the training data is scarce. The rest of this chapter is structured as follows: Sec. 6.1 introduces the LTH and presents the reasons that have motivated studying this phenomenon from a TL perspective. Sec. 6.2 and Sec. 6.3 present the experimental setup that was used throughout this chapter, while Sec. 6.4 and Sec. 6.5 present the main findings of our research. The chapter ends by contextualizing its content with respect to the existing literature in Sec. 6.6 and by identifying some potential avenues for future work in Sec. 6.7.

This chapter is based on the publication Sabatelli, Kestemont, and Geurts [157].

6.1 THE LOTTERY TICKET HYPOTHESIS

The “Lottery-Ticket-Hypothesis” (LTH) [50] states that within large randomly initialized neural networks, there exist smaller sub-networks which, if trained from their initial weights, can perform just as well as the fully trained unpruned network from which they are extracted. This happens to be possible because the weights of these sub-networks seem to be particularly well initialized before training starts, therefore making these smaller architectures suitable for learning (see Fig

[29](#) for an illustration). These sub-networks, i.e., the pruned structure and their initial weights, are called winning tickets, as they appear to have won the initialization lottery. Since winning tickets only contain a very limited amount of parameters, they yield faster training, inference, and sometimes even better final performance than their larger over-parametrized counterparts [\[50, 52\]](#). So far, winning tickets are typically identified by an iterative procedure that cycles through several steps of network training and weight pruning, starting from a randomly initialized unpruned network. While simple and intuitive, the resulting algorithm has, unfortunately, a high computational cost. Even though the resulting sparse networks can be trained efficiently and in isolation from their initial weights, the LTH idea has not yet led to more efficient solutions for training a sparse network than existing pruning algorithms that all also require to first fully train an unpruned network [\[41, 63, 104, 122, 240\]](#).

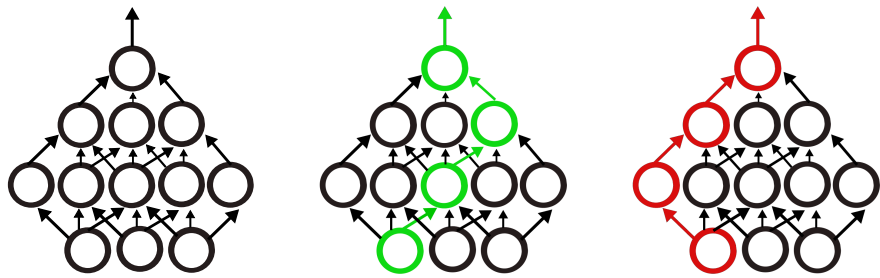


Figure 29: A visual representation of the LTH as introduced by Frankle and Carbin [\[50\]](#). Let us consider a simplified version of a two hidden layer feedforward neural network as is depicted in the first image on the left. The LTH states that within this neural network, there exist multiple smaller networks (represented in green), which can perform just as well as their larger counterpart. Training these sparse models from scratch successfully is only possible as long as their weights are initialized with the same values that were also used when the larger (black) model was initialized. Furthermore, the structure of these sparse models appears to be crucial as well, as it is not possible to randomly extract any subset of weights from an unpruned model and successfully train the resulting sparse network (represented in red in the last figure) from scratch. We visually represent the performance of models that are the winners of the LTH in the two plots reported in Figure 30.

Since the introduction of the idea of the LTH, several research works have focused on understanding what makes some weights so special to be the winners of the initialization lottery. Among the different tested approaches, which will be reviewed in Sec. 6.6, one research direction, in particular, has looked into how well winning ticket initializations can be transferred among different training settings (datasets and optimizers), an approach that aims at characteriz-

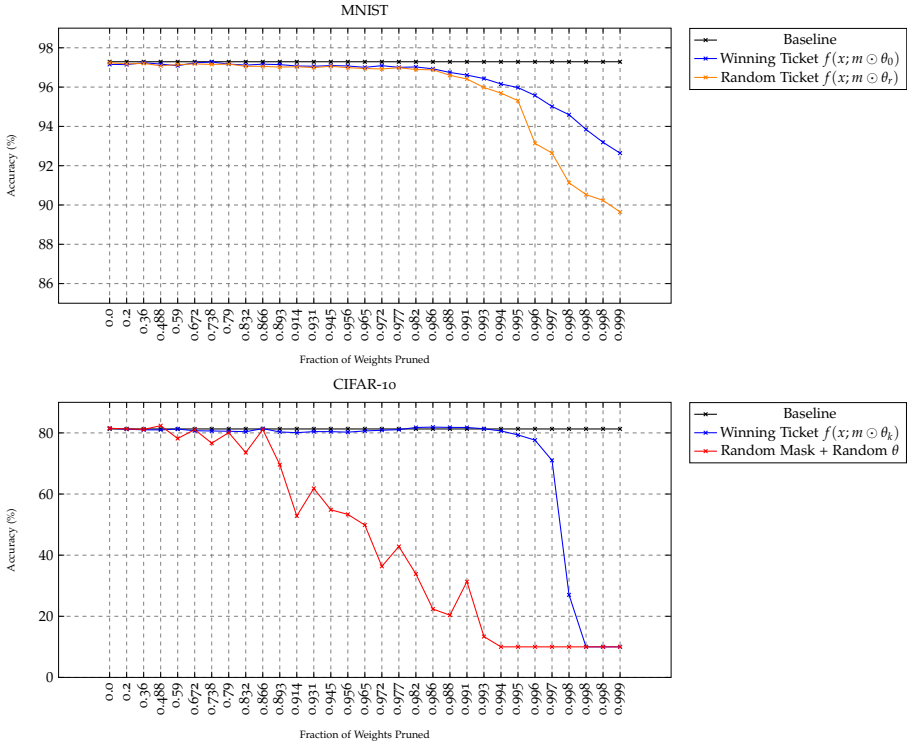


Figure 30: A visual representation of the performance of lottery winners that replicate the findings first presented by Frankle and Carbin [50]. In the first plot we consider a multilayer perceptron that gets trained on the MNIST dataset. After the network gets trained from scratch it obtains a final accuracy of $\approx 97\%$ as reported by the black line. We can observe that winning tickets $f(x; m \odot \theta_0)$ only start performing worse than the network they have been extracted from once a large fraction of their weights gets pruned. We can also observe how crucial it is to re-initialize the weights of the pruned models with the same weights that were used when initializing the unpruned model from scratch (θ_0). If random weights are used instead (θ_r), the pruned masks appear to be less robust to pruning (orange curve). In the second plot we show how important it is for a pruned model to come in the form of $f(x; \odot \theta_k)$ after training a ResNet-50 architecture on the CIFAR-10 dataset, since we show that it is not possible to simply extract any random subset of weights from a deep convolutional network and obtain a performance that is robust to pruning after randomly initializing the parameters of the model (red curve).

ing the winners of the LTH by studying to what extent their **inductive biases** are generic [123]. The most interesting findings of this study are that winning tickets generalize across datasets, within the natural image domain at least, and that tickets obtained from larger datasets typically generalize better. This opens the door to the transfer of winning tickets between datasets, which makes the high computational cost required to identify them much more acceptable in practice, as this cost has to be paid only once and can be shared across datasets.

In this chapter, we build on top of this latter work. While Morcos et al. [123] focused on the natural image domain, we investigate the possibility of transferring winning tickets obtained from the natural image domain to datasets in non-natural image domains. This question has an important practical interest as datasets in non-natural image domains are typically scarcer than datasets in natural image domains. They would, therefore, potentially benefit more from a successful transfer of sparse networks since the latter can be expected to require less data for training than large over-parametrized networks. Furthermore, besides studying their generalization capabilities, we also focus on another interesting property that characterizes models that win the LTH, and which so far has received less research attention. As originally presented by Frankle and Carbin [50], pruned models, which are the winners of the LTH, can yield a final performance that is better than the one obtained by larger over-parametrized networks. In this chapter we explore whether it is worth seeking such pruned models when training data is scarce, a scenario that is well known to constraint the training of deep neural networks. To answer these two questions, we carried out experiments on several datasets from two very different non-natural image domains: digital pathology and, similarly to Chapters 4 and 5, digital heritage.

6.2 DATASETS

We consider seven datasets that will serve as target domains \mathcal{D}_T , and that come from two different, unrelated sources: histopathology and digital heritage. Each dataset comes with its training, validation, and testing splits. Furthermore, the datasets change in size, resolution, and amount of labels that need to be classified. We report an overview about the size of these datasets in Table 11 while a visual representation of the samples constituting these datasets in Fig. 31. The Digital-PATHology (DP) data comes from the Cytomine [111] web application, the same open-source platform that allowed the creation of the MINERVA dataset described in the previous chapter. While Cytomine has collected many datasets over the years, in what follows, we have limited our analysis to a subset of four datasets that all represent tissues and cells from either human or animal organs. These datasets, which therefore correspond to the first four target tasks \mathcal{T}_T that will be considered throughout this chapter are: Human-LBA, Lung-Tissues, and Mouse-LBA (which were originally proposed in [124]), and Bone-Marrow (which comes from [81]). All four datasets have been used by Mormont, Geurts, and Marée [124], who, as described in Chapter 3, researched whether neural networks pre-trained on natural images could successfully be re-used in the DP domain. In this chapter, we explore whether an alternative to their transfer-learning approaches could be based on training pruned networks

that are the winners of the LTH. This will allow us to investigate the two research questions introduced in Sec. 6.1: we will explore whether winning initializations that are found on datasets of natural images do generalize to non-natural domains and whether sparse models winners of the LTH can perform better than larger unpruned models that get trained from scratch. Regarding the field of Digital-Humanities (DH) we use three novel, small datasets that all revolve around the target task \mathcal{T}_T that is the classification of artworks. We consider two different target tasks that were already studied in Chapter 4, namely type and artist classification. When it comes to the latter target task \mathcal{T}_T we use two different datasets, referred to as Artist ① and Artist ②, which purpose will be better explained in Sec. 6.5. All images are publicly available as part of the WikiArt gallery [142] and can also be found within the large popular OmniArt dataset [184]. Albeit as we have seen in Chapter 4 in DH it is possible to find large datasets, which cannot be said for the field of histopathology, it is worth mentioning that we have kept the size of these datasets intentionally small in order to fit the research questions introduced in Sec. 6.1.

Table 11: A brief overview of the seven different datasets which have been used in this work. As usual throughout this thesis N_t corresponds to the total amount of samples that are present in the dataset, while Q_t represents the number of classes.

Dataset	Training-Set	Validation-Set	Testing-Set	N_t	Q_t
Human-LBA	4051	346	1023	5420	9
Lung-Tissues	4881	562	888	6331	10
Mouse-LBA	1722	716	1846	4284	8
Bone-Marrow	522	130	639	1291	8
Artist ①	3103	389	389	3881	20
Type	2868	360	360	3588	20
Artist ②	2827	353	353	3533	19

6.3 EXPERIMENTAL SETUP

We follow an experimental set-up similar to the one that was introduced in [123] (and that has been validated by Gohil, Narayanan, and Jain [57]). Let us define a neural network $f(x; \theta)$ that gets randomly initialized with parameters $\theta_0 \sim \mathcal{D}_\theta$ and then trained for j iterations over an input space \mathcal{X} , and an output space \mathcal{Y} . At the end of training a percentage of the parameters in θ_j gets pruned, a procedure which results in a mask m . The parameters in θ_j which did not get pruned are then reset to the values they had at θ_k , where k represents an early training iteration. A winning ticket corresponds to the combination

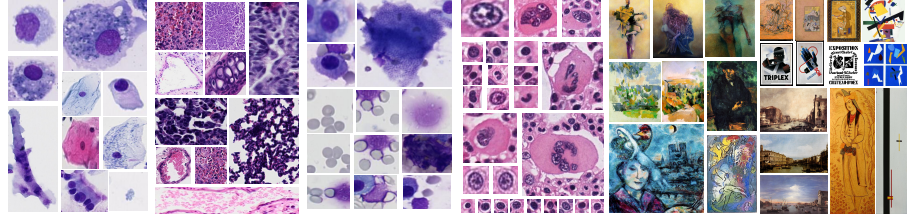


Figure 31: Some image samples that constitute the non-natural image datasets which have been used in this work. From left to right we have the Human-LBA, Lung-Tissues, Mouse-LBA and Bone-Marrow datasets, while finally we report some examples that represent artworks which come from the field of digital heritage and that are therefore similar to the images we have used for the experiments reported in Chapters 4 and 5.

between the previously obtained mask, and the parameters θ_k , and is defined as $f(x; m \odot \theta_k)$ ¹. Constructing a winning ticket with parameters θ_k , instead of θ_0 , is a procedure which is known as late-resetting [52], and is a simple but effective trick that makes it possible to stably find winning initializations in deep convolutional neural networks [52, 123]. In this study $f(x; \theta)$ comes in the form of a ResNet-50 architecture [63] which gets trained on three popular CV natural image datasets serving as source domains \mathcal{D}_S : CIFAR-10/100 and Fashion-MNIST (see Fig. 32 for a visualization). Following [63, 123], 31 winning tickets $f(x; m \odot \theta_k)$ of increasing sparsity are obtained from each of these three datasets by repeating 31 iterations of network training and magnitude pruning with a pruning rate p of 20%. Specifically, given a tensor \mathbf{T} representing the unpruned parameters in a layer, at each pruning iteration we first train the network for several epochs (using early stopping on the validation set as described in the appendix), and then remove all entries in channel c along dimension d as:

$$\left\{ \mathbf{T}_{[...,c,...]} : c_{\text{th}} \{ \mathbf{T}_{[...,i,...]} \}_{i=1}^d \|_1 \leq p \right\}, \quad (85)$$

where k_{th} is the rank of the k^{th} channel of \mathbf{T} along direction d according to the L_1 -based ranking [131]. The parameters θ_k that define each of the 31 tickets are then taken as the weights of the corresponding pruned networks at the k^{th} epoch of the first pruning iteration. Once these pruned networks are found, we aim at investigating whether their parameters θ_k contain inductive biases that allow them to generalize to the non-natural image domain. To do so, we replace the final fully connected layer of each winning ticket with a randomly initialized layer that has as many output nodes as there are classes to

¹ Note that this formulation generalizes the original version of the LTH [50] that we have represented in Fig. 29, where a winning ticket is obtained after resetting the unpruned parameters of the network to the values they had right after initialization, therefore defining a winning ticket as $f(x; m \odot \theta_0)$.



Figure 32: The three natural datasets constituting the source tasks \mathcal{T}_S that are necessary for finding winning tickets. From left to right samples from the CIFAR-10/100 and Fashion-MNIST datasets.

classify. We then fine-tune each of these networks on the non-natural target tasks \mathcal{T}_T considered in this study. At the end of training, we study the performance of each winning ticket in two different ways. First, we compare the performance of each network to the performance of a fully unpruned network that gets randomly initialized and trained from scratch. Second, we also compare the performance of winning tickets that have been found on a natural image dataset to 31 new sparse models that are the winners of the LTH on the considered target dataset. Since it is not known to which extent pruned networks that contain weights that are the winners of the LTH on a natural image dataset can generalize to target domains \mathcal{D}_T that do not contain natural images, we report the first results that investigate the potential of a novel transfer-learning scheme which has so far only been studied on datasets from the natural image domain. Moreover, testing the performance of sparse networks that contain winning tickets that are specific to a non-natural image target distribution also allows us to investigate whether it is worth pruning large networks with the hope of finding smaller models that might perform better than a large over-parametrized one. As mentioned in Sec. 6.1, pruned networks that are initialized with the winning weights can sometimes perform better than a fully unpruned network. Identifying such sparse networks leads to a very significant reduction of model size, which can be a very effective way of regularization when training data is scarce.

6.4 RESULTS

The results of all our experiments are visually reported in the plots of Fig. 33. Each line plot represents the final performance obtained by a pruned model containing a winning ticket initialization on the final testing set of our target datasets. This performance is reported on the y-axis of the plots, while on the x-axis we represent the fraction of weights that are pruned from the original ResNet-50 architec-

ture. As explained in the previous section, the performance of each winning ticket is compared to the performance obtained by an unpruned, over-parametrized architecture reported by the black dashed lines. The models that are the winners of the LTH on a natural image dataset are reported by the green, red and purple lines, while the blue lines report the winners of the LTH on a non-natural target dataset. Furthermore, when it comes to the latter lottery tickets, we also report the performance that is obtained by winning tickets that get randomly reinitialized ($f(x; m \odot \theta'_0)$ with $\theta'_0 \sim \mathcal{D}_\theta$). The orange lines report these results.

6.4.1 *On the Importance of Finding Winning Initializations*

We can start by observing that pruned models which happen to be the winners of the LTH either on a natural dataset or on a non-natural one can maintain a good final performance until large pruning rates are reached. This is particularly evident on the first three datasets, where models that keep only $\approx 1\%$ of their original weights barely suffer from any drop in performance. This gets a little bit less evident on the last three datasets, where the performance of winning ticket initializations that are directly found on the considered target dataset starts getting harmed once a fraction of $\approx 97\%$ of original weights are pruned. These results show that an extremely large part of the parameters of a ResNet-50 architecture can be considered superfluous, therefore confirming the LTH when datasets contain non-natural images. More importantly, we also observe that pruned models winners of the LTH, significantly outperform larger over-parametrized models that get trained from scratch. This can be very clearly seen in all plots where the performance of pruned models is always consistently better than what is reported by the black dashed line. To get a better sense of how much these pruned networks perform better than their larger unpruned counterparts, we report in Table 12 the performance that is obtained by the best performing pruned model, found over all 31 possible pruned models, and compare it to the performance of an unpruned architecture. The exact fraction of weights which is pruned from an original ResNet-50 architecture is reported in Table 13 for each configuration. We can observe that no matter which dataset has been used as source domain \mathcal{D}_S for finding a winning ticket initialization, all pruned networks reach a final accuracy that is significantly higher than the one that is obtained after training an unpruned model from scratch directly on the target task \mathcal{T}_T . While in most cases, the difference in terms of performance is of $\approx 10\%$ (see e.g., the Human-LBA, Lung-Tissues and the Type datasets), it is worth highlighting that there are other cases in which this difference is even larger. This is the case for the Mouse-LBA and Artist ① datasets where a winning ticket coming from the CIFAR-10 dataset performs more

than 20% better than a model trained from scratch. These results show that to maximize the performance of deep networks, it is always worth finding and training pruned models that are the winners of the LTH.

Table 12: The results comparing the performance that is obtained on the testing-set by the best pruned model winner of the LTH, and an unpruned architecture trained from scratch. The overall best performing model is reported in a green cell, while the second best one in a yellow cell. We can observe that pruned models winners of the LTH perform significantly better than a larger over-parametrized architecture that gets trained from scratch. As can be seen by the results obtained on the Mouse-LBA and Artist 1 datasets the difference in terms of performance can be particularly large ($\approx 20\%$).

Target-Dataset	Scratch-Training	CIFAR-10	CIFAR-100	Fashion-MNIST	Target-Ticket
Human-LBA	71.85 ± 1.12	79.17 ± 1.85	76.97 ± 0.73	77.32 ± 1.85	81.72 ± 0.39
Lung-Tissues	84.75 ± 0.81	88.90 ± 1.97	87.61 ± 0.90	87.61 ± 0.11	90.48 ± 0.16
Mouse-LBA	48.17 ± 1.18	74.20 ± 2.04	57.42 ± 0.48	52.27 ± 1.73	68.20 ± 3.79
Bone-Marrow	64.66 ± 1.36	71.75 ± 3.36	69.87 ± 0.39	68.77 ± 0.39	72.55 ± 0.46
Artist ①	45.88 ± 0.42	66.58 ± 1.54	65.55 ± 1.79	63.88 ± 0.12	58.74 ± 1.92
Type	41.36 ± 2.31	58.63 ± 2.97	60.56 ± 0.44	58.92 ± 0.59	50.44 ± 2.23

Table 13: Some additional information about the lottery winners which performance is reported in Table 12. For each winning ticket we report the fraction of weights that is pruned from an original ResNet-50 architecture and that therefore characterizes the level of sparsity of the overall best performing lottery ticket. The results in the Scratch-Training column are not reported since these are unpruned models that are trained from scratch.

Target-Dataset	Scratch-Training	CIFAR-10	CIFAR-100	Fashion-MNIST	Target-Ticket
Human-LBA	-	0.945	0.79	0.886	0.832
Lung-Tissues	-	0.977	0.977	0.672	0.965
Mouse-LBA	-	0.972	0.893	0.738	0.931
Bone-Marrow	-	0.866	0.988	0.931	0.914
Artist ①	-	0.972	0.993	0.991	0.931
Type	-	0.991	0.931	0.995	0.963

6.4.2 On the Generalization Properties of Lottery Winners

We then investigate whether natural image tickets can generalize to the non-natural setting, therefore accounting for the distribution shift between domains \mathcal{D} . Findings differ across datasets. When considering the datasets that come from the DP field, we can see that, in three out of four cases, winning tickets that are found on a natural image dataset get outperformed by sparse winning networks that come after training a model on the biomedical dataset. This is particularly evident in the results obtained on the Human-LBA and

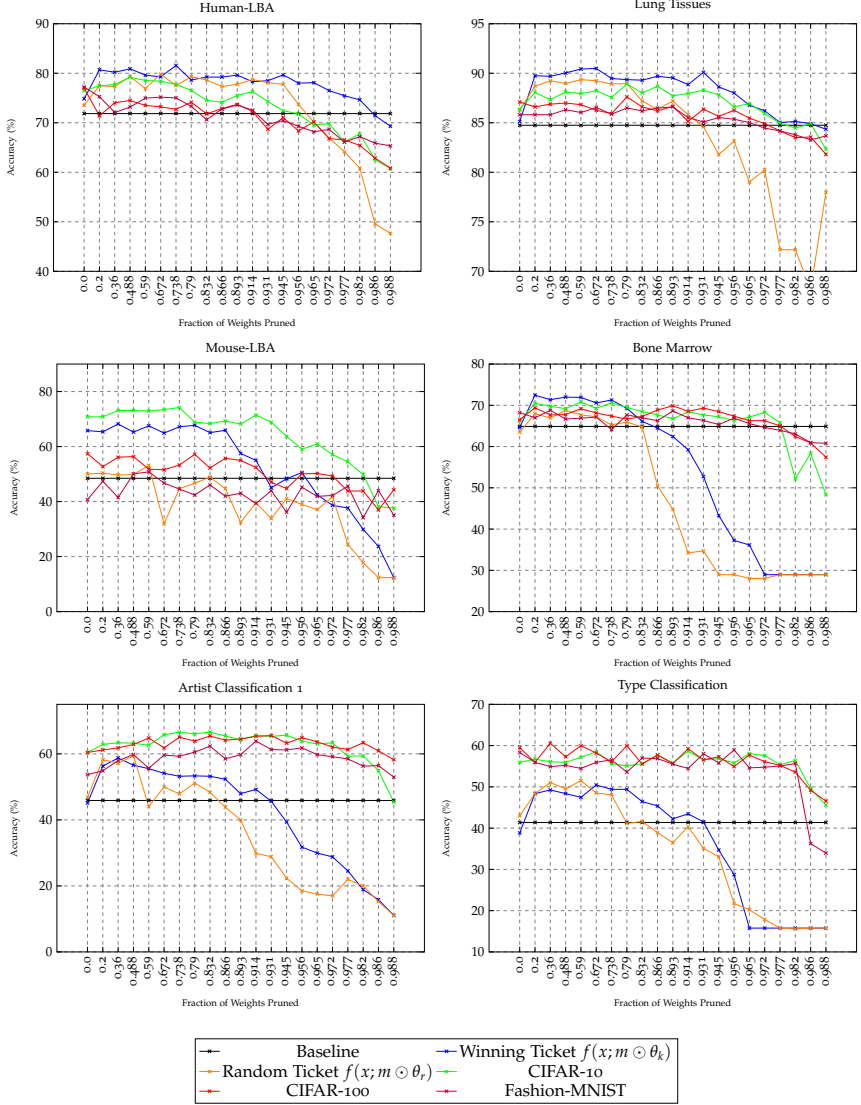


Figure 33: An overview of the results showing that sparse models that are the winners of the LTH (represented by the coloured lines) significantly outperform unpruned networks which get randomly initialized and trained from scratch (dashed black line). This happens to be the case on all tested datasets, no matter whether a winning initialization comes from a natural image source or not. It is however worth mentioning that, especially on the biomedical datasets, natural image tickets get outperformed by sparse networks that are the winners of the LTH on a biomedical dataset. On the other hand this is not the case when it comes to the classification of arts where natural image tickets outperform the ones which are found within artistic collections.

Lung-Tissues datasets, where the blue line plots consistently reach the highest testing-set accuracy. When it comes to the Bone-Marrow dataset, the difference in terms of performance between the best natural image ticket, in this case coming from the CIFAR-10 dataset, and

the one coming from the biomedical dataset, is less evident (see Table 12 for the exact accuracies). Furthermore, it is worth highlighting that on the Bone-Marrow dataset, albeit natural image models seem to get outperformed by the ones found on the biomedical dataset, the performance of the latter ones appears to be less stable once substantial pruning rates are reached. When it comes to the Mouse-LBA dataset, these results slightly differ. In fact, this dataset corresponds to the only case where a natural image source ticket outperforms a non-natural one. As can be seen, by the green line plot, pruned models coming from the CIFAR-10 dataset outperform the ones found on the Mouse-LBA dataset.

When focusing our analysis on the classification of arts, we see that the results change significantly from the ones obtained on the biomedical datasets. In this case, all of the natural image lottery winners, no matter the source tasks \mathcal{D}_S they were initially found on, outperform the same kind of models that were found after training a full network on the artistic collection. We can see from Table 12 that the final testing performance is similar among all of the best natural image tickets. Similar to what has been noticed on the Bone-Marrow dataset, we can again observe that tickets coming from a non-natural data distribution seem to suffer more from large pruning rates.

These results show both the potential and limitations that natural image winners of the LTH can offer when fine-tuned on non-natural images datasets. The results obtained on the artistic datasets suggest that winning initializations contain inductive biases that are strong enough to get at least successfully transferred to the artistic domain, therefore confirming some of the claims that were made by Morcos et al. [123]. However, it also appears that there are stronger limitations to the transferability of winning initializations which were not observed by Morcos et al. [123]. In fact, our results show that on DP data, the best strategy is to find a winning ticket directly on the biomedical dataset, and that winning initializations found on natural image datasets, albeit outperforming a randomly initialized unpruned network, perform worse than pruned models that are the winners of the LTH on a biomedical dataset.

6.5 ADDITIONAL STUDIES

To characterize the transferability of winning initializations even more while at the same time gaining a deeper understanding of the LTH, we have performed a set of three additional experiments which help us characterize this phenomenon better.

6.5.0.1 *Lottery Tickets VS fine-tuned pruned models*

So far, we have focused our transfer learning study on lottery tickets that come in the form of $f(x; m \odot \theta_k)$, where, as mentioned in Sec.

[6.3](#), θ_k corresponds to the weights that parametrize a neural network at a very early training iteration. This formalization is, however, different from the transfer learning scenarios that we have described in Chapter [3](#) and adapted in Chapters [4](#) and [5](#), where neural networks get transferred with the weights that are obtained at the end of the training process. We have therefore studied whether there is a difference in terms of performance between transferring and fine-tuning a lottery ticket with parameters θ_k , and the same kind of pruned network which is initialized with the weights that are obtained once the network is fully trained on a source task T_S . We define these kind of models as $f(x; m \odot \theta_i)$ where i stays for the last training iteration. We report some examples of this behaviour in the plots presented in Fig. [34](#), where we consider $f(x; m \odot \theta_i)$ models which were trained on the CIFAR-10 and CIFAR-100 datasets, and then transferred and fine-tuned on the Human-LBA dataset. We found that these models overall perform worse than lottery tickets while also being less robust to pruning. This also shows that on this dataset, the slightly inferior performance of the natural image tickets with respect to the target tickets is not due to the weight re-initialization.

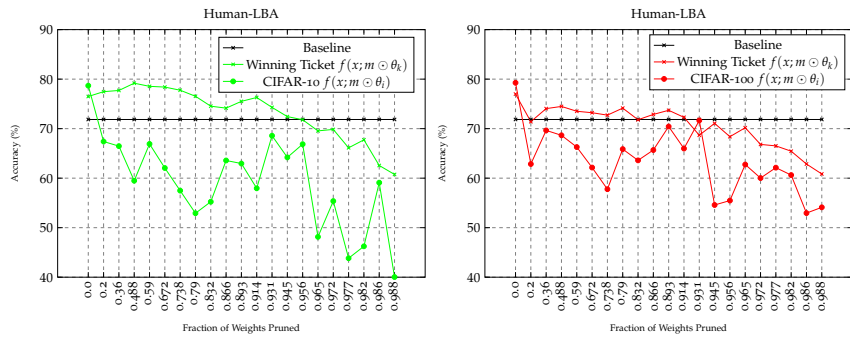


Figure 34: Our results showing the advantages of transferring lottery winners over pruned models that are fully fine-tuned on natural datasets (CIFAR-10/100). We can observe that their performance is overall inferior to the one of lottery tickets and that these models are significantly less robust to pruning. We believe that the reason behind their poor performance revolves around the fact that, once completely trained on a specific source task, and after having gone through the pruning stage, these models lose the necessary flexibility that is required for them to adapt to a new task.

6.5.0.2 Transferring tickets from similar non-natural domains

We investigated whether it is beneficial to fine-tune lottery winners that come from a natural image distribution instead of a related non-natural dataset. Specifically we tested whether winning tickets generated on the Human-LBA dataset generalize to the Mouse-LBA one (since both datasets are representative of the field of Live-Blood-Analysis),

and whether lottery winners coming from the Artist ① dataset generalized to the Artist ② one. We visually represent these results in Fig. 35. As one might expect, we found that it is beneficial to transfer winning tickets from a related source. Specifically, Human-LBA tickets can perform just as well as winning tickets that are generated on the Mouse-LBA dataset, while at the same time also being more robust to large pruning rates. When it comes to lottery winners found on the Artist ① dataset we have observed that these tickets can even outperform the ones generated on the Artist ② one. Overall these results confirm the claims that we made in Chapter 4 where we already highlighted the benefits that could come from transferring models that were trained on a similar source as the target task. This conclusion now also seems to hold for models that are the winners of the LTH.

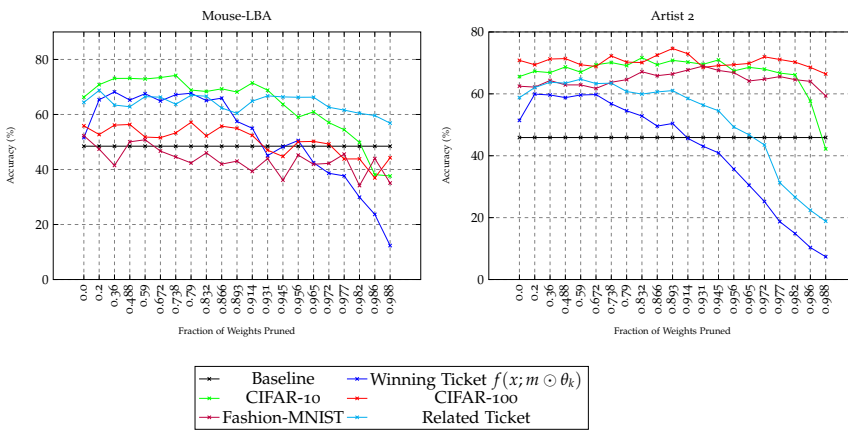


Figure 35: Our results showing the benefits of transferring lottery winners that have been identified on a related source task. We can observe that on the Mouse-LBA dataset, winning tickets that were obtained on the Human-LBA dataset are the ones that are the most robust ones to pruning, while on the Artist 2 dataset we can observe that lottery winners that have been obtained on the Artist 1 dataset are both more robust to pruning, while they also yield overall better performance.

6.5.0.3 On the size of the training set

We have observed from the blue line plots of Fig. 33 that there are cases in which lottery winners are very robust to extremely large pruning rates (see as an example the first and second plots), while there are other cases in which their performance deteriorates faster with respect to the fraction of weights that get pruned. The most robust performance is obtained by winning tickets that are generated on the Human-LBA and Lung-Tissues datasets, which are the two target datasets that contain the largest amount of training samples. Therefore, we have studied whether there is a relationship between the

size of the training data used for finding lottery winners and the robustness in terms of performance of the resulting pruned models. We generated lottery winners after incrementally reducing the size of the training data by 75%, 50% and 25%, and then investigated whether we could observe a similar drop in performance like the one we have observed in the last three blue line-plots of Fig. 33 once a large fraction of weights got pruned. Perhaps surprisingly, we have observed that this was not the case, and as can be seen, by the plots represented in Fig. 36, the performance of lottery winners that are found when using only 25% of the training set is just as stable as the one of winning tickets which are generated on the entire dataset. However, it is worth mentioning that, albeit the performance of such sparse models is robust, their final performance on the testing set is lower than the one obtained by winning tickets that have been trained on the full training data distribution.

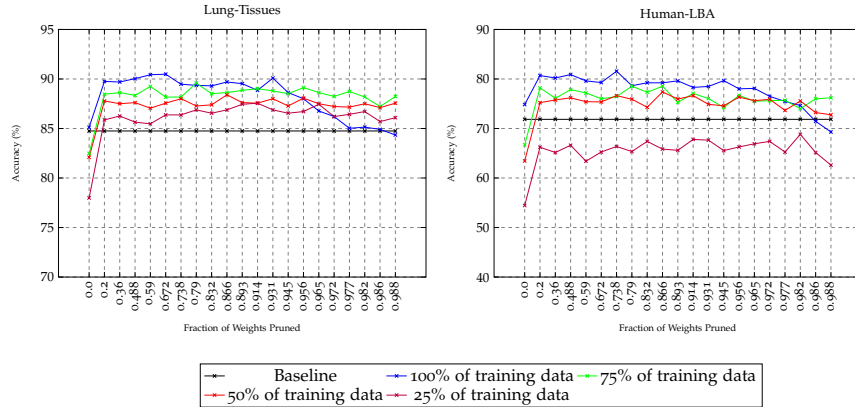


Figure 36: Our study showing that the robustness to large pruning rates of lottery winners does not depend from the size of the training dataset. We can observe that even when lottery tickets are trained on only 25% of the dataset their performance remains stable with respect to the fraction of pruned weights. These results suggest that the less stable performance of Bone-Marrow lottery tickets observed in Fig. 33 does not depend from the small training set.

6.6 RELATED WORK

The research presented in this chapter contributes to a better understanding of the LTH by exploring the generalization and transfer learning properties of lottery tickets. The closest approach to what has been presented in this work is undoubtedly the one presented by Morcos et al. [123], which shows that winning models can generalize across datasets of natural images and across different optimizers. As mentioned in Sec. 6.3, a large part of our experimental setup is based on this work. Besides the work presented in [123], there

have been other attempts that aimed to better understand the LTH after studying it from a transfer learning perspective. However, just as the study presented by Morcos et al. [123], all this research limited its analysis to natural images. Van Soelen and Sheppard [208] transfer winning tickets among different partitions of the CIFAR-10 dataset, while Mehta [115] shows that sparse models can successfully get transferred from the CIFAR-10 dataset to other object recognition tasks. While these results seem to suggest that lottery tickets contain inductive biases which are strong enough to generalize to different domains, it is worth highlighting that their transfer learning properties were only studied after considering the CIFAR-10 dataset as a possible source task \mathcal{T}_S for winning ticket initializations, a limitation which we overcome in this chapter. It is also worth mentioning that the research presented in this part of the dissertation is strongly connected to the work presented by Frankle et al. [52]. While the first paper that introduced the LTH limited its analysis to relatively simple neural architectures, such as multilayer perceptrons and convolutional networks, which were tested on small CV datasets, the presence of winning initializations in larger, more popular convolutional models such as the ones that we used in Chapter 4 trained on large datasets [155] was only first presented in [52]. Since we have used a ResNet-50 architecture [68], we have followed all the recommendations that were introduced by Frankle et al. [52] for successfully identifying the winners of the LTH in larger models. More specifically, we mention the late-resetting procedure, which resets the weights of a pruned model to the weights that are obtained after k training iterations instead of to the values which were used at the beginning of training (as explained in Sec. 6.3), a procedure which has shown to be related to *linear mode connectivity* [51]. While the work presented in this paper has limited its analysis to networks that minimize an objective function that is relevant for classification problems, it is worth noting that more recent approaches have identified lottery winners in different training settings. Yu et al. [228] have shown that winning initializations can be found when neural networks are trained on tasks ranging from natural language processing to reinforcement learning, while Sun et al. [185] successfully identify sparse winning models in a multi-task learning scenario. As future work, one could study whether lottery tickets can be found on different neural architectures and also whether they appear when neural networks are trained on CV tasks other than classification. To this end, the YOLO-V3 architecture used in Chapter 5 comes to mind, alongside CV tasks such as object detection and image segmentation.

6.7 CONCLUSION

We have investigated the transfer learning potential of pruned neural networks that are the winners of the LTH from datasets of natural images to datasets containing non-natural images. We have explored this in training conditions where the size of the training data is relatively small. All of the results presented in this chapter confirm that it is always beneficial to train a sparse model, winner of the LTH, instead of a larger over-parametrized one. Regarding our study on the transferability of winning tickets, we have reported the first results, which study this phenomenon under non-natural data distributions by using datasets coming from the fields of digital pathology and heritage. While for the case of artistic data, it seems that winning tickets from the natural image domain contain inductive biases which are strong enough to generalize to this specific domain, we have also shown that this approach can present stronger limitations when it comes to biomedical data. This probably stems from the fact that DP images are further away from natural images than artistic ones. We have also shown that lottery tickets perform significantly better than fully trained pruned models, that it is beneficial to transfer lottery winners from different but related, non-natural sources, and that the performance of lottery tickets is not dependent on the size of the training data. To conclude, we provide a better characterization of the LTH while simultaneously showing that when training data is limited, the performance of deep neural networks can get significantly improved by using lottery winners over larger over-parametrized ones.

Part III

TRANSFER LEARNING FOR DEEP
REINFORCEMENT LEARNING

THE DEEP QUALITY-VALUE LEARNING FAMILY OF ALGORITHMS

CONTRIBUTIONS AND OUTLINE

In the first part of this thesis we have thoroughly studied the level of transferability of deep neural networks that get trained in a supervised learning fashion. From the results of our studies we concluded that significant benefits can come from using pre-trained models over networks that get trained from scratch, and that transfer learning can be a valuable machine learning paradigm for studying the generalization properties of neural networks. So far we have always considered the setting in which, before getting trained on a new task, a model could rely on some **fixed** knowledge it had learned on a separate but related task. In this chapter however, we take a different approach: we develop a novel family of Deep Reinforcement Learning (DRL) algorithms, that instead of learning on top of what a model has learned in the past, rely on what is **simultaneously** being learned by a different, yet related model. The information that is being learned by one model can be transferred and used by a second one in a very dynamical fashion, which within the DRL context yields faster, more robust and better performance.

The structure of this chapter is the following: in Sec. 7.1 and Sec. 7.2 we provide the reader with some background information about the field of DRL and present the necessary mathematical notation that will be used throughout this chapter. In Sec. 7.4 we introduce the main algorithmic contributions of our research, the performance of which is studied from different perspectives in Sec. 7.5. The chapter ends with Sec. 7.6 and Sec. 7.7 which provide a set of additional studies that characterize the performance of our newly introduced algorithms even further, while providing insights about potential possible future work.

This chapter is based on the following two publications: Sabatelli et al. [158] and Sabatelli et al. [162]

7.1 INTRODUCTION

In value-based Reinforcement Learning (RL) the aim is to construct algorithms which learn *value functions* that are either able to estimate how good or bad it is for an agent to be in a particular state, or how

good it is for an agent to perform a particular action in a given state. Such functions are respectively denoted as the state-value function $V(s)$, and the state-action value function $Q(s, a)$ [188]. In Deep Reinforcement Learning (DRL) the aim is to approximate these value functions with e.g. deep convolutional neural networks [98], which can serve as universal function approximators and powerful feature extractors. Classic model-free RL algorithms like Q-Learning [214], Double Q-Learning [204] and SARSA [154] have all led to the development of a “deep” version of themselves in which the original RL update rules are expressed as objective functions that can be minimized by gradient descent [120, 205, 231]. Despite their successful applications [102], the aforementioned algorithms only aim at approximating the Q function, while completely ignoring the V function. This approach, however, is prone to issues that go back to standard RL literature. As shown by Van Hasselt, Guez, and Silver [205] the DQN algorithm [120] is known to overestimate the values of the Q function and requires an additional target network to not diverge (which role, as shown by Achiam, Knight, and Abbeel [2], is not yet fully understood). These overestimations can partially be corrected by the DDQN [205] algorithm, which, despite yielding stability improvements, does not always prevent its Q networks from diverging [**van2018deep**] and sometimes even underestimating the Q function. Furthermore, DRL algorithms are also extremely slow to train. In what follows, we introduce a new family of DRL algorithms based on the key idea of simultaneously learning the V function alongside the Q function with two separate neural networks. Our main insight is that by jointly approximating the V function and the Q function, the task of learning one of these value functions can be sped up if the model that is responsible for learning it, can rely on what is being learned by the model responsible for learning the remaining value function. We show that this simple, yet effective idea yields faster, more robust and better model-free Deep Reinforcement Learning.

7.2 PRELIMINARIES

We formally define the RL setting as a Markov Decision Process (MDP) where the main components are a finite set of states $\mathcal{S} = \{s^1, s^2, \dots, s^n\}$, a finite set of actions \mathcal{A} and a time-counter variable t . In each state $s_t \in \mathcal{S}$, the RL agent can perform an action $a_t \in \mathcal{A}(s_t)$ and transit to the next state as defined by a transition probability distribution $p(s_{t+1}|s_t, a_t)$. When moving from s_t to a successor state s_{t+1} the agent receives a reward signal r_t coming from the reward function $\mathfrak{R}(s_t, a_t, s_{t+1})$. The actions of the agent are selected based on its policy

$\pi : \mathcal{S} \rightarrow \mathcal{A}$ that maps each state to a particular action. For every state $s \in \mathcal{S}$, under policy π its *value function* V^π is defined as:

$$V^\pi(s) = \mathbb{E} \left[\sum_{k=0}^{\infty} \gamma^k r_{t+k} \middle| s_t = s, \pi \right], \quad (86)$$

which denotes the expected cumulative discounted reward that the agent will get when starting in state s and by following policy π thereafter. Similarly, we can also define the *state-action* value function Q for denoting the value of taking action a in state s based on policy π as:

$$Q^\pi(s, a) = \mathbb{E} \left[\sum_{k=0}^{\infty} \gamma^k r_{t+k} \middle| s_t = s, a_t = a, \pi \right]. \quad (87)$$

Both functions are computed with respect to the discount factor $\gamma \in [0, 1]$ which controls the trade-off between immediate and long term rewards. The goal of an RL agent is to find a policy π^* that realizes the optimal expected return:

$$V^*(s) = \max_{\pi} V^\pi(s), \text{ for all } s \in \mathcal{S} \quad (88)$$

and the optimal Q value function:

$$Q^*(s, a) = \max_{\pi} Q^\pi(s, a) \text{ for all } s \in \mathcal{S} \text{ and } a \in \mathcal{A}. \quad (89)$$

It is well-known that optimal value functions satisfy the Bellman optimality equation as given by

$$V^*(s_t) = \max_a \sum_{s_{t+1}} p(s_{t+1}|s_t, a) \left[\mathfrak{R}(s_t, a, s_{t+1}) + \gamma V^*(s_{t+1}) \right] \quad (90)$$

for the state-value function, and by

$$Q^*(s_t, a_t) = \sum_{s_{t+1}} p(s_{t+1}|s_t, a_t) \left[\mathfrak{R}(s_t, a_t, s_{t+1}) + \gamma \max_a Q^*(s_{t+1}, a) \right], \quad (91)$$

for the state-action value function. Both functions can either be learned via Monte Carlo methods or by Temporal-Difference (TD) learning [186], with the latter approach being so far the most popular choice among model-free RL algorithms [154, 204, 214].

7.3 RELATED WORK

While RL algorithms have been successfully combined with shallow neural networks for over two decades [195], the use of these algorithms with deeper architectures is more recent. The contribution which has established the potential of DRL can certainly be identified with the Deep-Q-Network (DQN), the first algorithm which uses

a convolutional neural network for successfully learning an approximation of the Q function from high dimensional inputs [120]. This approximation is learned by reshaping the popular Q-Learning algorithm introduced by Watkins and Dayan [214] to an objective function which can be minimized by gradient descent. The original Q-Learning algorithm learns the state-action value function as follows

$$Q(s_t, a_t) := Q(s_t, a_t) + \alpha [r_t + \gamma \max_{a \in \mathcal{A}} Q(s_{t+1}, a) - Q(s_t, a_t)] \quad (92)$$

where α corresponds to the learning rate. The DQN algorithm adapts this update rule to a differentiable loss function which can be used for training a neural network that is parametrized by θ . This objective function comes in the following form:

$$L(\theta) = \mathbb{E}_{\langle s_t, a_t, r_t, s_{t+1} \rangle \sim U(D)} \left[(r_t + \gamma \max_{a \in \mathcal{A}} Q(s_{t+1}, a; \theta^-) - Q(s_t, a_t; \theta))^2 \right]. \quad (93)$$

Within this loss there are two components which ensure stable training. The first one is the Experience-Replay memory buffer (D), first introduced by Lin [105], a buffer coming in the form of a queue which stores RL experiences $\langle s_t, a_t, r_t, s_{t+1} \rangle$. When it comes to the popular Atari Arcade Learning (ALE) [13] benchmark, the DQN algorithm uniformly samples mini-batches of 32 experiences for minimizing Eq. 93, a procedure which starts as soon as at least 50.000 experiences are stored within the queue. Furthermore, there is a second component which ensures stable training denoted as the target-network. DQN learns an approximation of the Q function via TD-Learning, meaning that the approximated Q -function is regressed towards TD-targets which are computed by the approximated Q function itself. The TD-target, defined as y_t^{DQN} , is expressed as follows:

$$y_t^{DQN} = r_t + \gamma \max_{a \in \mathcal{A}} Q(s_{t+1}, a; \theta^-), \quad (94)$$

and is computed by the target network θ^- instead from the online Q -network θ . The online network, and its target counterpart, have the exact same structure, with the main difference being that the parameters of the latter do not get optimized each time a mini-batch of experiences is sampled from the memory buffer. On the contrary its weights are temporally frozen and are only periodically updated with the θ weights (as defined by an appropriate hyperparameter). Given a training iteration i , differentiating the objective function of Eq. 93 with respect to θ gives the following gradient:

$$\nabla_{\theta_i} y_t^{DQN}(\theta_i) = \mathbb{E}_{\langle s_t, a_t, r_t, s_{t+1} \rangle \sim U(D)} \left[(r_t + \gamma \max_{a \in \mathcal{A}} Q(s_{t+1}, a; \theta_{i-1}^-) - Q(s_t, a_t; \theta_i)) \nabla_{\theta_i} Q(s_t, a_t; \theta_i) \right]. \quad (95)$$

Despite yielding super-human performance on most games coming from the ALE, DQN has shown to be suffering from the same issues which characterize the Q-Learning algorithm [204]. Among these issues we mention the overestimation bias of the Q-function which has been well characterized in the tabular setting by Van Hasselt [204] and later in the deep learning context by Van Hasselt, Guez, and Silver [205]. In short, DQN is prone to learn overestimated Q-values because the same values are used both for selecting an action ($\max_{a \in \mathcal{A}}$) and for evaluating it ($Q(s_{t+1}, a; \theta^-)$). As originally presented by Van Hasselt, Guez, and Silver [205] this becomes clearer when re-writing Eq. 94 as:

$$y_t^{DQN} = r_t + \gamma Q(s_{t+1}, \arg \max_{a \in \mathcal{A}} Q(s_{t+1}, a; \theta); \theta^-). \quad (96)$$

As a result, DQN tends to approximate the expected maximum value of a state, instead of its maximum expected value. To solve this problem the DDQN algorithm untangles the selection of an action from its evaluation by taking advantage of the target network θ^- . DDQN's target is the same as DQN's with the main difference being that the selection of an action, given by the online Q-network θ , and the evaluation of the resulting policy, given by θ^- , can get unbiased by symmetrically updating the two sets of weights (θ and θ^-). This can be achieved by regularly switching their roles during training.

Several extensions of DQN and DDQN have been proposed over the years, to make these algorithms learn faster and more data-efficient. We refer the reader to [102] for a more in-depth review of these contributions. Within this chapter, we are only interested in synchronous DRL algorithms which learn an approximation of a value function. This is achieved by following the same experimental setups that have been used for DQN and DDQN, and that will be reviewed in Sec. 7.5.1 of this chapter. Therefore, in what follows we will aim at comparing our novel DRL algorithms to DQN and DDQN only, while leaving their potential integration within more sophisticated DRL techniques as future work.

7.4 A NOVEL FAMILY OF DEEP REINFORCEMENT LEARNING ALGORITHMS

Just as much as DQN and DDQN are based on two tabular RL algorithms, so are the main contributions presented in this chapter. More specifically we extend two RL algorithms which were first introduced by Wiering [219] and then extended by Wiering and Van Hasselt [220] to the use of deep neural networks that serve as function approximators. Training these algorithms robustly is done by taking advantage of some of the techniques which have been reviewed in the previous section.

7.4.1 DQV-Learning

Our first contribution is the Deep Quality-Value (DQV) Learning algorithm, a novel DRL algorithm which aims at jointly approximating the V function alongside the Q function in an *on-policy* learning setting. This algorithm is based on the $QV(\lambda)$ algorithm [219], a tabular RL algorithm which learns the V function via the simplest form of TD-Learning [186], and uses the estimates that are learned by this value function to update the Q function in a Q-Learning resembling way. Specifically, after a transition $\langle s_t, a_t, r_t, s_{t+1} \rangle$, $QV(\lambda)$ uses the $TD(\lambda)$ learning rule [186] to update the V function for all states:

$$V(s) := V(s) + \alpha [r_t + \gamma V(s_{t+1}) - V(s_t)] e_t(s), \quad (97)$$

where α stands again for the learning rate and γ is the discount factor, while $e_t(s)$ are the eligibility traces [55, 138, 221] that are necessary for keeping track if a particular state has occurred before a certain time-step or not. These are updated for all states as follows:

$$e_t(s) = \gamma \lambda e_{t-1}(s) + \eta_t(s), \quad (98)$$

where $\eta_t(s)$ is an indicator function that returns a value of 1 whether a particular state occurred at time t and 0 otherwise. Before updating the V function, $QV(\lambda)$ updates the Q function first, and does this via the following update rule:

$$Q(s_t, a_t) := Q(s_t, a_t) + \alpha [r_t + \gamma V(s_{t+1}) - Q(s_t, a_t)]. \quad (99)$$

We take inspiration from this specific learning dynamic and aim at learning an approximation of both the V function, and the Q function, with two neural networks that are respectively parametrized by Φ and θ . To do so, we follow the same principles which have led to the development of the DQN algorithm and that reshape Eq. 92 to Eq. 93. Therefore, starting from Eq. 97, and after removing $e_t(s)$ for simplicity, we get the following objective function which is used by DQV for learning the state-value function:

$$L(\Phi) = \mathbb{E}_{\langle s_t, a_t, r_t, s_{t+1} \rangle \sim U(D)} \left[(r_t + \gamma V(s_{t+1}; \Phi^-) - V(s_t; \Phi))^2 \right], \quad (100)$$

while the following loss is minimized for learning the Q function when starting from Eq. 99:

$$L(\theta) = \mathbb{E}_{\langle s_t, a_t, r_t, s_{t+1} \rangle \sim U(D)} \left[(r_t + \gamma V(s_{t+1}; \Phi^-) - Q(s_t, a_t; \theta))^2 \right], \quad (101)$$

where D is again the Experience-Replay memory buffer, used for uniformly sampling batches of RL trajectories $\langle s_t, a_t, r_t, s_{t+1} \rangle$, and Φ^- is

the target-network used for the construction of the TD-errors. Please note that the role of this target network is different from its role within the DQN algorithm. In DQV this network corresponds to a copy of the network which approximates the state-value function and not the state-action value function. It is also worth noting that both networks learn from the same TD-target which comes in the following form:

$$y_t^{DQV} = r_t + \gamma V(s_{t+1}; \Phi^-). \quad (102)$$

The gradient with respect to both loss functions can be easily expressed similarly as done in Eq. 95 for the DQN algorithm.

7.4.2 DQV-Learning with Multilayer Perceptrons

We start by exploring whether this learning dynamic of jointly approximating two value functions simultaneously, and let the Q function bootstrap from the TD-targets that are learned from the V network can yield successful results on a set of preliminary experiments. To do so, we use two classic control problems that are well known in the RL literature: Acrobot [187] and Cartpole [11] with both environments being provided by the Open-AI Gym package [23]. We approximate the V function and the Q function with a two hidden layer Multilayer Perceptron (MLP) that is activated by a ReLU non linearity ($f(x) = \max(0, x)$) and compare the performance of DQV to the one of the DQN and the DDQN algorithms, which use the same MLP but for approximating the Q function only. Given the simplicity of these two control problems we did not integrate DQV with the target network Φ^- yet. Our preliminary results reported in Fig. 37, show the benefits that can come from training two separate networks with the update rules reported in Eq. 100 and Eq. 101. We can in fact observe that on both control problems DQV-Learning outperforms DQN and DDQN, by converging significantly faster.

7.4.3 DQV-Max Learning

Based on the successful results presented in Fig. 37 that highlight the potential benefits that could come from jointly approximating two value functions over one, we now introduce the Deep Quality-Value-Max (DQV-Max) algorithm, a novel DRL algorithm which builds on top of some of the ideas that characterize DQV. Similarly as done for DQV, we still aim at jointly learning an approximation of the V function and the Q function, but in this case, the goal is to do this with an *off-policy* learning scheme. To construct this algorithm we take inspiration from the QV-Max RL algorithm introduced by Wiering and Van Hasselt [220]. The key component of QV-Max is the use of the $\max_{a \in \mathcal{A}} Q(s_{t+1}, a)$ operator, which makes RL algorithms learn *off-*

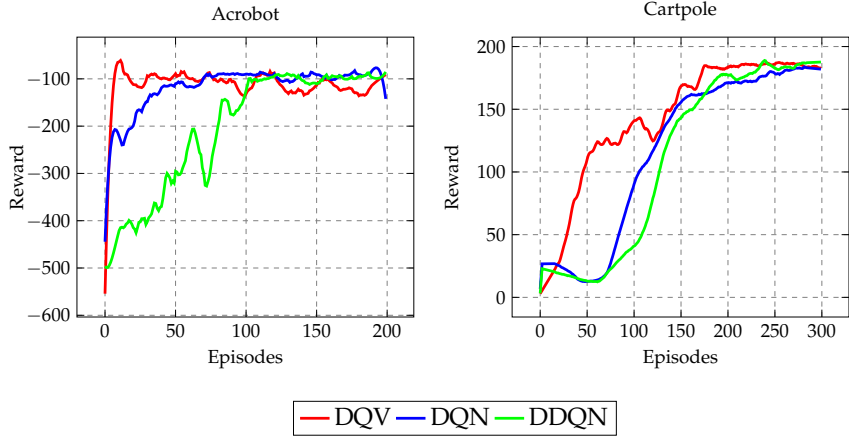


Figure 37: Our preliminary results that show the benefits in terms of convergence time that can come from jointly approximating the V function alongside the Q function. We can observe that the DQV-Learning algorithm yields faster convergence when compared to popular algorithms which only approximate the Q function: DQN and DDQN.

policy. We use this operator when approximating the V function and for computing TD-errors which correspond to the ones that are also used by the DQN algorithm. However, within DQV-Max, these TD-errors are used by the state-value network and not by the state-action value network. This results in the following loss which is used for learning the V function:

$$L(\Phi) = \mathbb{E}_{(s_t, a_t, r_t, s_{t+1}) \sim U(D)} \left[(r_t + \gamma \max_{a \in \mathcal{A}} Q(s_{t+1}, a; \theta^-) - V(s_t; \Phi))^2 \right]. \quad (103)$$

In this case the target network θ^- corresponds to the same target network that is used by DQN. The TD-error $r_t + \gamma \max_{a \in \mathcal{A}} Q(s_{t+1}, a; \theta^-)$ is however only used for learning the V function. When it comes to the Q function we use the same update rule that is presented in Eq. 101 with the only difference being that in this case no Φ^- target network is used. Despite requiring the computation of two different targets for learning, we noticed that DQV-Max did not benefit from using two distinct target networks, therefore its loss function for approximating the Q function is simply:

$$L(\theta) = \mathbb{E}_{(s_t, a_t, r_t, s_{t+1}) \sim U(D)} \left[(r_t + \gamma V(s_{t+1}; \Phi) - Q(s_t, a_t; \theta))^2 \right]. \quad (104)$$

The pseudocode of both DQV and DQV-Max is presented at the end of this thesis in Algorithm 1 which can be found in Appendix. The pseudocode is an adaptation of a standard DRL training loop

which corresponds to what is usually presented within the literature [120]. We just make explicit use of the hyperparameters `total_a` and `c` which ensure that enough actions have been performed by the agent before updating the weights of the target network. We also ensure via the hyperparameter `total_e`, that enough episodes are stored within the memory buffer (which has capacity \mathcal{N}) before starting to optimize the neural networks.

7.5 RESULTS

7.5.1 Global Evaluation

We evaluate the performance of DQV and DQV-Max on a subset of 15 games coming from the popular Atari-2600 benchmark [13]. Our newly introduced algorithms are compared against DQN and DDQN. To keep all the comparisons as fair as possible we follow the same experimental setup and evaluation protocol which was used in [120] and [205]. The only difference between DQV and DQV-Max, and DQN and DDQN is the exploration schedule which is used. Differently from the latter two algorithms, which use an epsilon-greedy strategy which has an ϵ starting value of 1.0, DQV and DQV-Max's exploration policy starts with an initial ϵ value of 0.5. All other hyperparameters, ranging from the size of the Experience-Replay memory buffer to the architectures of the neural networks, are kept the same among all algorithms. We refer the reader to the original DQN paper [120] for an in-depth overview of all these hyperparameters. The performance of the algorithms is tested based on the popular no-op action evaluation regime. At the end of the training, the learned policies are tested over a series of episodes for a total amount of 5 minutes of emulator time. All testing episodes start by executing a set of partially random actions to test the level of generalization of the learned policies. We present our results in Table 14 where the best performing algorithm is reported in a green cell while the second-best performing algorithm is reported in a yellow cell. As is common within the DRL literature, the table also reports the scores which would be obtained by an expert human player and by a random policy. When the scores over games are equivalent, we report in the green and yellow cells the fastest and second fastest algorithm with respect to its convergence time.

We can start by observing that DQV and DQV-Max successfully master all the environments on which they have been tested, with the only exception being the Montezuma's Revenge game. It is well-known that this game requires more sophisticated exploration strategies than the epsilon-greedy one [47], and was also not mastered by DQN and DDQN when these algorithms were introduced. We can also observe that there is no algorithm which performs best on all

Algorithm 1 DQV and DQV-Max Learning

Require: Experience Replay Queue D of maximum size N

Require: Q network with parameters θ ▷ Network required by DQV

Require: V networks with parameters Φ and Φ^- ▷ Networks required by DQV

Require: Q networks with parameters θ and θ^- ▷ Networks required by DQV-Max

Require: V network with parameters Φ ▷ Network required by DQV-Max

Require: total_a = 0

Require: total_e = 0

Require: c = 10000

Require: $\mathcal{N} = 50000$

1: **while** True **do**

2: set s_t as the initial state

3: **while** s_t is not terminal **do**

4: select $a_t \in \mathcal{A}$ for s_t with policy π (using the epsilon-greedy strategy)

5: get r_t and s_{t+1}

6: store $\langle s_t, a_t, r_t, s_{t+1} \rangle$ in D

7: $s_t := s_{t+1}$

8: total_e += 1

9: **if** total_e $\geq \mathcal{N}$ **then**

10: sample a minibatch $B = \{\langle s_t^i, a_t^i, r_t^i, s_{t+1}^i \rangle | i = 1, \dots, 32\}$ of size 32 from D

11: **for** i = 1 to 32 **do**

12: **if** s_{t+1}^i is terminal **then**

13: $y_t^i := r_t^i$ ▷ TD-Error for DQV

14: $v_t^i := r_t^i$ ▷ 1st TD-Error for DQV-Max

15: $q_t^i := r_t^i$ ▷ 2nd TD-Error for DQV-Max

16: **else**

17: $y_t^i := r_t^i + \gamma V(s_{t+1}^i, \Phi^-)$ ▷ TD-Error for DQV

18: $v_t^i := r_t^i + \gamma \max_{a \in \mathcal{A}} Q(s_{t+1}^i, a, \theta^-)$ ▷ 1st TD-Error for DQV-Max

19: $q_t^i := r_t^i + \gamma V(s_{t+1}^i, \Phi)$ ▷ 2nd TD-Error for DQV-Max

20: **end if**

21: **end for**

22: $\theta := \arg \min_{\theta} \sum_{i=1}^{32} (y_t^i - Q(s_t^i, a_t^i, \theta))^2$ ▷ Train the Q network for DQV

23: $\Phi := \arg \min_{\Phi} \sum_{i=1}^{32} (y_t^i - V(s_t^i, \Phi))^2$ ▷ Train the V network for DQV

24: $\theta := \arg \min_{\theta} \sum_{i=1}^{32} (q_t^i - Q(s_t^i, a_t^i, \theta))^2$ ▷ Train the Q network for DQV-Max

25: $\Phi := \arg \min_{\Phi} \sum_{i=1}^{32} (v_t^i - V(s_t^i, \Phi))^2$ ▷ Train the V network for DQV-Max

26: total_a += 1

27: **if** total_a = c **then**

28: $\Phi^- := \Phi$ ▷ Update the target V network in DQV

29: $\theta^- := \theta$ ▷ Update the target Q network in DQV-Max

30: total_a := 0

31: **end if**

32: **end if**

33: **end while**

34: **end while**

the tested environments even though, as highlighted by the green and yellow cells, the algorithms of the DQV-family seem to generally perform better than DQN and DDQN, with DQV-Max being the overall best performing algorithm in our set of experiments. When either DQV or DQV-Max are not the best performing algorithm (see for example the `Boxing` and `CrazyClimber` environments), we can still observe that our algorithms managed to converge to a policy which is not significantly worst than the one learned by DQN and DDQN. There is however one exception being the `RoadRunner` environment. In fact, in this game, DDQN significantly outperforms DQV and DQV-Max. It is also worth noting the results on the `BankHeist` and `Enduro` environments. Both DQN and DDQN failed to achieve super-human performance on these games, while DQV and DQV-Max successfully managed to obtain a significantly higher score than the one obtained by a professional human player. On the `BankHeist` environment DQV and DQV-Max obtain ≈ 400 points more than an expert human player, while on the `Enduro` environment their performance is almost three times better than the one obtained by DQN and DDQN.

Table 14: The results obtained by DQV and DQV-Max on a subset of 15 Atari games. We can see that our newly introduced algorithms have a comparable, and often even better performance than DQN and DDQN. As highlighted by the green cells the overall best performing algorithm in our set of experiments is DQV-Max while the second-best performing algorithm is DQV (as reported by the yellow cells). Specific attention should be given to the games `BankHeist` and `Enduro` where DQV and DQV-Max are the only algorithms which can master the game with a final super-human performance.

Environment	Random	Human	DQN [120]	DDQN [205]	DQV	DQV-Max
Asteroids	719.10	13156.70	1629.33	930.60	1445.40	1846.08
Bank Heist	14.20	734.40	429.67	728.30	1236.50	1118.28
Boxing	0.10	4.30	71.83	81.70	78.66	80.15
Crazy Climber	10780.50	35410.50	114103.33	101874.00	108600.00	1000131.00
Enduro	0.00	309.60	301.77	319.50	829.33	875.64
Fishing Derby	-91.70	5.50	-0.80	20.30	1.12	20.42
Frostbite	65.20	4334.70	328.33	241.50	271.86	281.36
Gopher	257.60	2321.00	8520.00	8215.40	8230.30	7940.00
Ice Hockey	-11.20	0.90	-1.60	-2.40	-1.88	-1.12
James Bond	29.00	406.70	576.67	438.00	372.41	440.80
Montezuma's Revenge	0.00	4366.70	0.00	0.00	0.00	0.00
Ms. Pacman	307.30	15693.40	2311.00	3210.00	3590.00	3390.00
Pong	-20.70	9.30	18.90	21.00	21.00	21.00
Road Runner	11.50	7845.00	18256.67	48377.00	39290.00	20700.00
Zaxxon	32.50	9173.30	4976.67	10182.00	10950.00	8487.00

7.5.2 Convergence Time

While DRL algorithms have certainly obtained impressive results on the Atari-2600 benchmark, it is also true that the amount of training time which is required by these algorithms can be very long. Over the years, several techniques, ranging from Prioritized Experience Replay (PER) [212] to the Rainbow extensions introduced by Hessel et al. [72], have been proposed to reduce the training time of DRL algorithms. It is therefore natural to investigate whether jointly approximating the V function alongside the Q function can lead to significant benefits in this behalf. Unlike the Q function, the state-value function is not dependent on the set of possible actions that the agent may take, and therefore requires fewer parameters to converge. Since DQV and DQV-Max use the estimates of the V network to train the Q function, it is possible that the Q function could directly benefit from these estimates and as a result converge faster than when regressed towards itself (as happens in DQN).

We use two self-implemented versions of DQN and DDQN for comparing the convergence time that is required during training by all the tested algorithms on three increasingly complex Atari games: Boxing, Pong and Enduro. Our results, reported in Fig. 38, show that DQV and DQV-Max converge significantly faster than DQN and DDQN, therefore confirming the preliminary results which we reported in Fig. ??, and highlighting once again the benefits of jointly approximating two value functions instead of one when it comes to the overall convergence time that is required by the algorithms. Even though, as presented in Table 14, DQV and DQV-Max do not always significantly outperform DQN and DDQN in terms of the final cumulative reward which is obtained, it is worth noting that these algorithms require significantly less training episodes to converge on all tested games. This benefit makes our two novel algorithms faster alternatives within model-free DRL.

7.5.3 Quality of the Learned Value Functions

It is well-known that the combination of RL algorithms with function approximators can yield DRL algorithms that diverge. The popular Q-Learning algorithm is known to result in unstable learning both if linear [201] and non-linear functions are used when approximating the Q function [van2018deep]. This divergence according to Sutton and Barto [188] is caused by the interplay of three elements that are known as the '*Deadly Triad*' of DRL. The elements of this triad are:

- *a function approximator*: which is used for learning an approximation of a value function that could not be learned in the tabular RL setting due to a too large state-action space.

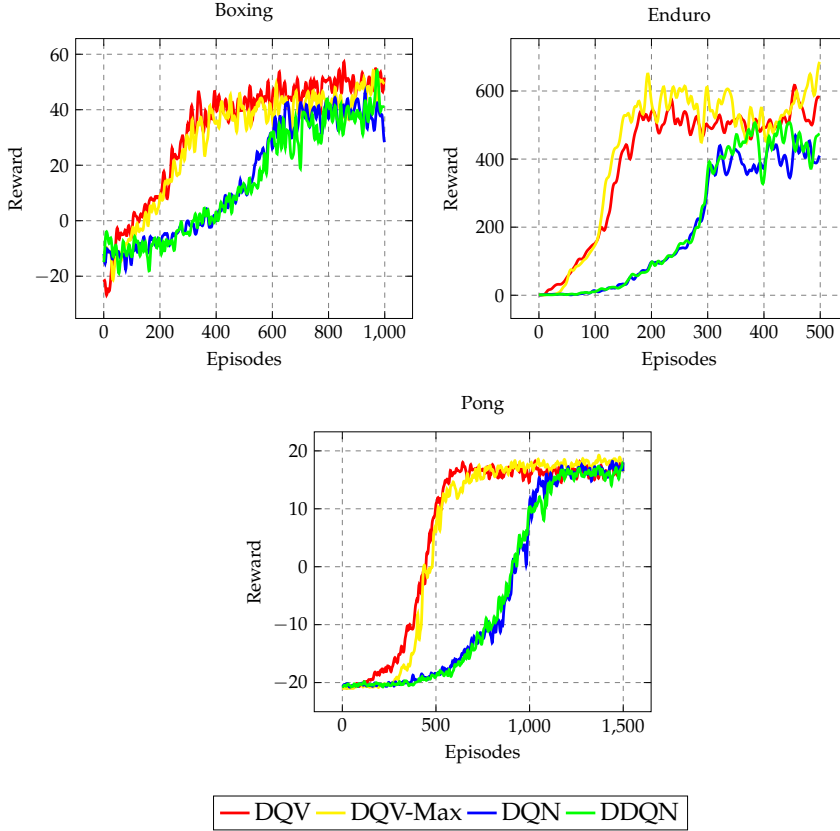


Figure 38: Learning curves obtained during training on three different Atari games by DQV and DQV-Max, and DQN and DDQN. We can observe that on these games both DQV and DQV-Max converge significantly faster than DQN and DDQN and that they obtain higher cumulative rewards on the Enduro environment.

- *bootstrapping*: when the algorithms use a future estimated value for learning the same kind of estimate.
- *off-policy learning*: when a future estimated value is different from the one which would be computed by the policy the agent is following.

van2018deep have shown that the ‘*Deadly Triad*’ is responsible for enhancing one of the most popular biases that characterize the Q-Learning algorithm: the overestimation bias of the Q function [204]. It is therefore natural to study how DQV and DQV-Max relate to the ‘*Deadly Triad*’ of DRL, and to investigate up to what extent these algorithms suffer from the overestimation bias of the Q function. To do this we monitor the estimates that are given by the network that is responsible for approximating the Q function. More specifically, at training time, we compute the averaged $\max_{a \in \mathcal{A}} Q(s_{t+1}, a)$ over a set (n) of full evaluation episodes as defined by

$$\frac{1}{n} \sum_{t=1}^n \max_{a \in \mathcal{A}} Q(s_{t+1}, a; \theta). \quad (105)$$

As suggested by Van Hasselt, Guez, and Silver [205] these estimates can then be compared to the averaged discounted return of all visited states that comes from an agent that has already concluded training. By analyzing whether the Q values which are estimated while training differ from the ones which should be predicted by the end of it, it is possible to quantitatively characterize the level of divergence of DRL algorithms. We report our results in Figs. 39, 40, 41 and 42 where the black full lines correspond to the value estimates that come from each algorithm at training time, while the coloured lines correspond to the actual averaged discounted return that is given by an already trained agent.

We can start by observing that the values denoting the averaged discounted return obtained by each algorithm differ among agents. This is especially the case when it comes to the Enduro environment, and is a result which is in line with what has been presented in Table 12: DQV and DQV-Max lead to better final policies than DQN and DDQN. Furthermore, when we compare these baseline values to the value estimates that are obtained during training, we can observe that the ones obtained by the DQN algorithm significantly diverge from the ones which should be predicted by the end of training. This behavior is known to be caused by the overestimation bias of the Q function which can be corrected by the DDQN algorithm. By analyzing the value estimates of DQV and DQV-Max we can observe that both algorithms produce value estimates which are more similar to the ones computed by DDQN than to the ones given by DQN. This is especially the case for DQV, in fact its value estimates nicely correspond to the averaged discounted return baseline, both on the Pong environment and on the Enduro environment. The estimates coming from DQV-Max, however, seem to diverge more when compared to DQV and DDQN's ones. This is clearer on the Enduro environment, where the algorithm does show some divergence. However, we can also observe that this divergence is less strong when compared to DQN's one. The value estimates of the latter algorithm keep growing over time, while DQV-Max's ones get bounded while training progresses. This results in smaller estimated Q values. We believe that there are mainly two reasons why our algorithms suffer less from the overestimation bias of the Q function. When it comes to DQV, we believe that this algorithm suffers less from this bias since it is an *on-policy* learning algorithm. Such algorithms are trained on exploration actions with lower Q values. Because of its *on-policy* learning scheme, DQV also does not present one element of the '*Deadly Triad*', which might help reducing divergence. When it comes to DQV-Max, we believe that the reason why this algorithm does not diverge as much as DQN can be found in the way it approximates the Q function. One key component of the '*Deadly Triad*', is that divergence occurs if the Q function is learned by regressing towards itself. As given by Eq. 104

we can see that this does not hold for DQV-Max, since the Q function bootstraps with respect to estimates that come from the V network. We believe that this specific learning dynamic, which also holds for the DQV algorithm, makes our algorithms less prone to estimate large Q values.

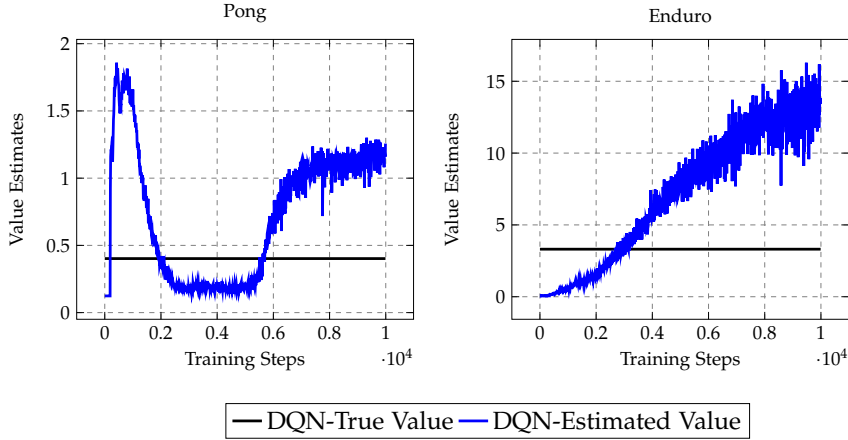


Figure 39: Results investigating the extent to which the DQN algorithm suffers from the overestimation bias of the Q function. We can observe that on the Pong environment during the early stages of training, the $\max_{a \in \mathcal{A}} Q(s_{t+1}, a)$ estimates quickly grow, while on the Enduro game the values estimated by the Q network keep indefinitely growing, therefore making the algorithm significantly diverge from the real return that is obtained by a trained agent.

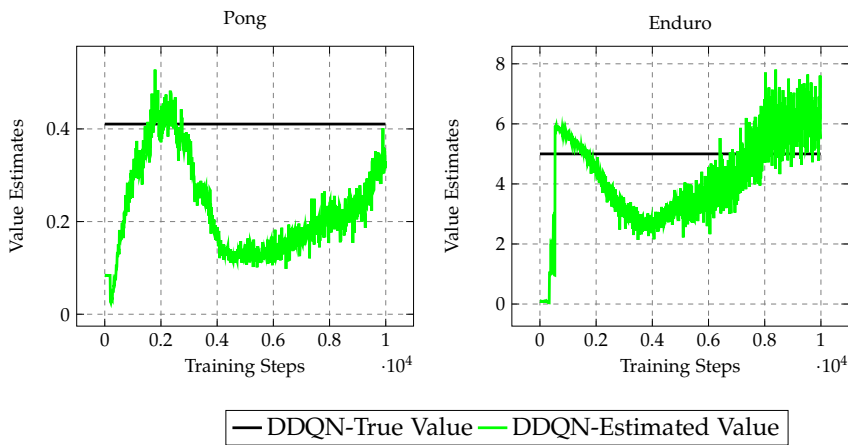


Figure 40: Results investigating the extent to which the DDQN algorithm suffers from the overestimation bias of the Q function. We can observe that compared to the analysis presented in Fig. 39, the DDQN algorithm prevents its Q -Network from diverging since on both Atari environments the $\max_{a \in \mathcal{A}} Q(s_{t+1}, a)$ estimates do not diverge from the observed real return of a trained agent. Results that replicate the findings reported by [van2018deep](#).

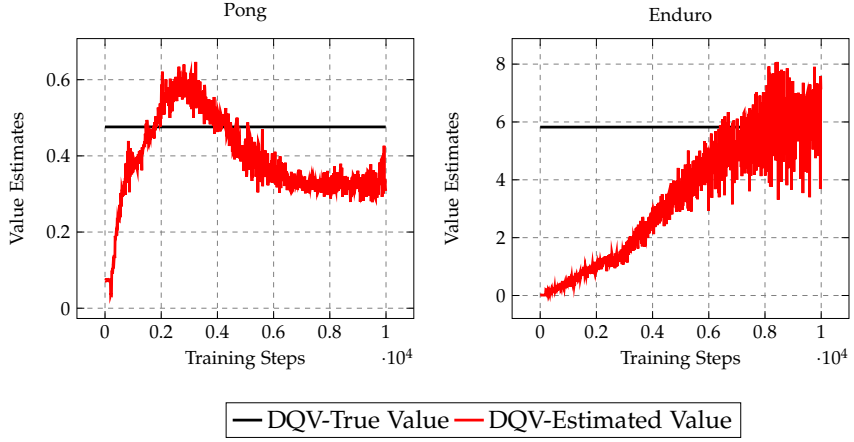


Figure 41: Results investigating the extent to which the DQV algorithm suffers from the overestimation bias of the Q function. We can observe that the performance of the algorithm is similar to the one observed in Fig. 40 for the DDQN algorithm. On both environments the estimated cumulative reward does not diverge from the real return that is obtained by the end of training, therefore suggesting that DQV-Learning does not suffer from the overestimation bias of the Q function. It is also worth noting the difference between the real return obtained by the DQN and the DDQN algorithms on the Enduro environment, and the one obtained by DQV. As can be seen by the black line, the real return obtained by a DQV agent is higher than DQN and DDQN's one, a result which shows that DQV converges to a better policy than DQN and DDQN.

7.6 ADDITIONAL STUDIES

As introduced in Sec. 7.4 DQV and DQV-Max use two separate neural networks for approximating the Q function and the V function. To verify whether two different architectures are needed for making both algorithms perform well, we have experimented with a series of variants of the DQV-Learning algorithm. The aim of these experiments is that of reducing the number of trainable parameters that are required by the original version of DQV, and investigate whether its performance could get harmed when reducing the capacity of the algorithm. The studied DQV's extensions are the following:

1. *Hard-DQV*: a version of DQV which uses one single common neural network for approximating both the Q and the V functions. An additional output node, needed for estimating the value of a state, is added next to the output nodes which estimate the different Q values. The parameters of this algorithm are therefore ‘hardly-shared’ among the agent, and provide the benefit of halving the total amount of trainable parameters of DQV. The different outputs of the network get then alternatively optimized according to Eq. 100 and 101.

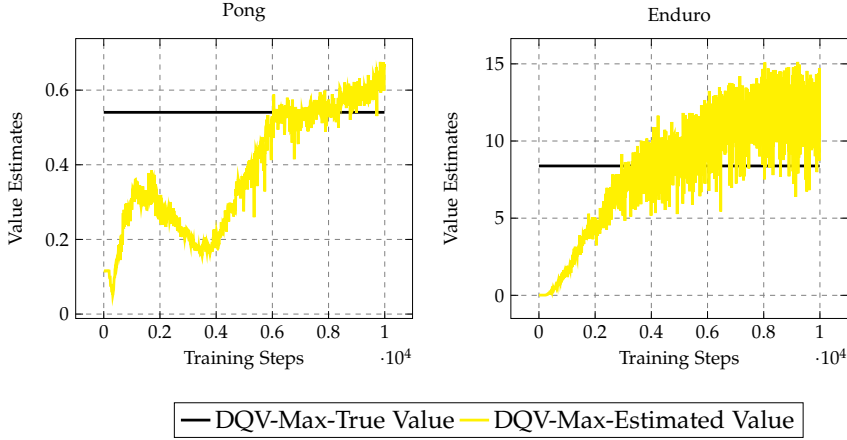


Figure 42: Results investigating the extent to which the DQV-Max algorithm suffers from the overestimation bias of the Q function. We can observe that on the Pong environment the value estimates of the algorithm are comparable to the ones of DDQN and DQV, therefore showing the DQV-Max also diverges significantly less than DQN. On the Enduro environment we can observe that the algorithm does diverge, although, differently from what is reported in Fig. 39, the $\max_{a \in \mathcal{A}} Q(s_{t+1}, a)$ estimates seem to converge towards an upper bound (≈ 15). Similarly to what is reported in Fig. 41 we can again observe that the real return obtained by a trained agent is higher compared to the one obtain by DQN, DDQN and DQV, therefore confirming the results presented in Table 14 which see the DQV-Max algorithm as the best performing algorithm on the Enduro game.

2. *Dueling-DQV*: a slightly more complicated version of Hard-DQV which adds one specific hidden layer before the output nodes that estimate the Q and V functions. In this case, the outputs of the neural network which learn one of the two value functions, partly benefit from some specific weights that are not shared within the neural network. This approach is similar to the one used by the ‘Dueling-Architecture’ presented by Wang et al. [212], therefore the name Dueling-DQV. While it is well established that three convolutional layers are needed [120, 205] for learning the Q function, the same might not be true when it comes to learning the V function. We thus report experiments with three different versions of Dueling-DQV: Dueling-1st, Dueling-2nd, and Dueling-3rd. The difference between these methods is simply the location of the hidden layer which precedes the output that learns the V function. It can be positioned after the first convolutional layer, the second or the third one. Training this architecture is done as for Hard-DQV.
3. *Tiny-DQV*: the neural architectures used by DQV and DQV-Max that approximate the V function and the Q function follow the one which was initially introduced by the DQN algorithm [120].

This corresponds to a three-hidden layer convolutional neural network which is followed by a fully connected layer of 512 hidden units. The first convolutional layer has 32 channels while the last two layers have 64 channels. In Tiny-DQV we reduce the number of trainable parameters of DQV by reducing the number of channels at each convolution operation. Tiny-DQV only uses 8 channels after the first convolutional layer and 16 at the second and third convolutional layers. Furthermore, the size of the final fully connected layer is reduced to only 128 hidden units. The choice of this architecture is motivated by the work presented in [van2018deep] which studies the role of the capacity of the DDQN algorithm. Unlike the Hard-DQV and Dueling-DQV extensions, the parameters of Tiny-DQV are not shared at all among the networks that are responsible for approximating the V function and the Q function.

The results obtained by these alternative versions of DQV are presented in Figs. 43, 44 and 45 where we report the learning curves obtained by the tested algorithms on six different Atari games. Each DQV extension is directly compared to the original DQV algorithm. We can observe that all the extensions of DQV, which aim at reducing the number of trainable parameters of the algorithm, fail in performing as well as the original DQV algorithm. Starting from Fig.43 we can observe that *Hard-DQV* does not only yield significantly lower rewards (see the results obtained on *Boxing*) but also presents more unstable training (as highlighted by the results obtained on the *Pong* environment). Lower rewards and unstable training also characterize the *Tiny-DQV* algorithm (see results on *BankHeist* and *CrazyClimber* reported in Fig.45). Overall the most promising extensions of DQV are its *Dueling* counterparts, we have observed in particular that the best performing architecture over most of our experiments was the *Dueling-DQV-3rd* one. As can be seen by the results reported in Fig. 44 on the *Pong* environment we can observe that *Dueling-DQV-3rd* has a comparable performance to DQV, even though it converges slower. Unfortunately, *Dueling-DQV-3rd* still shows some limitations, in particular when tested on more complicated environments such as *Enduro*, we can observe that it under-performs DQV with ≈ 200 points. It is also worth mentioning that the idea of approximating the V function before the Q function explored by *Dueling-DQV-1st* and *Dueling-DQV-2nd* yielded negative results.

7.7 DISCUSSION AND CONCLUSION

We have presented two novel model-free DRL algorithms which in addition to learning an approximation of the Q function also aim at learning an approximation of the V function. We have compared DQV and DQV-Max Learning to DRL algorithms which only learn

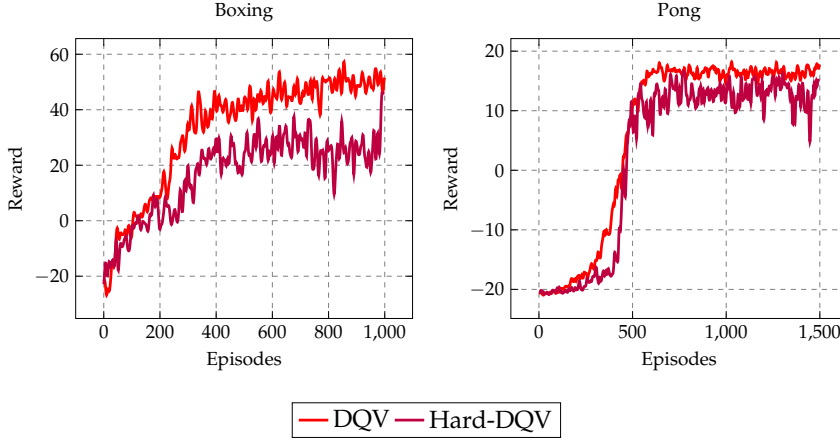


Figure 43: Our results which aim to approximate the V and the Q function with a unique, shared parameterized network, an approach that is heavily inspired by multi-task learning studies that can be found in supervised learning [27, 125, 232]. We can see that this extension of DQV, named Hard-DQV, significantly underperforms the original DQV-Learning algorithm.

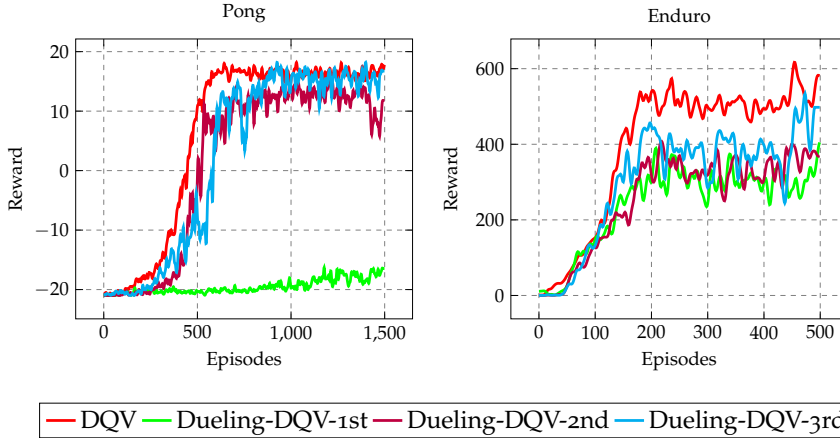


Figure 44: Our extensions of DQV that aim to reduce the amount of trainable parameters of the algorithm by following an approach similar to the one presented by Wang et al. [212] when “Dueling Networks” for DRL have been introduced. We can observe that among all the three Dueling-DQV extensions, only the Dueling-DQV-3rd one yielded good performance, but as highlighted by the results obtained on the Enduro environment, its performance is still inferior when compared to the one of the original DQV algorithm.

an approximation of the Q function, and showed the benefits which come from jointly approximating two value functions over one. Our newly introduced algorithms learn significantly faster than DQN and DDQN and show that approximating both the V function and the Q function can yield significant benefits both in an *on-policy* learning setting as in an *off-policy* learning one. This specific training dynamic

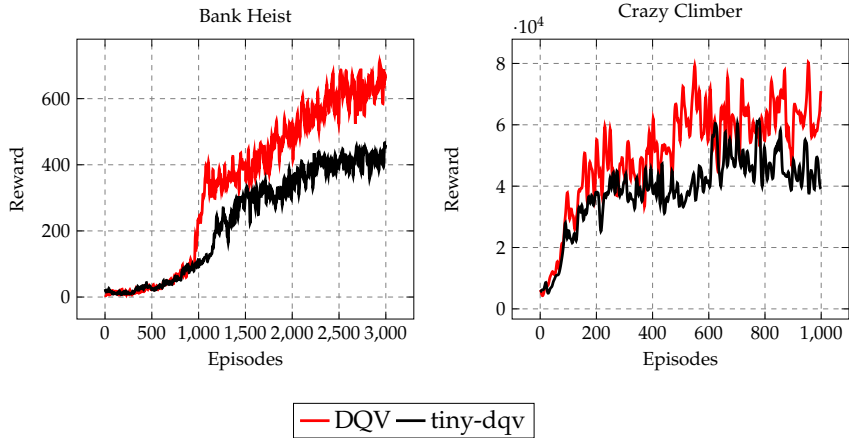


Figure 45: Learning curves obtained when reducing the capacity of the convolutional networks that approximate the V and the Q functions. We can observe that albeit each value function is approximated with its own parametrized network, the tiny-dqv extension still yields worse performance. These results highlight that it is not sufficient to simply have two separate neural networks for DQV to perform well, but that a crucial role in DQV's performance is played by the capacity of the networks that are used as well.

allows for a better learned Q function which makes DQV and DQV-Max less prone to estimate unrealistically large Q values. All these benefits come however at a price: to successfully learn two value functions, two separate neural networks with enough capacity are required.

We identify several directions for further research that focus on the following points: an integration of the algorithms of the DQV-family with all the extensions which have improved the DQN algorithm over the years; an integration of DQV and DQV-Max within an Actor-Critic framework which will allow us to tackle continuous-control problems, and lastly, a study of how the algorithms of the DQV-family will perform in a Batch-DRL setting. It has been shown that DRL algorithms fail when learning from a fixed data set of trajectories instead of dynamically interacting with the environment [54]. This is due to a phenomenon known as extrapolation error. We will investigate to what extent jointly learning two value functions instead of one will cope with this additional DRL bias.

8

ON THE TRANSFERABILITY OF DEEP-Q NETWORKS

9

CONCLUDING REMARKS

Part IV
APPENDIX

BIBLIOGRAPHY

- [1] Martín Abadi, Paul Barham, Jianmin Chen, Zhifeng Chen, Andy Davis, Jeffrey Dean, Matthieu Devin, Sanjay Ghemawat, Geoffrey Irving, Michael Isard, et al. “Tensorflow: A system for large-scale machine learning.” In: *12th {USENIX} symposium on operating systems design and implementation ({OSDI} 16)*. 2016, pp. 265–283.
- [2] Joshua Achiam, Ethan Knight, and Pieter Abbeel. “Towards Characterizing Divergence in Deep Q-Learning.” In: *arXiv preprint arXiv:1903.08894* (2019).
- [3] Sandro Ackermann, Kevin Schawinski, Ce Zhang, Anna K Weigel, and M Dennis Turp. “Using transfer learning to detect galaxy mergers.” In: *Monthly Notices of the Royal Astronomical Society* (2018).
- [4] Nancy Allen. “Collaboration through the Colorado digitization project.” In: *First Monday* 5.6 (2000).
- [5] Ahmed Alqaraawi, Martin Schuessler, Philipp Weiß, Enrico Costanza, and Nadia Berthouze. “Evaluating saliency map explanations for convolutional neural networks: a user study.” In: *Proceedings of the 25th International Conference on Intelligent User Interfaces*. 2020, pp. 275–285.
- [6] Andrew Arnold, Ramesh Nallapati, and William W Cohen. “A comparative study of methods for transductive transfer learning.” In: *Seventh IEEE international conference on data mining workshops (ICDMW 2007)*. IEEE. 2007, pp. 77–82.
- [7] Kai Arulkumaran, Marc Peter Deisenroth, Miles Brundage, and Anil Anthony Bharath. “Deep reinforcement learning: A brief survey.” In: *IEEE Signal Processing Magazine* 34.6 (2017), pp. 26–38.
- [8] Nishanth Arun, Nathan Gaw, Praveer Singh, Ken Chang, Mehak Aggarwal, Bryan Chen, Katharina Hoebel, Sharut Gupta, Jay Patel, Mishka Gidwani, et al. “Assessing the (un) trustworthiness of saliency maps for localizing abnormalities in medical imaging.” In: *arXiv preprint arXiv:2008.02766* (2020).
- [9] Nikolay Banar, Matthia Sabatelli, Pierre Geurts, Walter Daelemans, and Mike Kestemont. “Transfer Learning with Style Transfer between the Photorealistic and Artistic Domain.” In: (2021).

- [10] André Barreto, Will Dabney, Rémi Munos, Jonathan J Hunt, Tom Schaul, Hado P van Hasselt, and David Silver. "Successor features for transfer in reinforcement learning." In: *Advances in neural information processing systems*. 2017, pp. 4055–4065.
- [11] Andrew G Barto, Richard S Sutton, and Charles W Anderson. "Neuronlike adaptive elements that can solve difficult learning control problems." In: *IEEE transactions on systems, man, and cybernetics* 5 (1983), pp. 834–846.
- [12] Marc G Bellemare, Will Dabney, and Rémi Munos. "A distributional perspective on reinforcement learning." In: *International Conference on Machine Learning*. PMLR. 2017, pp. 449–458.
- [13] Marc G Bellemare, Yavar Naddaf, Joel Veness, and Michael Bowling. "The arcade learning environment: An evaluation platform for general agents." In: *Journal of Artificial Intelligence Research* 47 (2013), pp. 253–279.
- [14] Richard Bellman. "Dynamic programming." In: *Science* 153.3731 (1966), pp. 34–37.
- [15] Dimitri P Bertsekas. "Value and policy iterations in optimal control and adaptive dynamic programming." In: *IEEE transactions on neural networks and learning systems* 28.3 (2015), pp. 500–509.
- [16] Dimitri P Bertsekas. *Reinforcement learning and optimal control*. Athena Scientific Belmont, MA, 2019.
- [17] Dimitri P Bertsekas and John N Tsitsiklis. "Neuro-dynamic programming: an overview." In: *Proceedings of 1995 34th IEEE conference on decision and control*. Vol. 1. IEEE. 1995, pp. 560–564.
- [18] Dimitri P Bertsekas et al. *Dynamic programming and optimal control: Vol. 1*. Athena scientific Belmont, 2000.
- [19] Francesco Bidoia, Matthia Sabatelli, Amirhossein Shantia, Marco A. Wiering, and Lambert Schomaker. "A Deep Convolutional Neural Network for Location Recognition and Geometry based Information." In: *Proceedings of the 7th International Conference on Pattern Recognition Applications and Methods, ICPRAM 2018, Funchal, Madeira - Portugal, January 16-18, 2018*. 2018, pp. 27–36.
- [20] Mariusz Bojarski, Anna Choromanska, Krzysztof Choromanski, Bernhard Firner, Larry Jackel, Urs Muller, and Karol Zieba. "VisualBackProp: efficient visualization of CNNs." In: *arXiv preprint arXiv:1611.05418* (2016).
- [21] Léon Bottou and Olivier Bousquet. "13 the tradeoffs of large-scale learning." In: *Optimization for machine learning* (2011), p. 351.

- [22] Nicolas Boulanger-Lewandowski, Yoshua Bengio, and Pascal Vincent. "Audio Chord Recognition with Recurrent Neural Networks." In: *ISMIR*. Citeseer. 2013, pp. 335–340.
- [23] Greg Brockman, Vicki Cheung, Ludwig Pettersson, Jonas Schneider, John Schulman, Jie Tang, and Wojciech Zaremba. "Openai gym." In: *arXiv preprint arXiv:1606.01540* (2016).
- [24] Tom B Brown, Benjamin Mann, Nick Ryder, Melanie Subbiah, Jared Kaplan, Prafulla Dhariwal, Arvind Neelakantan, Pranav Shyam, Girish Sastry, Amanda Askell, et al. "Language models are few-shot learners." In: *arXiv preprint arXiv:2005.14165* (2020).
- [25] Lucian Busoniu, Robert Babuska, Bart De Schutter, and Damien Ernst. *Reinforcement learning and dynamic programming using function approximators*. Vol. 39. CRC press, 2010.
- [26] Lucian Buşoniu, Damien Ernst, Bart De Schutter, and Robert Babuška. "Approximate reinforcement learning: An overview." In: *2011 IEEE symposium on adaptive dynamic programming and reinforcement learning (ADPRL)*. IEEE. 2011, pp. 1–8.
- [27] Rich Caruana. "Multitask learning." In: *Machine learning* 28.1 (1997), pp. 41–75.
- [28] Rich Caruana, Steve Lawrence, and C Lee Giles. "Overfitting in neural nets: Backpropagation, conjugate gradient, and early stopping." In: *Advances in neural information processing systems*. 2001, pp. 402–408.
- [29] Aditya Chattpadhyay, Anirban Sarkar, Prantik Howlader, and Vineeth N Balasubramanian. "Grad-cam++: Generalized gradient-based visual explanations for deep convolutional networks." In: *2018 IEEE Winter Conference on Applications of Computer Vision (WACV)*. IEEE. 2018, pp. 839–847.
- [30] François Chollet. "Xception: Deep learning with depthwise separable convolutions." In: *arXiv preprint* (2016).
- [31] François Chollet et al. *Keras*. 2015.
- [32] Tarin Clanuwat, Mikel Bober-Irizar, Asanobu Kitamoto, Alex Lamb, Kazuaki Yamamoto, and David Ha. "Deep learning for classical Japanese literature." In: *arXiv preprint arXiv:1812.01718* (2018).
- [33] Djork-Arné Clevert, Thomas Unterthiner, and Sepp Hochreiter. "Fast and accurate deep network learning by exponential linear units (elus)." In: *arXiv preprint arXiv:1511.07289* (2015).
- [34] Wenyuan Dai, Qiang Yang, Gui-Rong Xue, and Yong Yu. "Self-taught clustering." In: *Proceedings of the 25th international conference on Machine learning*. 2008, pp. 200–207.

- [35] Navneet Dalal and Bill Triggs. "Histograms of oriented gradients for human detection." In: *2005 IEEE computer society conference on computer vision and pattern recognition (CVPR'05)*. Vol. 1. Ieee. 2005, pp. 886–893.
- [36] Li Deng, Geoffrey Hinton, and Brian Kingsbury. "New types of deep neural network learning for speech recognition and related applications: An overview." In: *2013 IEEE international conference on acoustics, speech and signal processing*. IEEE. 2013, pp. 8599–8603.
- [37] Jacob Devlin, Ming-Wei Chang, Kenton Lee, and Kristina Toutanova. "Bert: Pre-training of deep bidirectional transformers for language understanding." In: *arXiv preprint arXiv:1810.04805* (2018).
- [38] Emily I Dolan. *MIMO: Musical Instrument Museums Online*. 2017.
- [39] H Domínguez Sánchez, M Huertas-Company, M Bernardi, S Kaviraj, JL Fischer, TMC Abbott, FB Abdalla, J Annis, S Avila, D Brooks, et al. "Transfer learning for galaxy morphology from one survey to another." In: *Monthly Notices of the Royal Astronomical Society* 484.1 (2019), pp. 93–100.
- [40] Jeff Donahue, Yangqing Jia, Oriol Vinyals, Judy Hoffman, Ning Zhang, Eric Tzeng, and Trevor Darrell. "Decaf: A deep convolutional activation feature for generic visual recognition." In: *International conference on machine learning*. PMLR. 2014, pp. 647–655.
- [41] Xin Dong, Shangyu Chen, and Sinno Pan. "Learning to prune deep neural networks via layer-wise optimal brain surgeon." In: *Advances in Neural Information Processing Systems*. 2017, pp. 4857–4867.
- [42] John Duchi, Elad Hazan, and Yoram Singer. "Adaptive subgradient methods for online learning and stochastic optimization." In: *Journal of machine learning research* 12.7 (2011).
- [43] Stamatatos Efstathios. "A survey of modern authorship attribution methods." In: *Journal of the American Society for Information Science and Technology* 3 (2009), pp. 538–556. DOI: [10.1002/asi.21001](https://doi.org/10.1002/asi.21001).
- [44] Mark Everingham, Luc Van Gool, Christopher KI Williams, John Winn, and Andrew Zisserman. "The pascal visual object classes (voc) challenge." In: *International journal of computer vision* 88.2 (2010), pp. 303–338.
- [45] Jesse Farebrother, Marlos C Machado, and Michael Bowling. "Generalization and regularization in DQN." In: *arXiv preprint arXiv:1810.00123* (2018).

- [46] William Fedus, Prajit Ramachandran, Rishabh Agarwal, Yoshua Bengio, Hugo Larochelle, Mark Rowland, and Will Dabney. “Revisiting fundamentals of experience replay.” In: *International Conference on Machine Learning*. PMLR. 2020, pp. 3061–3071.
- [47] Meire Fortunato, Mohammad Gheshlaghi Azar, Bilal Piot, Jacob Menick, Ian Osband, Alex Graves, Vlad Mnih, Remi Munos, Demis Hassabis, Olivier Pietquin, et al. “Noisy networks for exploration.” In: *arXiv preprint arXiv:1706.10295* (2017).
- [48] Vincent François-Lavet, Raphaël Fonteneau, and Damien Ernst. “How to Discount Deep Reinforcement Learning: Towards New Dynamic Strategies.” In: *NIPS 2015 Workshop on Deep Reinforcement Learning*. 2015.
- [49] Vincent François-Lavet, Peter Henderson, Riashat Islam, Marc G Bellemare, and Joelle Pineau. “An introduction to deep reinforcement learning.” In: *arXiv preprint arXiv:1811.12560* (2018).
- [50] Jonathan Frankle and Michael Carbin. “The lottery ticket hypothesis: Finding sparse, trainable neural networks.” In: *arXiv preprint arXiv:1803.03635* (2018).
- [51] Jonathan Frankle, Gintare Karolina Dziugaite, Daniel M Roy, and Michael Carbin. “Linear mode connectivity and the lottery ticket hypothesis.” In: *arXiv preprint arXiv:1912.05671* (2019).
- [52] Jonathan Frankle, G Karolina Dziugaite, DM Roy, and M Carbin. “Stabilizing the Lottery Ticket Hypothesis.” In: *arXiv preprint arXiv:1903.01611* (2019).
- [53] Scott Fujimoto, Herke Hoof, and David Meger. “Addressing function approximation error in actor-critic methods.” In: *International Conference on Machine Learning*. PMLR. 2018, pp. 1587–1596.
- [54] Scott Fujimoto, Edoardo Conti, Mohammad Ghavamzadeh, and Joelle Pineau. “Benchmarking Batch Deep Reinforcement Learning Algorithms.” In: *arXiv preprint arXiv:1910.01708* (2019).
- [55] Matthieu Geist, Bruno Scherrer, et al. “Off-policy learning with eligibility traces: a survey.” In: *J. Mach. Learn. Res.* 15.1 (2014), pp. 289–333.
- [56] Daniel George, Hongyu Shen, and EA Huerta. “Deep Transfer Learning: A new deep learning glitch classification method for advanced LIGO.” In: *arXiv preprint arXiv:1706.07446* (2017).
- [57] Varun Gohil, S Deepak Narayanan, and Atishay Jain. “One ticket to win them all: generalizing lottery ticket initializations across datasets and optimizers.” In: *ReScience-C* (2020).

- [58] Nicolas Gonthier, Yann Gousseau, Said Ladjal, and Olivier Bonfait. “Weakly supervised object detection in artworks.” In: *Proceedings of the European Conference on Computer Vision (ECCV) Workshops*. 2018, pp. 0–0.
- [59] Ian Goodfellow, Yoshua Bengio, and Aaron Courville. *Deep learning*. MIT press, 2016.
- [60] Alan Green and Sean Ferguson. “RIdIM: cataloguing music iconography since 1971.” In: *Fontes artis musicae* (2013), pp. 1–8.
- [61] Tuomas Haarnoja, Aurick Zhou, Pieter Abbeel, and Sergey Levine. “Soft actor-critic: Off-policy maximum entropy deep reinforcement learning with a stochastic actor.” In: *International Conference on Machine Learning*. PMLR. 2018, pp. 1861–1870.
- [62] Travis Hammond, Dirk Jelle Schaap, Matthias Sabatelli, and Marco A Wiering. “Forest Fire Control with Learning from Demonstration and Reinforcement Learning.” In: *2020 International Joint Conference on Neural Networks (IJCNN)*. IEEE. 2020, pp. 1–8.
- [63] Song Han, Huizi Mao, and William J Dally. “Deep compression: Compressing deep neural networks with pruning, trained quantization and huffman coding.” In: *arXiv preprint arXiv:1510.00149* (2015).
- [64] Hado Philip van Hasselt. *Insights in reinforcement learning: formal analysis and empirical evaluation of temporal-difference learning algorithms*. Utrecht University, 2011.
- [65] Ji He, Jianshu Chen, Xiaodong He, Jianfeng Gao, Lihong Li, Li Deng, and Mari Ostendorf. “Deep reinforcement learning with a natural language action space.” In: *arXiv preprint arXiv:1511.04636* (2015).
- [66] Kaiming He, Ross Girshick, and Piotr Dollár. “Rethinking imagenet pre-training.” In: *Proceedings of the IEEE/CVF International Conference on Computer Vision*. 2019, pp. 4918–4927.
- [67] Kaiming He, Xiangyu Zhang, Shaoqing Ren, and Jian Sun. “Delving deep into rectifiers: Surpassing human-level performance on imagenet classification.” In: *Proceedings of the IEEE international conference on computer vision*. 2015, pp. 1026–1034.
- [68] Kaiming He, Xiangyu Zhang, Shaoqing Ren, and Jian Sun. “Deep residual learning for image recognition.” In: *Proceedings of the IEEE conference on computer vision and pattern recognition*. 2016, pp. 770–778.

- [69] Peter Henderson, Riashat Islam, Philip Bachman, Joelle Pineau, Doina Precup, and David Meger. "Deep reinforcement learning that matters." In: *Thirty-Second AAAI Conference on Artificial Intelligence*. 2018.
- [70] Kevin Hernandez-Diaz, Fernando Alonso-Fernandez, and Josef Bigun. "Periocular recognition using CNN features off-the-shelf." In: *2018 International conference of the biometrics special interest group (BIOSIG)*. IEEE. 2018, pp. 1–5.
- [71] J Fernando Hernandez-Garcia and Richard S Sutton. "Understanding Multi-Step Deep Reinforcement Learning: A Systematic Study of the DQN Target." In: *arXiv preprint arXiv:1901.07510* (2019).
- [72] Matteo Hessel, Joseph Modayil, Hado Van Hasselt, Tom Schaul, Georg Ostrovski, Will Dabney, Dan Horgan, Bilal Piot, Mohammad Azar, and David Silver. "Rainbow: Combining improvements in deep reinforcement learning." In: *Thirty-Second AAAI Conference on Artificial Intelligence*. 2018.
- [73] Matteo Hessel, Hado van Hasselt, Joseph Modayil, and David Silver. "On inductive biases in deep reinforcement learning." In: *arXiv preprint arXiv:1907.02908* (2019).
- [74] Namgyu Ho and Yoon-Chul Kim. "Evaluation of transfer learning in deep convolutional neural network models for cardiac short axis slice classification." In: *Scientific reports* 11.1 (2021), pp. 1–11.
- [75] Sepp Hochreiter and Jürgen Schmidhuber. "Long short-term memory." In: *Neural computation* 9.8 (1997), pp. 1735–1780.
- [76] Neil Houlsby, Andrei Giurgiu, Stanislaw Jastrzebski, Bruna Morrone, Quentin De Laroussilhe, Andrea Gesmundo, Mona Attariyan, and Sylvain Gelly. "Parameter-efficient transfer learning for NLP." In: *International Conference on Machine Learning*. PMLR. 2019, pp. 2790–2799.
- [77] Jeremy Howard and Sebastian Ruder. "Universal language model fine-tuning for text classification." In: *arXiv preprint arXiv:1801.06146* (2018).
- [78] Minyoung Huh, Pulkit Agrawal, and Alexei A Efros. "What makes ImageNet good for transfer learning?" In: *arXiv preprint arXiv:1608.08614* (2016).
- [79] Tommi Jaakkola, Satinder P Singh, and Michael I Jordan. "Reinforcement learning algorithm for partially observable Markov decision problems." In: *Advances in neural information processing systems* (1995), pp. 345–352.

- [80] Ou Jin, Nathan N Liu, Kai Zhao, Yong Yu, and Qiang Yang. “Transferring topical knowledge from auxiliary long texts for short text clustering.” In: *Proceedings of the 20th ACM international conference on Information and knowledge management*. 2011, pp. 775–784.
- [81] Philipp Kainz, Harald Burgsteiner, Martin Asslaber, and Helmut Ahammer. “Training echo state networks for rotation-invariant bone marrow cell classification.” In: *Neural Computing and Applications* 28.6 (2017), pp. 1277–1292.
- [82] Lukasz Kaiser, Mohammad Babaeizadeh, Piotr Milos, Blazej Osinski, Roy H Campbell, Konrad Czechowski, Dumitru Erhan, Chelsea Finn, Piotr Kozakowski, Sergey Levine, et al. “Model-based reinforcement learning for atari.” In: *arXiv preprint arXiv:1903.00374* (2019).
- [83] Dmitry Kalashnikov, Alex Irpan, Peter Pastor, Julian Ibarz, Alexander Herzog, Eric Jang, Deirdre Quillen, Ethan Holly, Mrinal Kalakrishnan, Vincent Vanhoucke, et al. “Qt-opt: Scalable deep reinforcement learning for vision-based robotic manipulation.” In: *arXiv preprint arXiv:1806.10293* (2018).
- [84] Ibrahem Kandel and Mauro Castelli. “The effect of batch size on the generalizability of the convolutional neural networks on a histopathology dataset.” In: *ICT express* 6.4 (2020), pp. 312–315.
- [85] Nitish Shirish Keskar, Dheevatsa Mudigere, Jorge Nocedal, Mikhail Smelyanskiy, and Ping Tak Peter Tang. “On large-batch training for deep learning: Generalization gap and sharp minima.” In: *arXiv preprint arXiv:1609.04836* (2016).
- [86] Diederik P Kingma and Jimmy Ba. “Adam: A method for stochastic optimization.” In: *arXiv preprint arXiv:1412.6980* (2014).
- [87] James Kirkpatrick, Razvan Pascanu, Neil Rabinowitz, Joel Veness, Guillaume Desjardins, Andrei A Rusu, Kieran Milan, John Quan, Tiago Ramalho, Agnieszka Grabska-Barwinska, et al. “Overcoming catastrophic forgetting in neural networks.” In: *Proceedings of the national academy of sciences* 114.13 (2017), pp. 3521–3526.
- [88] Qiuqiang Kong, Yin Cao, Turab Iqbal, Yuxuan Wang, Wenwu Wang, and Mark D Plumley. “Panns: Large-scale pretrained audio neural networks for audio pattern recognition.” In: *IEEE/ACM Transactions on Audio, Speech, and Language Processing* 28 (2020), pp. 2880–2894.
- [89] George Konidaris and Andrew Barto. “Autonomous shaping: Knowledge transfer in reinforcement learning.” In: *Proceedings of the 23rd international conference on Machine learning*. 2006, pp. 489–496.

- [90] Simon Kornblith, Jonathon Shlens, and Quoc V Le. "Do Better ImageNet Models Transfer Better?" In: *arXiv preprint arXiv:1805.08974* (2018).
- [91] Simon Kornblith, Jonathon Shlens, and Quoc V Le. "Do better imagenet models transfer better?" In: *Proceedings of the IEEE/CVF Conference on Computer Vision and Pattern Recognition*. 2019, pp. 2661–2671.
- [92] Stephen H Lane, David A Handelman, and Jack J Gelfand. "Theory and development of higher-order CMAC neural networks." In: *IEEE Control Systems Magazine* 12.2 (1992), pp. 23–30.
- [93] Pat Langley. "Transfer of knowledge in cognitive systems." In: *Talk, workshop on Structural Knowledge Transfer for Machine Learning at the Twenty-Third International Conference on Machine Learning*. 2006.
- [94] Romain Laroche and Merwan Barlier. "Transfer reinforcement learning with shared dynamics." In: *Proceedings of the AAAI Conference on Artificial Intelligence*. Vol. 31. 1. 2017.
- [95] Alessandro Lazaric. "Transfer in reinforcement learning: a framework and a survey." In: *Reinforcement Learning*. Springer, 2012, pp. 143–173.
- [96] Alessandro Lazaric, Marcello Restelli, and Andrea Bonarini. "Reinforcement learning in continuous action spaces through sequential monte carlo methods." In: *Advances in neural information processing systems* 20 (2007), pp. 833–840.
- [97] Alessandro Lazaric, Marcello Restelli, and Andrea Bonarini. "Transfer of samples in batch reinforcement learning." In: *Proceedings of the 25th international conference on Machine learning*. 2008, pp. 544–551.
- [98] Yann LeCun, Yoshua Bengio, and Geoffrey Hinton. "Deep learning." In: *nature* 521.7553 (2015), p. 436.
- [99] Donghun Lee, Boris Defourny, and Warren B Powell. "Bias-corrected q-learning to control max-operator bias in q-learning." In: *2013 IEEE Symposium on Adaptive Dynamic Programming and Reinforcement Learning (ADPRL)*. IEEE. 2013, pp. 93–99.
- [100] Donghun Lee and Warren B Powell. "Bias-corrected Q-learning with multistate extension." In: *IEEE Transactions on Automatic Control* 64.10 (2019), pp. 4011–4023.
- [101] Pascal Leroy, Damien Ernst, Pierre Geurts, Gilles Louppe, Jonathan Pisane, and Matthia Sabatelli. "QVMix and QVMix-Max: Extending the Deep Quality-Value Family of Algorithms to Cooperative Multi-Agent Reinforcement Learning." In: *Proceedings of the AAAI-21 Workshop on Reinforcement Learning in Games*, p. 8.

- [102] Yuxi Li. "Deep reinforcement learning: An overview." In: *arXiv preprint arXiv:1701.07274* (2017).
- [103] Timothy P Lillicrap, Jonathan J Hunt, Alexander Pritzel, Nicolas Heess, Tom Erez, Yuval Tassa, David Silver, and Daan Wierstra. "Continuous control with deep reinforcement learning." In: *arXiv preprint arXiv:1509.02971* (2015).
- [104] Ji Lin, Yongming Rao, Jiwen Lu, and Jie Zhou. "Runtime neural pruning." In: *Advances in Neural Information Processing Systems*. 2017, pp. 2181–2191.
- [105] Long-Ji Lin. "Self-improving reactive agents based on reinforcement learning, planning and teaching." In: *Machine learning* 8.3-4 (1992), pp. 293–321.
- [106] Tsung-Yi Lin, Michael Maire, Serge Belongie, James Hays, Pietro Perona, Deva Ramanan, Piotr Dollár, and C Lawrence Zitnick. "Microsoft coco: Common objects in context." In: *European conference on computer vision*. Springer. 2014, pp. 740–755.
- [107] Jun S Liu and Rong Chen. "Sequential Monte Carlo methods for dynamic systems." In: *Journal of the American statistical association* 93.443 (1998), pp. 1032–1044.
- [108] Libin Liu and Jessica Hodgins. "Learning to schedule control fragments for physics-based characters using deep q-learning." In: *ACM Transactions on Graphics (TOG)* 36.3 (2017), pp. 1–14.
- [109] David G Lowe. "Distinctive image features from scale-invariant keypoints." In: *International journal of computer vision* 60.2 (2004), pp. 91–110.
- [110] Andrew L Maas, Awni Y Hannun, Andrew Y Ng, et al. "Rectifier nonlinearities improve neural network acoustic models." In: *Proc. icml*. Vol. 30. 1. Citeseer. 2013, p. 3.
- [111] Raphaël Marée, Loïc Rollus, Benjamin Stévens, Renaud Hoyoux, Gilles Louppe, Rémy Vandaele, Jean-Michel Begon, Philipp Kainz, Pierre Geurts, and Louis Wehenkel. "Collaborative analysis of multi-gigapixel imaging data using Cytomine." In: *Bioinformatics* 32.9 (2016), pp. 1395–1401.
- [112] Dominic Masters and Carlo Luschi. "Revisiting Small Batch Training for Deep Neural Networks." In: *arXiv preprint arXiv:1804.07612* (2018).
- [113] Warren S McCulloch and Walter Pitts. "A logical calculus of the ideas immanent in nervous activity." In: *The bulletin of mathematical biophysics* 5.4 (1943), pp. 115–133.
- [114] Neville Mehta, Sriraam Natarajan, Prasad Tadepalli, and Alan Fern. "Transfer in variable-reward hierarchical reinforcement learning." In: *Machine Learning* 73.3 (2008), p. 289.

- [115] Rahul Mehta. "Sparse Transfer Learning via Winning Lottery Tickets." In: *arXiv preprint arXiv:1905.07785* (2019).
- [116] Thomas Mensink and Jan Van Gemert. "The rijksmuseum challenge: Museum-centered visual recognition." In: *Proceedings of International Conference on Multimedia Retrieval*. 2014, pp. 451–454.
- [117] Thomas Mensink, Jasper Uijlings, Alina Kuznetsova, Michael Gygli, and Vittorio Ferrari. "Factors of Influence for Transfer Learning across Diverse Appearance Domains and Task Types." In: *arXiv preprint arXiv:2103.13318* (2021).
- [118] Tomas Mikolov, Kai Chen, Greg Corrado, and Jeffrey Dean. "Efficient estimation of word representations in vector space." In: *arXiv preprint arXiv:1301.3781* (2013).
- [119] Volodymyr Mnih, Koray Kavukcuoglu, David Silver, Alex Graves, Ioannis Antonoglou, Daan Wierstra, and Martin Riedmiller. "Playing atari with deep reinforcement learning." In: *arXiv preprint arXiv:1312.5602* (2013).
- [120] Volodymyr Mnih, Koray Kavukcuoglu, David Silver, Andrei A Rusu, Joel Veness, Marc G Bellemare, Alex Graves, Martin Riedmiller, Andreas K Fidjeland, Georg Ostrovski, et al. "Human-level control through deep reinforcement learning." In: *Nature* 518.7540 (2015), p. 529.
- [121] Volodymyr Mnih, Adria Puigdomenech Badia, Mehdi Mirza, Alex Graves, Timothy Lillicrap, Tim Harley, David Silver, and Koray Kavukcuoglu. "Asynchronous methods for deep reinforcement learning." In: *International conference on machine learning*. 2016, pp. 1928–1937.
- [122] Pavlo Molchanov, Stephen Tyree, Tero Karras, Timo Aila, and Jan Kautz. "Pruning convolutional neural networks for resource efficient inference." In: *arXiv preprint arXiv:1611.06440* (2016).
- [123] Ari Morcos, Haonan Yu, Michela Paganini, and Yuandong Tian. "One ticket to win them all: generalizing lottery ticket initializations across datasets and optimizers." In: *Advances in Neural Information Processing Systems*. 2019, pp. 4933–4943.
- [124] Romain Mormont, Pierre Geurts, and Raphaël Marée. "Comparison of deep transfer learning strategies for digital pathology." In: *Proceedings of the IEEE Conference on Computer Vision and Pattern Recognition Workshops*. 2018, pp. 2262–2271.
- [125] Romain Mormont, Pierre Geurts, and Raphaël Marée. "Multi-task pre-training of deep neural networks for digital pathology." In: *IEEE journal of biomedical and health informatics* (2020).
- [126] Karthik Narasimhan, Tejas Kulkarni, and Regina Barzilay. "Language understanding for text-based games using deep reinforcement learning." In: *arXiv preprint arXiv:1506.08941* (2015).

- [127] Yurii E Nesterov. "A method for solving the convex programming problem with convergence rate $O(1/k^2)$." In: *Dokl. akad. nauk Sssr.* Vol. 269. 1983, pp. 543–547.
- [128] Kien Nguyen, Clinton Fookes, Arun Ross, and Sridha Sridharan. "Iris recognition with off-the-shelf CNN features: A deep learning perspective." In: *IEEE Access* 6 (2017), pp. 18848–18855.
- [129] Johan S Obando-Ceron and Pablo Samuel Castro. "Revisiting Rainbow: Promoting more insightful and inclusive deep reinforcement learning research." In: *arXiv preprint arXiv:2011.14826* (2020).
- [130] Maxime Oquab, Leon Bottou, Ivan Laptev, and Josef Sivic. "Learning and transferring mid-level image representations using convolutional neural networks." In: *Proceedings of the IEEE conference on computer vision and pattern recognition*. 2014, pp. 1717–1724.
- [131] Michela Paganini and Jessica Zosa Forde. "Bespoke vs. Pr\ et-a-Porter Lottery Tickets: Exploiting Mask Similarity for Trainable Sub-Network Finding." In: *arXiv preprint arXiv:2007.04091* (2020).
- [132] Sinno Jialin Pan and Qiang Yang. "A survey on transfer learning." In: *IEEE Transactions on knowledge and data engineering* 22.10 (2009), pp. 1345–1359.
- [133] Emilio Parisotto, Jimmy Lei Ba, and Ruslan Salakhutdinov. "Actor-mimic: Deep multitask and transfer reinforcement learning." In: *arXiv preprint arXiv:1511.06342* (2015).
- [134] Jooyoung Park and Irwin W Sandberg. "Approximation and radial-basis-function networks." In: *Neural computation* 5.2 (1993), pp. 305–316.
- [135] Ross Parry. "Digital heritage and the rise of theory in museum computing." In: *Museum management and Curatorship* (2005), pp. 333–348.
- [136] Adam Paszke, Sam Gross, Soumith Chintala, Gregory Chanan, Edward Yang, Zachary DeVito, Zeming Lin, Alban Desmaison, Luca Antiga, and Adam Lerer. "Automatic differentiation in pytorch." In: (2017).
- [137] Fabian Pedregosa, Gaël Varoquaux, Alexandre Gramfort, Vincent Michel, Bertrand Thirion, Olivier Grisel, Mathieu Blondel, Peter Prettenhofer, Ron Weiss, Vincent Dubourg, et al. "Scikit-learn: Machine learning in Python." In: *the Journal of machine Learning research* 12 (2011), pp. 2825–2830.
- [138] Jing Peng and Ronald J Williams. "Incremental multi-step Q-learning." In: *Machine Learning Proceedings 1994*. Elsevier, 1994, pp. 226–232.

- [139] Andreas Pentaliotis and Marco Wiering. "Variation-resistant Q-learning: Controlling and Utilizing Estimation Bias in Reinforcement Learning for Better Performance." In: (2021).
- [140] Matthew E Peters, Sebastian Ruder, and Noah A Smith. "To tune or not to tune? adapting pretrained representations to diverse tasks." In: *arXiv preprint arXiv:1903.05987* (2019).
- [141] Matthew E Peters, Mark Neumann, Mohit Iyyer, Matt Gardner, Christopher Clark, Kenton Lee, and Luke Zettlemoyer. "Deep contextualized word representations." In: *arXiv preprint arXiv:1802.05365* (2018).
- [142] Fred Phillips and Brandy Mackintosh. "Wiki Art Gallery, Inc.: A case for critical thinking." In: *Issues in Accounting Education* 26.3 (2011), pp. 593–608.
- [143] Martin L Puterman. "Markov decision processes." In: *Handbooks in operations research and management science* 2 (1990), pp. 331–434.
- [144] Martin L Puterman. *Markov decision processes: discrete stochastic dynamic programming*. John Wiley & Sons, 2014.
- [145] Pengjiang Qian, Yizhang Jiang, Zhaohong Deng, Lingzhi Hu, Shouwei Sun, Shitong Wang, and Raymond F Muzic. "Cluster prototypes and fuzzy memberships jointly leveraged cross-domain maximum entropy clustering." In: *IEEE transactions on cybernetics* 46.1 (2015), pp. 181–193.
- [146] Pavlo M Radiuk et al. "Impact of training set batch size on the performance of convolutional neural networks for diverse datasets." In: *Information Technology and Management Science* 20.1 (2017), pp. 20–24.
- [147] Aniruddh Raghu, Matthieu Komorowski, Leo Anthony Celi, Peter Szolovits, and Marzyeh Ghassemi. "Continuous state-space models for optimal sepsis treatment: a deep reinforcement learning approach." In: *Machine Learning for Healthcare Conference*. PMLR. 2017, pp. 147–163.
- [148] Joseph Redmon and Ali Farhadi. "YOLO9000: better, faster, stronger." In: *Proceedings of the IEEE conference on computer vision and pattern recognition*. 2017, pp. 7263–7271.
- [149] Joseph Redmon and Ali Farhadi. "Yolov3: An incremental improvement." In: *arXiv preprint arXiv:1804.02767* (2018).
- [150] Frank Rosenblatt. "The perceptron: a probabilistic model for information storage and organization in the brain." In: *Psychological review* 65.6 (1958), p. 386.
- [151] Corby Rosset, Chenyan Xiong, Minh Phan, Xia Song, Paul Bennett, and Saurabh Tiwary. "Knowledge-Aware Language Model Pretraining." In: *arXiv preprint arXiv:2007.00655* (2020).

- [152] Sebastian Ruder. "An overview of gradient descent optimization algorithms." In: *arXiv preprint arXiv:1609.04747* (2016).
- [153] David E Rumelhart, Geoffrey E Hinton, and Ronald J Williams. "Learning representations by back-propagating errors." In: *nature* 323.6088 (1986), pp. 533–536.
- [154] Gavin A Rummery and Mahesan Niranjan. *On-line Q-learning using connectionist systems*. Vol. 37. University of Cambridge, Department of Engineering Cambridge, England, 1994.
- [155] Olga Russakovsky, Jia Deng, Hao Su, Jonathan Krause, Sanjeev Satheesh, Sean Ma, Zhiheng Huang, Andrej Karpathy, Aditya Khosla, Michael Bernstein, et al. "Imagenet large scale visual recognition challenge." In: *International journal of computer vision* 115.3 (2015), pp. 211–252.
- [156] Matthia Sabatelli. *Learning to Play Chess with Minimal Lookahead and Deep Value Neural Networks*. Tech. rep. Faculty of Science and Engineering, 2017.
- [157] Matthia Sabatelli, Mike Kestemont, and Pierre Geurts. "On the transferability of winning tickets in non-natural image datasets." In: (2021), pp. 59–69.
- [158] Matthia Sabatelli, Gilles Louppe, Pierre Geurts, and Marco Wiering. "Deep Quality-Value (DQV) Learning." In: *Advances in Neural Information Processing Systems, Deep Reinforcement Learning Workshop*. Montreal. 2018.
- [159] Matthia Sabatelli, Mike Kestemont, Walter Daelemans, and Pierre Geurts. "Deep transfer learning for art classification problems." In: *Proceedings of the European Conference on Computer Vision (ECCV) Workshops*. 2018, pp. 631–646.
- [160] Matthia Sabatelli, Francesco Bidoia, Valeriu Codreanu, and Marco Wiering. "Learning to Evaluate Chess Positions with Deep Neural Networks and Limited Lookahead." In: *7th International Conference on Pattern Recognition Applications and Methods*. 2018.
- [161] Matthia Sabatelli, Gilles Louppe, Pierre Geurts, and Marco A Wiering. "Approximating two value functions instead of one: towards characterizing a new family of Deep Reinforcement Learning algorithms." In: *arXiv preprint arXiv:1909.01779* (2019).
- [162] Matthia Sabatelli, Gilles Louppe, Pierre Geurts, and Marco A Wiering. "The deep quality-value family of deep reinforcement learning algorithms." In: *2020 International Joint Conference on Neural Networks (IJCNN)*. IEEE. 2020, pp. 1–8.

- [163] Matthia Sabatelli, Nikolay Banar, Marie Cocriamont, Eva Coudyzer, Karine Lasaracina, Walter Daelemans, Pierre Geurts, and Mike Kestemont. "Advances in Digital Music Iconography: Benchmarking the detection of musical instruments in unrestricted, non-photorealistic images from the artistic domain." In: *DHQ: Digital Humanities Quarterly* 15.1 (2021).
- [164] Iman Sajedian, Heon Lee, and Junsuk Rho. "Design of high transmission color filters for solar cells directed by deep Q-learning." In: *Solar Energy* 195 (2020), pp. 670–676.
- [165] Adriel Saporta, Xiaotong Gui, Ashwin Agrawal, Anuj Pareek, Steven QH Truong, Chanh DT Nguyen, Van-Doan Ngo, Jayne Seekins, Francis G Blankenberg, Andrew Ng, et al. "Deep learning saliency maps do not accurately highlight diagnostically relevant regions for medical image interpretation." In: *medRxiv* (2021).
- [166] Stefan Schaal, Auke Jan Ijspeert, Aude Billard, Sethu Vijayakumar, and Jean-Arcady Meyer. "Estimating future reward in reinforcement learning animats using associative learning." In: (2004).
- [167] Tom Schaul, John Quan, Ioannis Antonoglou, and David Silver. "Prioritized experience replay." In: *arXiv preprint arXiv:1511.05952* (2015).
- [168] Juergen Schmidhuber. "Reinforcement Learning Upside Down: Don't Predict Rewards—Just Map Them to Actions." In: *arXiv preprint arXiv:1912.02875* (2019).
- [169] Robin M Schmidt, Frank Schneider, and Philipp Hennig. "Descending through a Crowded Valley—Benchmarking Deep Learning Optimizers." In: *arXiv preprint arXiv:2007.01547* (2020).
- [170] John Schulman, Philipp Moritz, Sergey Levine, Michael Jordan, and Pieter Abbeel. "High-dimensional continuous control using generalized advantage estimation." In: *arXiv preprint arXiv:1506.02438* (2015).
- [171] John Schulman, Sergey Levine, Pieter Abbeel, Michael Jordan, and Philipp Moritz. "Trust region policy optimization." In: *International conference on machine learning*. PMLR. 2015, pp. 1889–1897.
- [172] John Schulman, Filip Wolski, Prafulla Dhariwal, Alec Radford, and Oleg Klimov. "Proximal policy optimization algorithms." In: *arXiv preprint arXiv:1707.06347* (2017).
- [173] Ramprasaath R Selvaraju, Michael Cogswell, Abhishek Das, Ramakrishna Vedantam, Devi Parikh, and Dhruv Batra. "Grad-cam: Visual explanations from deep networks via gradient-based localization." In: *Proceedings of the IEEE international conference on computer vision*. 2017, pp. 618–626.

- [174] Pierre Sermanet, David Eigen, Xiang Zhang, Michaël Mathieu, Rob Fergus, and Yann LeCun. "Overfeat: Integrated recognition, localization and detection using convolutional networks." In: *arXiv preprint arXiv:1312.6229* (2013).
- [175] Ali Sharif Razavian, Hossein Azizpour, Josephine Sullivan, and Stefan Carlsson. "CNN features off-the-shelf: an astounding baseline for recognition." In: *Proceedings of the IEEE conference on computer vision and pattern recognition workshops*. 2014, pp. 806–813.
- [176] Arjun Sharma et al. "Adapting off-the-shelf CNNs for word spotting & recognition." In: *2015 13th International Conference on Document Analysis and Recognition (ICDAR)*. IEEE. 2015, pp. 986–990.
- [177] Karen Simonyan, Andrea Vedaldi, and Andrew Zisserman. "Deep inside convolutional networks: Visualising image classification models and saliency maps." In: *arXiv preprint arXiv:1312.6034* (2013).
- [178] Karen Simonyan and Andrew Zisserman. "Very deep convolutional networks for large-scale image recognition." In: *arXiv preprint arXiv:1409.1556* (2014).
- [179] Satinder Singh, Andrew G Barto, and Nuttapong Chentanez. *Intrinsically motivated reinforcement learning*. Tech. rep. MASSACHUSETTS UNIV AMHERST DEPT OF COMPUTER SCIENCE, 2005.
- [180] Satinder Singh, Tommi Jaakkola, Michael L Littman, and Csaba Szepesvári. "Convergence results for single-step on-policy reinforcement-learning algorithms." In: *Machine learning* 38.3 (2000), pp. 287–308.
- [181] James E Smith and Robert L Winkler. "The optimizer's curse: Skepticism and postdecision surprise in decision analysis." In: *Management Science* 52.3 (2006), pp. 311–322.
- [182] Nitish Srivastava, Geoffrey Hinton, Alex Krizhevsky, Ilya Sutskever, and Ruslan Salakhutdinov. "Dropout: a simple way to prevent neural networks from overfitting." In: *The journal of machine learning research* 15.1 (2014), pp. 1929–1958.
- [183] Eric Van den Steen. "Rational overoptimism (and other biases)." In: *American Economic Review* 94.4 (2004), pp. 1141–1151.
- [184] Gjorgji Strezoski and Marcel Worring. "Omniart: a large-scale artistic benchmark." In: *ACM Transactions on Multimedia Computing, Communications, and Applications (TOMM)* 14.4 (2018), pp. 1–21.

- [185] Tianxiang Sun, Yunfan Shao, Xiaonan Li, Pengfei Liu, Hang Yan, Xipeng Qiu, and Xuanjing Huang. "Learning Sparse Sharing Architectures for Multiple Tasks." In: *arXiv preprint arXiv:1911.05034* (2019).
- [186] Richard S Sutton. "Learning to predict by the methods of temporal differences." In: *Machine learning* 3.1 (1988), pp. 9–44.
- [187] Richard S Sutton. "Generalization in reinforcement learning: Successful examples using sparse coarse coding." In: *Advances in neural information processing systems*. 1996, pp. 1038–1044.
- [188] Richard S Sutton and Andrew G Barto. *Reinforcement learning: An introduction*. MIT press, 2018.
- [189] Richard S Sutton, David A McAllester, Satinder P Singh, Yishay Mansour, et al. "Policy gradient methods for reinforcement learning with function approximation." In: *NIPS*. Vol. 99. Cite-seer. 1999, pp. 1057–1063.
- [190] Richard Stuart Sutton. "Temporal credit assignment in reinforcement learning." In: (1984).
- [191] Christian Szegedy, Vincent Vanhoucke, Sergey Ioffe, Jon Shlens, and Zbigniew Wojna. "Rethinking the inception architecture for computer vision." In: *Proceedings of the IEEE Conference on Computer Vision and Pattern Recognition*. 2016, pp. 2818–2826.
- [192] Nima Tajbakhsh, Jae Y Shin, Suryakanth R Gurudu, R Todd Hurst, Christopher B Kendall, Michael B Gotway, and Jianming Liang. "Convolutional neural networks for medical image analysis: Full training or fine tuning?" In: *IEEE transactions on medical imaging* 35.5 (2016), pp. 1299–1312.
- [193] Hong Hui Tan and King Hann Lim. "Review of second-order optimization techniques in artificial neural networks backpropagation." In: *IOP Conference Series: Materials Science and Engineering*. Vol. 495. 1. IOP Publishing. 2019, p. 012003.
- [194] Matthew E Taylor, Nicholas K Jong, and Peter Stone. "Transferring instances for model-based reinforcement learning." In: *Joint European conference on machine learning and knowledge discovery in databases*. Springer. 2008, pp. 488–505.
- [195] Gerald Tesauro. "TD-Gammon, a self-teaching backgammon program, achieves master-level play." In: *Neural computation* 6.2 (1994), pp. 215–219.
- [196] Sebastian Thrun and Anton Schwartz. "Issues in using function approximation for reinforcement learning." In: *Proceedings of the Fourth Connectionist Models Summer School*. Hillsdale, NJ. 1993, pp. 255–263.

- [197] Tijmen Tieleman and Geoffrey Hinton. "Lecture 6.5-rmsprop: Divide the gradient by a running average of its recent magnitude." In: *COURSERA: Neural networks for machine learning* (2012), pp. 26–31.
- [198] Andrea Tirinzoni, Rafael Rodriguez Sanchez, and Marcello Restelli. "Transfer of value functions via variational methods." In: *Advances in Neural Information Processing Systems*. 2018, pp. 6179–6189.
- [199] Andrea Tirinzoni, Andrea Sessa, Matteo Pirotta, and Marcello Restelli. "Importance weighted transfer of samples in reinforcement learning." In: *International Conference on Machine Learning*. PMLR. 2018, pp. 4936–4945.
- [200] Huan-Hsin Tseng, Yi Luo, Sunan Cui, Jen-Tzung Chien, Randall K Ten Haken, and Issam El Naqa. "Deep reinforcement learning for automated radiation adaptation in lung cancer." In: *Medical physics* 44.12 (2017), pp. 6690–6705.
- [201] John N Tsitsiklis and Benjamin Van Roy. "An analysis of temporal-difference learning with function approximation." In: *IEEE transactions on automatic control* 42.5 (1997), pp. 674–690.
- [202] Jacob Tyo and Zachary Lipton. "How transferable are the representations learned by deep q agents?" In: *arXiv preprint arXiv:2002.10021* (2020).
- [203] Bram Van Ginneken, Arnaud AA Setio, Colin Jacobs, and Francesco Ciompi. "Off-the-shelf convolutional neural network features for pulmonary nodule detection in computed tomography scans." In: *2015 IEEE 12th International symposium on biomedical imaging (ISBI)*. IEEE. 2015, pp. 286–289.
- [204] Hado Van Hasselt. "Double Q-learning." In: *Advances in Neural Information Processing Systems*. 2010, pp. 2613–2621.
- [205] Hado Van Hasselt, Arthur Guez, and David Silver. "Deep reinforcement learning with double Q-learning." In: *Thirtieth AAAI Conference on Artificial Intelligence*. 2016.
- [206] Hado Van Hasselt, Yotam Doron, Florian Strub, Matteo Hessel, Nicolas Sonnerat, and Joseph Modayil. "Deep Reinforcement Learning and the Deadly Triad." In: *arXiv preprint arXiv:1812.02648* (2018).
- [207] Harm Van Seijen, Mehdi Fatemi, and Arash Tavakoli. "Using a logarithmic mapping to enable lower discount factors in reinforcement learning." In: *arXiv preprint arXiv:1906.00572* (2019).
- [208] Ryan Van Soelen and John W Sheppard. "Using winning lottery tickets in transfer learning for convolutional neural networks." In: *2019 International Joint Conference on Neural Networks (IJCNN)*. IEEE. 2019, pp. 1–8.

- [209] Vladimir Vapnik. "Principles of risk minimization for learning theory." In: *Advances in neural information processing systems*. 1992, pp. 831–838.
- [210] Limin Wang, Yu Qiao, and Xiaoou Tang. "Action recognition and detection by combining motion and appearance features." In: *THUMOS14 Action Recognition Challenge 1.2* (2014), p. 2.
- [211] Zheng Wang, Yangqiu Song, and Changshui Zhang. "Transferred dimensionality reduction." In: *Joint European conference on machine learning and knowledge discovery in databases*. Springer. 2008, pp. 550–565.
- [212] Ziyu Wang, Tom Schaul, Matteo Hessel, Hado Van Hasselt, Marc Lanctot, and Nando Freitas. "Dueling Network Architectures for Deep Reinforcement Learning." In: *International Conference on Machine Learning*. 2016, pp. 1995–2003.
- [213] Ziyu Wang, Victor Bapst, Nicolas Heess, Volodymyr Mnih, Remi Munos, Koray Kavukcuoglu, and Nando de Freitas. "Sample efficient actor-critic with experience replay." In: *arXiv preprint arXiv:1611.01224* (2016).
- [214] Christopher JCH Watkins and Peter Dayan. "Q-learning." In: *Machine learning* 8.3-4 (1992), pp. 279–292.
- [215] Qinglai Wei, Derong Liu, and Hanquan Lin. "Value iteration adaptive dynamic programming for optimal control of discrete-time nonlinear systems." In: *IEEE Transactions on cybernetics* 46.3 (2015), pp. 840–853.
- [216] Stuart Weibel, John Kunze, Carl Lagoze, and Misha Wolf. *Dublin core metadata for resource discovery*. Tech. rep. 1998.
- [217] Marco A Wiering. "Explorations in efficient reinforcement learning." PhD thesis. University of Amsterdam, 1999.
- [218] Marco A Wiering. "Convergence and divergence in standard and averaging reinforcement learning." In: *European Conference on Machine Learning*. Springer. 2004, pp. 477–488.
- [219] Marco A Wiering. "QV (lambda)-learning: A new on-policy reinforcement learning algorithm." In: *Proceedings of the 7th European Workshop on Reinforcement Learning*. 2005, pp. 17–18.
- [220] Marco A Wiering and Hado Van Hasselt. "The QV family compared to other reinforcement learning algorithms." In: *Adaptive Dynamic Programming and Reinforcement Learning, 2009. AD-PRL'09. IEEE Symposium on*. IEEE. 2009, pp. 101–108.
- [221] Marco Wiering and Jürgen Schmidhuber. "Speeding up Q (λ)-learning." In: *European Conference on Machine Learning*. Springer. 1998, pp. 352–363.

- [222] Ronald J Williams. "Simple statistical gradient-following algorithms for connectionist reinforcement learning." In: *Machine learning* 8.3-4 (1992), pp. 229–256.
- [223] Jos van de Wolfshaar, Mahir F Karaaba, and Marco A Wiering. "Deep convolutional neural networks and support vector machines for gender recognition." In: *Computational Intelligence, 2015 IEEE Symposium Series on*. IEEE. 2015, pp. 188–195.
- [224] R. Wollheim. *On Art and the Mind. Essays and Lectures*. Allen Lane, 1972.
- [225] Han Xiao, Kashif Rasul, and Roland Vollgraf. "Fashion-mnist: a novel image dataset for benchmarking machine learning algorithms." In: *arXiv preprint arXiv:1708.07747* (2017).
- [226] Saining Xie, Ross Girshick, Piotr Dollár, Zhuowen Tu, and Kaiming He. "Aggregated residual transformations for deep neural networks." In: *Computer Vision and Pattern Recognition (CVPR), 2017 IEEE Conference on*. IEEE. 2017, pp. 5987–5995.
- [227] Corinna Cortes Yann LeCun and Christopher J. C. Burges. *The MNIST database of handwritten digits*. <http://yann.lecun.com/exdb/mnist/>, 1994. 1996.
- [228] Haonan Yu, Sergey Edunov, Yuandong Tian, and Ari S Morcos. "Playing the lottery with rewards and multiple languages: lottery tickets in RL and NLP." In: *arXiv preprint arXiv:1906.02768* (2019).
- [229] Guido Zarrella and Amy Marsh. "Mitre at semeval-2016 task 6: Transfer learning for stance detection." In: *arXiv preprint arXiv:1606.03784* (2016).
- [230] Matthew D Zeiler and Rob Fergus. "Visualizing and understanding convolutional networks." In: *European conference on computer vision*. Springer. 2014, pp. 818–833.
- [231] Dongbin Zhao, Haitao Wang, Kun Shao, and Yuanheng Zhu. "Deep reinforcement learning with experience replay based on SARSA." In: *2016 IEEE Symposium Series on Computational Intelligence (SSCI)*. IEEE. 2016, pp. 1–6.
- [232] Sheng-hua Zhong, Xingsheng Huang, and Zhiqiao Xiao. "Fine-art painting classification via two-channel dual path networks." In: *International Journal of Machine Learning and Cybernetics* 11.1 (2020), pp. 137–152.
- [233] Yang Zhong, Josephine Sullivan, and Haibo Li. "Face attribute prediction using off-the-shelf CNN features." In: *2016 International Conference on Biometrics (ICB)*. IEEE. 2016, pp. 1–7.
- [234] Yi-Tong Zhou and Rama Chellappa. "Computation of optical flow using a neural network." In: *ICNN*. 1988, pp. 71–78.

- [235] Rong Zhu and Mattia Rigotti. "Self-correcting Q-Learning." In: *arXiv preprint arXiv:2012.01100* (2020).
- [236] Xiaofeng Zhu, Zi Huang, Yang Yang, Heng Tao Shen, Changsheng Xu, and Jiebo Luo. "Self-taught dimensionality reduction on the high-dimensional small-sized data." In: *Pattern Recognition* 46.1 (2013), pp. 215–229.
- [237] Xiaofeng Zhu, Xuelong Li, Shichao Zhang, Chunhua Ju, and Xindong Wu. "Robust joint graph sparse coding for unsupervised spectral feature selection." In: *IEEE transactions on neural networks and learning systems* 28.6 (2016), pp. 1263–1275.
- [238] Zhuangdi Zhu, Kaixiang Lin, and Jiayu Zhou. "Transfer Learning in Deep Reinforcement Learning: A Survey." In: *arXiv preprint arXiv:2009.07888* (2020).
- [239] Fuzhen Zhuang, Zhiyuan Qi, Keyu Duan, Dongbo Xi, Yongchun Zhu, Hengshu Zhu, Hui Xiong, and Qing He. "A comprehensive survey on transfer learning." In: *Proceedings of the IEEE* 109.1 (2020), pp. 43–76.
- [240] Zhuangwei Zhuang, Mingkui Tan, Bohan Zhuang, Jing Liu, Yong Guo, Qingyao Wu, Junzhou Huang, and Jinhui Zhu. "Discrimination-aware channel pruning for deep neural networks." In: *Advances in Neural Information Processing Systems*. 2018, pp. 875–886.

DECLARATION

Put your declaration here.

Saarbrücken, September 2015

Matthia Sabatelli

COLOPHON

This document was typeset using the typographical look-and-feel `classicthesis` developed by André Miede. The style was inspired by Robert Bringhurst's seminal book on typography "*The Elements of Typographic Style*". `classicthesis` is available for both L^AT_EX and LyX:

<https://bitbucket.org/amiede/classicthesis/>

Happy users of `classicthesis` usually send a real postcard to the author, a collection of postcards received so far is featured here:

<http://postcards.miede.de/>

Final Version as of July 15, 2021 (classicthesis version 4.2).